uOttawa

L'Université canadienne
Canada's university

FACULTÉ DES ÉTUDES SUPÉRIEURES ET POSTOCTORALES

uOttawa

L'Université canadienne
Canada's university

FACULTY OF GRADUATE AND POSDOCTORAL STUDIES

Huijian Zhan

AUTEUR DE LA THÈSE / AUTHOR OF THESIS

M.A.Sc. (Mechanical Engineering)

GRADE / DEGREE

Department of Mechanical Engineering

FACULTÉ, ÉCOLE, DÉPARTEMENT / FACULTY, SCHOOL, DEPARTMENT

Static and Dynamic Analysis of Toroidal LPG Tanks

TITRE DE LA THÈSE / TITLE OF THESIS

David Redekop

DIRECTEUR (DIRECTRICE) DE LA THÈSE / THESIS SUPERVISOR

CO-DIRECTEUR (CO-DIRECTRICE) DE LA THÈSE / THESIS CO-SUPERVISOR

EXAMINATEURS (EXAMINATRICES) DE LA THÈSE / THESIS EXAMINERS

Ming Liang

Xin Wang

Gary W. Slater

Le Doyen de la Faculté des études supérieures et postdoctorales / Dean of the Faculty of Graduate and Postdoctoral Studies

STATIC AND DYNAMIC ANALYSIS OF TOROIDAL LPG TANKS

H.J. Zhan

A thesis submitted to

the Faculty of Graduate and Postdoctoral Studies

in partial fulfillment of the requirements

for the degree of

MASTER OF APPLIED SCIENCE

in Mechanical Engineering

UNIVERSITY OF OTTAWA

Your file Votre référence
ISBN: 978-0-494-41687-7
Our file Notre référence
ISBN: 978-0-494-41687-7

Abstract

Liquefied petroleum gas (LPG) is considered clean, safe and cheap, offering a viable alternative to conventional fuels. Nowadays, the use of LPG as a fuel source in motor vehicles is steadily increasing. The LPG tanks in motor vehicles can be of toroidal shape. The toroidal LPG tanks are generally of non-circular cross-section, and may be supported at points, lines or patches on the surface. Among the mechanical properties of interest for toroidal LPG tanks are the static behavior under internal pressure, the vibration characteristics, the buckling and collapse loads, and the properties under impact loading arising from accident conditions.

In the current work, a shell-theory finite element analysis is carried out of toroidal LPG tanks, with non-circular cross-section. The analysis serves to determine the natural frequencies, the buckling and collapse pressures, and the deformation of impacted tanks. The differential quadrature method is used as an alternate means in the vibration analysis. A variety of support conditions are considered, including lines of support at the inner and outer equators of the tank. For validation, comparison is made with previously published results for stress, vibration and buckling of circular and elliptical toroidal shells, and impact deformation of spherical and cylindrical shells. Finally, a parametric study is carried out to determine the influence on the natural frequency, buckling and collapse pressures, and the deformation of the impacted tanks, of shell size, shell thickness, material properties, and support conditions.

Acknowledgements

I am deeply grateful to my supervisor, Dr. D. Redekop, for his patient and invaluable suggestions in the writing of this thesis. In my two-year study, I benefited enormously from his guidence. His enthusiasm and preciseness toward this research area taught me how to become a qualified engineer. His continuous encouragement helped me overcome the difficulties in my studies and research.

I would also like to express my gratitude to all the members of the Department of Mechannical Engineering who made contributions toward my studies and research.

Finally, the most special thanks are given to my dear parents for their encouragement and support during my study.

Content

List of tables

List of figures

Nomenclature

A_2	semi-axis of the square profile
a, b	the semi-minor and semi-major axes of the ellipse
C	bend radius of the toroidal shell
D	outer diameter of the toroidal LPG tank
d	projectile diameter
E	Young's modulus
E_s	the shear strain energy
E_k	initial kinetic energy
E_{bm}	bending strain energy
$\mathbf{e_1}, \mathbf{e_2}, \mathbf{e_n}$	unit vectors of the orthogonal basis
$\mathbf{F}$	load vector
${}^{T}\mathbf{F}$	consistent nodal force vector
${}^{T+\Delta T}\mathbf{F}^{(i-1)}$	the consistent nodal force vector corresponding to the element stresses due to the displacement vector ${}^{T+\Delta T}\mathbf{U}^{(i-1)}$
F	shell reactive force
F_c^s	the collapse force for the shell
F_c	the collapse load for the equivalent circular plate
f_1	parameter, defined as $f_1 = (a \cdot \cos\psi)^{\frac{1}{2n-1}}$
f_2	parameter, defined as $f_2 = (b \cdot \sin\psi)^{\frac{1}{2n-1}}$
G	parameter, defined as $G = \left(f_1^{2n} + f_2^{2n}\right)^{\frac{1}{2n}}$

H	transverse height of the toroidal LPG tank
i, j, k	Cartesian unit vectors
K	system stiffness matrix
${}^{T_1}K$	stiffness matrix of the structural system at time T_1
${}^{T_1}K_{NL}$	geometrically nonlinear part of ${}^{T_1}K$
${}^{T}K$	tangent stiffness matrix at time T
${}^{T+\Delta T}K^{(i-1)}$	the tangent stiffness matrix base on solution calculated at the end of iteration (i-1) at time $T+\Delta T$
K_m^s	membrane stiffness
K_m	membrane stiffness for the equivalent circular plate
k_1, k_2	curvature components of the toroidal shell
L	parameter, defined as $L = \frac{\partial \mathbf{e_n}}{\partial \phi} \cdot \frac{\partial \mathbf{R}}{\partial \phi}$
m	mass of the projectile
M_0, N_0	plastic capacities for the shell
N	parameter, defined as $N = \frac{\partial \mathbf{e_n}}{\partial \psi} \cdot \frac{\partial \mathbf{R}}{\partial \psi}$
p	internal pressure
q_1, q_2	orthogonal coordinate system
R	radius vector
R	radius of the spherical shell
R_o	horizontal radial projection of the spherical shell
R_2	radius of the lobed corners of squarish toroidal shell B

R_d	dimple radius
${}^{T_1}\mathbf{R}$, ${}^{T_0}\mathbf{R}$	externally applied load vectors at time T_1 and T_0
${}^{T+\Delta T}\mathbf{R}$	the externally applied load vector at time $T+\Delta T$
r	Cartesian unit vector, defined as $r=r(q_2)$
r_c	radius of the cross-section for the toroidal shell
T	time
t	thickness of shells
$\mathbf{U}$, ${}^{T}\mathbf{U}$	displacement vector
$\Delta\mathbf{U}^{(i)}$	the incremental displacement vector in iteration (i)
V	volumes of the toroidal LPG tank
v	initial velocity of the projectile
w	radial outward displacement
W_0, w_0	central deflection
x_1, y, z	Cartesian coordinates
α	experimental parameter
α_1, α_2	Lamé parameters
β	hardening parameter
β_0	parameter, defined as $\beta_0 = (\varphi_0/2\pi)^{\frac{1}{2}}$
θ	meridional angular coordinate for squarish toroidal shell B
γ_i	buckling eigenvalue
λ	frequency parameter, defined by $\lambda = \rho a_o^2 \omega^2 (1-\mu^2)/E$
λ_i	the critical buckling load factor for mode i
μ	Poisson's ratio

ρ	mass density
σ_0	bending stress
σ_y	yield stress
Φ	angle measured clockwise from the upper crown of the cross-section for a circular/elliptical toroidal shell
ϕ	circumferential angular coordinate
ϕ_i	the buckling shape for mode i
φ_0	angle subtended at the center of the sphere
ψ	meridional angular coordinate for squarish toroidal shell A
ω	natural frequency

Chapter 1: Introduction

1.1 Development of LPG

The preservation of the environment is one of the most important current issues for engineers. Conventional fuel is causing many severe environmental problems, and the price of gasoline is continuing to rise. Liquefied petroleum gas (LPG), which is clean, safe and cheap (the price of LPG is much lower than gasoline), is currently being cited as a viable alternative fuel. It burns readily in air and can be used in heating, cooking and automobiles, and is thus more environmentally friendly.

The development of environmentally friendly cars is a step towards achieving a cleaner environment. LPG vehicles produce less harmful carbon dioxide emissions than traditional gasoline-powered vehicles. Currently, several governments are encouraging the LPG industry with financial support. Thus an increasing number of LPG related products are being produced. Concerning motor vehicles, there are currently nine million LPG vehicles in the world, and the number is increasing rapidly.

1.2 Toroidal LPG tanks

LPG can change from a gaseous state to a liquid one, when subjected to pressure (approximate 800 *kPa* or 120 *psi*). That means, at normal temperatures and pressures, LPG will evaporate, and thus it needs to be stored in pressurized tanks. In an LPG tank, in order to allow for thermal expansion, generally 80%-85% of its capacity is filled, while the ratio between the volumes of the vaporized gas and the liquefied gas is around 250:1 (www.lpg-solutions.co.uk).

LPG tanks usually are made of thick carbon steel. They thus may be considered safer than conventional fuel tanks, which are normally made from very thin sheet steel or even plastic. There are now two main types of LPG tanks; cylindrical and toroidal. Toroidal tanks are increasingly being used in vehicles, as they can satisfy space-limited installation requirements. Additionally, because they present a doubly curved surface to the outside, toroidal tanks have better crashworthiness than cylindrical tanks, which are vulnerable if hit broadside on. Also the valve of the toroidal tank can be located in a protected position at the intrados of the tank.

In most cases toroidal LPG tanks are installed in the spare wheel well in the trunk of a motor vehicle. The tanks can be installed horizontally or vertically (Figs. 1.1 and 1.2). The tanks allow installation with minimum loss of trunk space in vehicles such as in a classic Range Rover or Jeep Cherokee.

Compared to cylindrical tanks, toroidal tanks can be a good solution for those wanting to maintain load or trunk space. However, because the structure of a toroidal tank is difficult to produce, its cost can be higher than a cylindrical LPG tank. In Canada, to convert a conventional vehicle to an LPG one, it would generally cost about $5,500 CAD (www.propanegas.ca).

1.3 Shell theory

Shell structures are widely used in engineering. A shell structure can be defined as a body enclosed between two closely spaced and curved surfaces. The behavior of a shell is governed by the membrane and the bending properties of an appropriate reference surface. In a shell, the membrane and the bending behaviors are coupled. For analyzing this behavior,

many different linear and non-linear shell theories have been developed. Most of them are first-order theories based on the Kirchhoff-Love hypothesis, while others are second-order theories based on the Mindlin hypothesis. The Sanders shell theory is one of the most accurate first-order theories.

In this thesis, the Sanders theory is adapted in a differential quadrature method (DQM) approach for the vibration analysis of toroidal LPG tanks. Details of the Sanders theory are discussed by Sanders (1959). The Mindlin theory is used in the finite element analysis of the study.

1.4 Finite element method (FEM)

In the current study, the finite element method (FEM) is used as the main tool of analysis. Its convenience and accuracy permit easy application to many problems, which are difficult to solve by other methods. This method combines several mathematical concepts to produce a system of linear or nonlinear equations and has two characteristics that distinguish it from other numerical procedures:

(1) The method utilizes an integral formulation to generate a system of algebraic equations.

(2) The method uses continuous piecewise smooth functions for approximating the unknown quantity or quantities.

In the FEM, the actual structure is subdivided into a number of small elements. Polynomial shape functions are employed to approximate the displacements and stresses in each element. The physical model is comprised of the elements which connect to other adjacent elements through discrete nodes. Known loads acting on the structure are

represented as forces, applied at the nodes. The solution requires using these known loads and element stiffnesses to solve for unknown displacements. The displacements are then used to find element results such as force per unit length, stress, strain, etc..

Nowadays, the FEM is widely used for solving linear and nonlinear problems in engineering. In the linear FEM analysis, two assumptions are involved. Firstly the stress in the material is exactly proportional to strain. Secondly, the structure deforms exactly proportional to the loads, as long as the supports are the same. Nonlinear FEM analysis involves systems that have large displacements or advanced material behavior such as plastic yielding, buckling, or failure. Another type of non-linearity involves contact between the structure and other components or supports.

In this thesis, two commercial FEM softwares ADINA and LS-DYNA are used. ADINA is used in the vibration and buckling and collapse analysis of toroidal LPG tanks. This software is a one-system program for comprehensive finite element analysis of structures, fluids, and fluid flows with structural interactions. It can be used in either linear or nonlinear static and dynamic structural analysis. The nonlinearities can include material nonlinearities, large deformations and contact conditions. Static, frequency, or transient analysis can be performed accurately and effectively.

LS-DYNA is employed in this study to obtain the dynamic response of toroidal LPG tanks impacted by projectiles. This software is widely used by automobile, aerospace, military, manufacturing, and bioengineering companies. LS-DYNA is most often used to simulate automotive crashworthiness and occupant safety, sheetmetal forming, structural failure etc. LS-DYNA was preferred for impact analysis because it can provide highly nonlinear transient dynamic finite element analysis using explicit time integration.

1.5 Structure of the thesis

This thesis covers vibration, buckling and collapse, and impact analysis of toroidal LPG tanks. Validation studies were carried out to ensure accuracy of the results. Parametric studies were carried out to indicate the influence of geometric and material properties on the results. Tables and figures are presented, and programs of the analysis are given in appendices. Finally conclusions are given and suggestions are made for further research.

The first chapter of the thesis introduces the background of LPG tanks, theories of shells, and the FEM.

The second chapter reviews previous research work related to the analyses of vibration, buckling, collapse and impact of shell structures. Theories developed by other researchers are reviewed. These theories were used in this thesis for validating the numerical results of toroidal LPG tanks simulated by the FEM softwares ADINA and LS-DYNA.

In Chapter 3, the characteristics of stress and vibration of toroidal LPG tanks were studied. A computer program, based on the differential quadrature method (DQM) was modified to validate work on circular and elliptical toroidal tanks. The program served to provide some results for the vibration of the tanks. A new DQM program was developed for squarish cross-sections, but the results obtained proved unreliable. A discussion about the results is presented at the end of this chapter.

In Chapter 4, the buckling and collapse of toroidal LPG tanks were studied, using again the ADINA software. The buckling and collapse pressures of toroidal LPG tanks with different geometric, material and loading were obtained. The effect of the variation of parameters on the behavior of toroidal LPG tanks was determined.

In Chapter 5, the FEM software LS-DYNA was used to determine the impact characteristics of toroidal LPG tanks. Impact by a cylindrical projectile was assumed. A theory developed by other researchers was employed to compare with the numerical results.

In Chapter 6, conclusions for the three chapters, 3, 4 and 5 are drawn. Discussions and comments on the results are also included.

Chapter 2: Literature review

2.1 Introduction

The use of toroidal shells and curved pipes in industrial applications is extending every year. Well known applications include piping systems for power stations, storage tanks for rockets, and protective devices for nuclear fuel cells. In the road transport industry the use of conventional fuels has led to serious environmental problems. An encouraging recent development has been the introduction of liquid petroleum gas (LPG) as a fuel source in motor cars. LPG is a versatile, multi-purpose fuel that is highly portable, clean burning and non-toxic, offering a viable alternative to conventional fuels. Thus, in recent years one of the newer applications of toroidal shells is for LPG storage tanks in motor vehicles. The toroidal LPG tanks are made of thick steel and are generally of non-circular cross-section. These tanks usually are designed to take the place of the spare wheels, and can be mounted vertically or horizontally in the trunks of vehicles.

Based on the applications mentioned above, a number of theories and methods have been developed for solving toroidal shell problems in statics and dynamics. However, no prior study on toroidal LPG tanks has been carried out. In this chapter, a review is presented here of the research work related to toroidal shell structures.

2.2 Stress and vibration analysis of toroidal shells

Toroidal shells have been widely studied in the past half-century. Among the mechanical properties for toroidal shells, the static behavior under internal pressure and the vibration characteristic are of great interest to researchers and engineers.

Sutcliffe (1971) conducted research on the stress analysis of toroidal shells of elliptical cross-section. He obtained the stress and deflection distributions in both circular and elliptical toroidal shells, loaded by internal pressure, through solving six first-order differential equations.

Yamada, et al. (1989) have analyzed the free vibration of a toroidal shell with elliptical cross-section. They established the equations of vibration of a toroidal shell based upon Love's first-approximation theory. They then expressed the equations in a matrix differential equation by using the transfer matrix method. The frequency equations were derived in terms of the elements of the transfer matrix determined by the numerical integration of the matrix equation.

Ming, Pan and Norton (2001) presented results on the free vibration of elastic circular toroidal shells. Their analysis was based upon the linear Sanders thin shell theory. They used beam functions to describe the motion along the meridional axis of a toroidal shell, and employed trigonometric functions to represent the deformation of the cross section. In the process of the analysis, they found that once the employed beam functions satisfied the end conditions, the natural frequencies and mode shapes of toroidal shells could be predicted using the proposed method with negligible error.

2.3 Buckling and collapse of toroidal shells

Engineers for a long time considered that for shells subjected to internal pressure buckling could not occur. Then in 1956, a failure of an internally pressurised torispherical head occurred at Avon, California. An intensive toroidal shell buckling study then followed. Galletly (1998) showed that this phenomenon could in fact theoretically happen.

Later Galletly (1998), and Combescure and Galletly (1999) did a series of researches on elastic and plastic buckling analysis of toroidal shells with circular and elliptical cross-sections, using two independent shell buckling programs BOSOR5 and INCA. In their researches, a number of parameters were studied. They were *C/b*, *b/t* and *k* (*C* is the bend radius of the toroidal shells, *a* and *b* are the semi-major and semi-minor axes of the ellipse, *t* is the thickness of the shell, *k=a/b*). They found that the plastic internal buckling pressures were much lower than their elastic counterparts for the smaller values of *k* (<= *1.5*). The plastic internal buckling pressures of elliptic toroidal shells are, more or less, proportional to the shell thickness and *C/b* ratio for the smaller values of *k* (<=*1.5*). The internal buckling pressures decrease rapidly when k increases in elastic buckling, and the pressures are approximately proportional to the square of the wall thickness. Some brief studies on toroidal shells of oblate (*k<1.0*) elliptical cross-section were also carried out in their researches. These showed that internal pressure buckling could also occur. Their researches have provided many valuable results for the study of the buckling of toroidal shells subjected to internal pressures. Their data are used in this study to compare with the results obtained using ADINA.

Blachut and Jaiswal (2000) developed an appropriate equation for the identification of configurations for which either bifurcation or collapse governs the stability of elliptical and circular toroidal shells under external pressure. The arc length method is used to determine the magnitudes of the collapse pressures. A study of imperfection sensitivities of elastic and elastic-plastic buckling load to initial, localized and global shape deviation is also presented in their paper. As well, they studied the influence of the boundary conditions and a series of geometrical parameters on the buckling pressures. The results indicate that the lowest

buckling load is obtained while either the inner or the outer equator is constrained. The number of points of the discrete constraints does not influence the magnitude of buckling pressure. Elliptical toroidal shells are sensitive to initial geometrical shape deviations. For a given set of boundary conditions, failure by collapse or bifurcation depends on the magnitude of the yield point of material and on the (C/r_c) ratio. When the C/r_c ratio is small enough, the toroidal shell fails by collapse. Sensitivity of the buckling pressure to the (a/b) ratio has also been examined. The buckling strength of closed toroidal with either prolate or oblate elliptical cross-section is much higher than the buckling load of a similar toroidal with circular cross-section.

Redekop (2005) presented results for buckling pressures of orthotropic thin shells with circular cross-sections under normal pressure, by using the differential quadrature method (DQM). The Sanders-Budiansky theory was employed. In the research, results obtained by DQM have good agreement with previous work and FEM results. The results of the buckling analysis of 10 orthotropic models indicate that the modulus ratio E_1/E_2 has great influence on the buckling pressure, while the boundary conditions shows less effect. The buckling pressure decreases with the increment of C/r_c ratio (C is the bend radius, and r_c is the radius of the circular cross-section).

2.4 Impact of toroidal shells

The impact behavior of a shell strongly depends on the external loading intensity. Under a sufficiently low impact velocity, the shell executes elastic vibrations and does not experience any permanent deformation, the energy being dissipated through structural damping or by mechanical transfer to the supports. Under medium impact velocity, the

plastic regime is reached and permanent deformation of the shell results. With a further increase of impact velocity, the shell is perforated (Zhong and Ruiz, 1990).

In a plate impact problem, because the thickness and width of the plate are much smaller than its length, the deformation characteristic that is of the greatest interest is the central deflection. Hence, only one parameter, the central deflection, is needed to describe the plate impact problem. For a spherical shell impact problem, the geometry becomes more complicated. Beside the central deflection, the meridional extension of the deflected shape (dimple) has to be considered. Therefore, the central polar deflection and meridional extension of the dimple are the two necessary parameters of the spherical shell impact problem. Models for the deformations of a spherical shell in an impact problem are of two types: non-axisymmetric deformation and axisymmetric deformation (Fig. 2.1).

Studies on the non-axisymmetric deformation were made by many authors. Based on experimental observations, Zhong and Ruiz (1990) established a simple plastic damage model, which was described as a truncated normal prismoid. It served to predict the permanent deformation of a spherical shell subjected to concentrate missile impact with high velocity (up to 120 *m/s*). The theory was non-axisymmetric, and made use of an energy balance. Some factors, like strain-rate, strain-hardening, etc. were neglected in model. Their model can provide a prediction of the damage of thin-walled spherical shells within 80% of the experimental results. However, this method does not apply within the range of very small deformations, when the central displacement is of the order of the shell thickness. The study also indicates that for a spherical shell loaded by a solid cylindrical indenter, there is a minimum mass for the indenter below which no buckling occurs, and the solution resembles that for a point load. Therefore, for simplicity, i.e. avoiding buckling, researchers often limit

the radius of projectiles in a certain range, which is larger than the thickness of the shell, and smaller than the radius of the shell.

Gupta and Venkatesh (2004) conducted numerous experiments on aluminum hemispherical shells, of radius to mean thickness ratio values between 13 and 85, impacted by a gravity drop hammer. Many typical deformed profiles of spherical shells, including axisymmetric and non-axisymmetric deformations, were obtained in their experiments, and numerical analysis was also done by using the FEM program FORGE2. In the experiments, it is observed that three stages of the deformation occur, viz small-displacement elastic, formation of axisymmetric inward dimple, and developing of non-axisymmetric integral number of lobes. Initially for a small depth of the inward dimple, perfectly axisymmetric geometry in combination with axisymmetric shell end conditions results in axisymmetric dimple formation. However, as the deformation progresses, a release of in-plane boundary conditions makes the boundary condition non-axisymmetric, and hence the transition to a non-axisymmetric deformations. This deformation pattern is of interest, as it has applicability to doubly curved shells in general.

Several theoretical and experimental studies were carried out based on the assumption of axisymmetric deflection of spherical shells. Applying Pogorelov's theory, Ning et al. (1999, 2006) assumed that a spherical shell impacted by a projectile forms a mirror-like reflection (dimple), and the deformation of the spherical shell could be separated into three regions (mirror-reflected zone, ridge zone, and outer zone). The Perzyna-Symonds constitutive equations were used to describe the four-parameter constitutive equations of the spherical shell. An axisymmetric displacement mode of the spherical shell, which contained a time factor, was assumed in their work. The result of the central deflection from their

theoretical model gives predictions within about 60%-88% of the experimental results, and the radius of dimple is within 77%-90% of the experimental data.

Witmer et al. (1963) found their axisymmetric theoretical equations had a large discrepancy compared with the experimental data. In their experiments, the patterns of the deformation of spherical shells were not axisymmetrical. The discrepancy indicated that their axisymmetric theory was not valid for the cases of the non-axisymmetric deformation.

Wen and Jones (1996) assumed that if a structure has a load-deflection characteristic similar to that of another structure, under the same type of loading or equivalent loading, then these two structures may be viewed as equivalent to each other in terms of their response. With this assumption, they modified their theoretical solution for a circular plate to obtain solutions for spherical and cylindrical shells. They obtained reasonable agreement with experimental data.

Chapter 3: Vibration analysis

3.1 Introduction

Toroidal shells have been applied to space structures, fusion reactors, fuel tanks, etc.. Nowadays, with the development of environmentally friendly vehicles, liquefied petroleum gas (LPG) is being used extensively. Thus the toroidal shell structure has been used in the storage tanks of motor vehicles. In practice, the vibration analysis is an important part of the design process for such tanks. Analytical solutions are useful either in the form of a primary solution or as a means of supplementing results determined using the finite element method (FEM).

Most previous work on toroidal shells or tanks has been carried out for circular or elliptical cross-sections, and only a few studies on toroidal shells with non-circular/elliptical cross-section could be found. Galletly and Blachut (1995) carried out a buckling analysis of toroidal shells with some part-cylindrical, part-spherical cross-sections. Stress and vibration analysis of toroidal shells of elliptical cross-section were conducted, respectively, by Sutcliffe (1971) and by Yamada et al. (1981). Further work on vibration of toroidal shells, of various cross-sections, has been done by Wang and Redekop (2005), and Xu and Redekop (2006).

This chapter describes a vibration analysis of a toroidal LPG tank with non-circular cross-section (Fig. 3.1), under several different support conditions. The analysis provides vibration data for a practical toroidal LPG tank, and indicates some of its important mechanical characteristics. The analysis was carried out using the FEM. Validation of the procedure was by comparison of results with problems cited in the literature for toroidal tanks of circular or elliptical cross-section. Two validation problems were considered, for

static stress conditions, and for free vibration. A parametric study was then conducted of a typical toroidal LPG tank, designed for vertical or horizontal installation in an automotive application. The influence on the natural frequency of the shell size, wall thickness, material properties, and support conditions was determined. Natural frequency values were tabulated, and mode shapes were plotted. A supplemental study, making use of a differential quadrature method (DQM) solution, indicates the effect on the frequencies of varying the position of a single circumferential line of support. An attempt was made to develop a special DQM program for the vibration problem of a squarish toroidal tank. However, this DQM program did not give satisfactory results, in comparison with the data obtain from FEM simulation and experiments.

3.2 Finite element method (FEM)

3.2.1 FEM software ADINA

The commercial FEM software ADINA 8.2 was used in this chapter to obtain the natural frequencies and mode shapes for toroidal LPG tanks.

In ADINA, the basic equation solved in the stress analysis of the validation is:

$$K \cdot \mathbf{U} = \mathbf{F} \tag{3.1}$$

where K is the stiffness matrix, $\mathbf{U}$ is the displacement vector, and $\mathbf{F}$ is the load vector. For the vibration problem the equation solved is:

$$K \cdot \phi_i = \omega_i^2 \cdot M \cdot \phi_i \tag{3.2}$$

where K and M are the system stiffness and mass matrices corresponding to the time of solution start, ϕ_i and ω_i are respectively the angular frequencies and mode shapes for mode i. Additionally, for a pre-stress vibration problem, the analysis is performed in two runs. In

the first run, the preload is applied in a static analysis. In the second run, the analysis is restarted from the last solution of the first run, and then a frequency analysis is performed. Instructions for use of the ADINA software for vibration analysis are given in Appendix I.1.

3.2.2 Shell element in ADINA

A 4-node 24 degree-of-freedom shell element was used to mesh for the toroidal LPG tanks in the entire stress and vibration study. Also, an 8-node 48 degree-of-freedom shell element was used in the validation section for checking the convergence of the finite element model. Both 4-node and 8-node shell elements available in ADINA, were used, with a small displacement/small strain formulation. In ADINA, shell elements follow the Mindlin plate theory. This theory accounts for rotations due to shear. The elements also follow the two basic assumptions of shell theory (ADINA Theory and Modeling Guide, 2004):

(1) Material particles that originally lie on a straight line "normal" to the mid-surface of the structure remain on that straight line during the deformations.

(2) The stress in the direction normal to the mid-surface of the structure is zero.

The most effective element for analysis of general shells is the 4-node shell element, because this element does not lock and has a high predictive capability (ADINA User Interface Primer, 2004).

3.2.3 Finite element model for toroidal LPG tanks

The finite element model of a toroidal LPG tank is built using ADINA. The model is simplified relative to a commercial product by removing the nozzle on the tank. A view of

the simplified model is given in Fig. 3.1. For the analysis, the detailed geometrical data of the LPG tank was not available in tabulated form, and thus the geometric dimensions of the model were obtained by measurements. Hence the results may not be entirely exact, but it is contended that the influence of the various parameters on the properties of the tanks can still be observed.

In the validation and parametric studies of the vibration analysis, the material of the model is defined as homogeneous and isotropic. The detailed information about the material is given in the section 3.4.

The boundary conditions are determined by the work environment and the installation requirements. Different boundary conditions of the LPG tank are considered according to the different installation modes. In the parametric study, the effects of various boundary conditions on the vibration properties of a toroidal LPG tank are considered.

3.3 Differential quadrature method

The DQM is a numerical technique for analyzing problems in engineering (Shu, 2000). It was first developed by Bellman and his associates in the early 1970s. The basis of the DQM is to approximate the derivative of a function by a linear weighted sum of all the functional values at all mesh points along a coordinate direction. A key procedure is to determine a-priori the weighting coefficients for the discretization of a derivative of any order. With the effort of many researchers, the improvement of the computation of the weighting coefficients has made the DQM a powerful tool for numerical analysis.

In the DQM, for determining the weighting coefficients, the distribution of grid points has to be first specified. By writing a Fourier series in the circumferential direction, the

vibration problem of a toroidal shell can be reduced to one mathematical dimension. The variable in the differential equations is the meridional angle Φ (Fig. 3.2). Hence, one needs only to select sampling points along an arbitrary meridional line. Then the derivatives of a function can be replaced by a linear weighted sum that consists of the product of displacements at the sampling points and weighting coefficients. The weighting coefficients are computed by choosing a set of test or trial functions. Replacing the derivatives in the governing differential equations with the weighted sum, transformed DQM vibration equations are obtained. In the DQM theory, the vibration equations are expressed in terms of the Lamé parameters, curvatures, and their derivatives.

In this chapter, to provide a second means of validating the FEM results, the DQM approach is used. An existing DQM program (Wang and Redekop, 2005) was modified to analyze the linear vibration of toroidal LPG tanks of isotropic material. The modified DQM program produced valid results in the free vibration analysis of the toroidal shells with circular and elliptical cross-sections. However, when the modified DQM approach was applied to a toroidal shell with a squarish cross-section, large differences arose in comparison with the FEM results. Owing to these differences, the theory developed is placed in the appendix section of this study.

In Appendix II, details of the equations of the Lamé parameters, curvatures and their derivatives for two squarish toroidal shells are presented. Figures in that appendix indicate that the toroidal shell with a squarish cross-section has some discontinuity in the derivatives of the Lamé parameters and curvatures. This kind of discontinuity does not arise in the cases of the circular and elliptical cross-sections. Therefore the discontinuity may be the cause for the discrepancies in the results.

As indicated in Appendix II, two separate systems for describing the geometry of the toroidal shells with squarish cross-sections (Figs. II.3.1 and II.4.1) were used. The distribution of the DQM sampling points varied, and the natural frequencies obtained based on these two systems differed considerably. The second system which provides the sampling points with much more even spacing gave better results than the first one. Although the results based on the second system are closer to the results of FEM simulation, large errors still exist.

3.4 Results of validation study

3.4.1 Stress analysis

Two studies, related to stress analysis and vibration analysis, were carried out to validate the FEM modeling and method of solution. The stress analysis was for a toroidal shell of circular cross-section, previously considered by Sutcliffe (1971). The geometry, material, and loading was defined by:

$$C=9\ in;\ r_c=6\ in;\ t=0.3\ in;\ E=30x10^6\ lb/in^2;\ \mu=0.3;\ p=E*10^4 \qquad (3.1)$$

where C is the bend radius, r_c is radius of the circular cross-section, t is the wall thickness (Fig. 3.2), E is the Young's modulus, μ is the Poisson's ratio, and p is the internal pressure. The model was built using ADINA, and only 1/8 of a toroidal shell is considered (Fig. 3.3), because the structure of the toroidal shell is symmetric and it is convenient using ADINA to apply the boundary conditions on the coordinate planes bordering the structure.

The convergence of the FEM results for the radial displacement and bending stress are indicated in Table 3.1. In the values given for the mesh density the first and second numbers indicate respectively the elements in the meridional and circumferential directions.

Convergence is clearly indicated, for both the displacement and stress. Results for the radial displacement and bending stress are given in Table 3.2 for various values of Φ, where Φ is the angle measured clockwise from the upper crown of the cross-section. The FEM values for both the radial displacement and the bending stress show close agreement with the values of Sutcliffe (1971). In the comparison of the values of the radial displacement, only the result for Φ of -90° has a comparatively large difference. For the other values of Φ, the errors of the comparison of the radial displacements are less than 0.5%. In the comparison of the values of the bending stress, most of the errors are less than 7%.

3.4.2 Free vibration analysis

For the validation of the vibration solution, comparison was made with results given by Yamada et al. (1989) for a toroidal shell with an elliptical cross-section. The geometry and material was defined by:

$$b/a=2.0;\ C/r_c=2.5;\ t/r_c=0.01;\ E=0.207x10^{12}\ Pa,\ \mu=0.3,\ \rho=7800\ kg/m^3 \qquad (3.2)$$

where a and b are the semi-minor and semi-major axes of the ellipse, and ρ is the mass density. Results for the vibration study are given in Table 3.3. The frequency parameter λ, used in Yamada et al. (1989), is defined as $\lambda = \rho a_o^2 \omega^2 (1-\mu^2)/E$. Three sets of results are given for the FEM, covering meshes of size 30x90, 60x180, and 120x360 (Fig. 3.4). It is seen that there is convergence of the FEM results (Table 3.3), as well as good agreement with the values of Yamada et al. (1989). The maximum error in the comparison of FEM results for the frequency parameter λ for the first six modes with results from Yamada et al. (1989) is 1.9%.

3.5 Results of parametric study on vibration analysis

A parametric study was made to determine the effects of several factors on the vibration characteristics of toroidal LPG tanks. The factors considered were shell size, shell thickness, material properties, shell cross-section, and type of support. It was found in a preliminary study that including internal pressure had little effect on the frequencies, and thus all the results presented herein are for un-pressurized toroidal tanks.

Three sizes of shells A, B, C (Fig. 3.5) were considered, representing the range in sizes marketed by a particular manufacturer. The outside diameter D, transverse height H and volumes V of these three tanks are given in Table 3.4. The thickness of each of the shells was taken as 8 mm, and the material properties were taken as:

$$E=0.207x10^{12}\,Pa,\ \mu=0.3,\ \rho=7800\ kg/m3 \tag{3.3}$$

The cross-section for the first and third shells (Fig. 3.5a, 3.5c) was obtained by scaling down or up the cross-section of the second shell. In Table 3.5 the first six natural frequencies are given for each shell. The results indicate that the range in fundamental frequency, from largest to smallest shell, is of the order of 43.7%.

In Table 3.6 results are presented that indicate the effect of the wall thickness on the natural frequencies. The shell size considered corresponds to tank B. Three values for thickness were considered: 6 *mm*, 8 *mm*, and 10 *mm*. In the table results are given for the first six natural frequencies (*rad/s*) for each of the shell cases. The results indicate a range in the fundamental frequency, from thinnest to thickest shell, of 16.4%. The first six mode shapes for shell B (D= 600 *mm*, H=250 *mm*, t=8 *mm*) are given in Fig. 3.6.

In Table 3.7 results are given that indicate the effect of changing the type of support for the shell. Four types of support are considered (see Fig. 3.7):

(a) Point support: constraint at six equally spaced points along the circumferential line 1,

(b) Line support 1: constraint along the entire circumferential line 1,

(c) Line support 2: constraint along the entire circumferential line 2,

(d) Surface support: constraint over the entire surface 1.

The results of the table indicate that the natural frequencies of the model increase passing from point support, to line support, and then to surface support. It is evident that positioning of the line has a considerable effect on the natural frequencies, and thus this topic is considered in greater depth in the following.

In Table 3.8 results are given that indicate the effect of the material properties, as well as the cross-sectional shape, on the natural frequencies. The shell size corresponds to tank B, and the thickness is 8mm. In column 1 of the table results are given for a shell with ovaloid cross-section and with material properties given by Eqn. (3.3). In column 2 results are given for a shell with ovaloid cross-section but with material properties defined by E=0.193x10^{12} Pa, μ=0.3, ρ=8000 kg/m^3. Lastly in column 3 results are given for a shell of circular cross-section, with the same volume as the shells of columns 1, 2, and with material properties defined by Eqn. (3.3). Comparing values for fundamental frequencies in the three cases, a maximum difference of 32.8% is observed.

In the parametric study it was indicated that the magnitude of the natural frequencies depends strongly on the type of support. To study this topic in greater detail use was made of a DQM solution for a circular toroidal shell (Wang and Redekop, 2005; Xu and Redekop, 2006). An analysis was carried out using the DQM method that gave the fundamental frequency of free vibration for different positions of a circumferential line of support.

The DQM method given by Wang and Redekop (2005) was modified to permit positioning of a circumferential line support at an arbitrary angular position θ of the cross-section. The results for a circular toroidal shell of the positioning of supports give some indication of the comparable effect on toroidal LPG tanks. The results for a shell of circular section with bend radius C=1 *m*, cross-section radius r_c=0.25 *m*, thickness t=2.5 *mm*, and material properties given by Eqn. (3.1) are shown in Fig. 3.8. The abscissa indicates the angle θ (measured counter-clockwise from the extrados) for the line of support, while the ordinate the corresponding magnitude of the fundamental frequency. It is seen that the maximum frequency of 680 *rad/s* corresponds to the θ values of about 90° and 270°. The value of the frequency corresponds to results given by Wang and Redekop (2005). The figure indicates in fact that spikes in frequency occur if the lines of support line lie in the intervals $80^\circ < \theta < 100^\circ$ and $260^\circ < \theta < 280^\circ$.

3.6 Conclusion

A vibration study was conducted of a toroidal LPG tank. Stress and frequencies computed by ADINA agree well with the results given by other researchers. Frequencies obtained by ADINA converge as the mesh is refined. The effect on the frequencies of the wall thickness, boundary conditions, tank size and material properties were found in the parametric study. It was shown that wall thickness and tank size have significant effects on the vibration characteristics of toroidal LPG tanks. The type of the support also has an important effect, while the material properties have a lesser influence. A DQM approach to the vibration problem of squarish toroidal tanks did not lead to reasonable results and the details are provided in Appendix II.

Chapter 4: Buckling and collapse analysis

4.1 Introduction

Since they serve as containers, toroidal LPG tanks must be able to safely resist specified values of pressure. Knowledge of the stability and collapse properties are of great importance for the safe use of toroidal LPG tanks. Thus, the determination of the minimum values of the buckling and collapse pressures of toroidal LPG tanks is an important step in the design of these tanks.

In this chapter, the buckling and collapse analysis of toroidal LPG tanks is considered. The theories of the buckling and collapse analysis are introduced. Both the buckling and collapse analysis of toroidal LPG tanks were carried out using the finite element method (FEM) software ADINA. Also, a parametric study was made to indicate the effect of various parameters on the buckling and collapse behavior of the LPG tanks. Details for the ADINA buckling and collapse analysis of shells are given in Appendices I.2-I.3.

4.2 Finite element method

4.2.1 Linearized buckling analysis

A buckling problem, which serves to determine the critical buckling load of a structure, is a typical eigenvalue problem. To solve a buckling problem by using the linearized buckling method in ADINA, the classical formulation is employed:

$$ {}^{T_1}K\phi_i = \gamma_t({}^{T_1}K - {}^{T_1}K_{NL})\phi_i,\ \gamma_t > 0 \qquad (4.1) $$

where ${}^{T_1}K$ is the stiffness matrix of the structural systems at time T_1, ${}^{T_1}K_{NL}$ is the geometrically nonlinear part of ${}^{T_1}K$, ϕ_i is the buckling shape for mode i, and the critical buckling load factor λ_i for mode i is related to the eigenvalue γ_i using:

$$\lambda_i = \frac{1}{1-\gamma_i} \tag{4.2}$$

The critical load factor, λ_i is multiplied by the load applied to the structure to determine the critical load. In the present work only the first buckling mode is of interest, so only λ_1 is determined (ADINA Theory and Modeling Guide, 2004).

In the linearized buckling analysis, the critical (buckling) load vector is determined from the critical load factor using:

$$\mathbf{R}_{cri} = {}^{T_0}\mathbf{R} + \lambda_i({}^{T_1}\mathbf{R} - {}^{T_0}\mathbf{R}) \text{ for mode i} \tag{4.3}$$

where ${}^{T_1}\mathbf{R}$ and ${}^{T_0}\mathbf{R}$ are the externally applied load vectors at time T_1 and T_0 (ADINA Theory and Modeling Guide, 2004).

Additionally, in the linearized buckling analysis, ADINA will run automatically in two steps; the first step is static analysis, and then the second step is mode analysis. The value of the prescribed load (internal pressure for LPG tanks) must be set, then the buckling load factor is obtained. The factor is multiplied with the prescribed load, and the product will be the critical buckling pressure. However, if the prescribed load is chosen either too high or too low relative to the real buckling load, the result calculated by the linearized buckling modulus will not be accurate. Hence, choosing an appropriate load level is very important.

4.2.2 Collapse analysis

Collapse analysis is a nonlinear static analysis (in this study, the nonlinearity comes

from the nonlinear material property and large displacements). To determine the plastic collapse pressure a number of methods based on the pressure–strain graph can be applied. The plastic collapse pressure is the maximum pressure a structure made of perfectly plastic material can sustain. The collapse pressure has been reached, when the material can no longer restrain large displacements.

In ADINA, the method of load-displacement incrementation with full Newton iterations without line search is used to determine the minimum collapse pressure of toroidal LPG tanks. The following algorithm hence is used when equilibrium iteration is performed:

$$ {}^{T+\Delta T}K^{(i-1)} \cdot \Delta \mathbf{U}^{(i)} = {}^{T+\Delta T}\mathbf{R} - {}^{T+\Delta T}\mathbf{F}^{(i-1)} \tag{4.4} $$

$$ {}^{T+\Delta T}\mathbf{U}^{(i)} = {}^{T+\Delta T}\mathbf{U}^{(i-1)} + \Delta \mathbf{U}^{(i)} \tag{4.5} $$

where ${}^{T+\Delta T}K^{(i-1)}$ is the tangent stiffness matrix base on solution calculated at the end of iteration (i-1) at time $T+\Delta T$; ${}^{T+\Delta T}\mathbf{R}$ is the externally applied load vector at time $T+\Delta T$; ${}^{T+\Delta T}\mathbf{F}^{(i-1)}$ is the consistent nodal force vector corresponding to the element stresses due to the displacement vector ${}^{T+\Delta T}\mathrm{U}^{(i-1)}$; $\Delta \mathrm{U}^{(i)}$ is the incremental displacement vector in iteration (i).

In this chapter, the material behavior is modeled by a bilinear stress-strain relationship with isotropic hardening. The maximum stress failure criterion is used to determine, during the analysis, whether the material has failed. A collapse analysis of a structure requires an incremental load analysis. The stiffness matrix of the elements is reformed at each load step and in each iteration. It is necessary to specify the time functions for the variation of the applied load (the internal pressure). A pressure range has to be estimated first, within the range of which the collapse pressure of the model could be expected. Small load steps are used near the collapse pressure. Once a section of the model reaches yielded, the analysis stops, and then the collapse pressure can be found.

4.2.3 Finite element model description

The models considered herein are simplified relative to commercial products, as nozzle, brackets etc. are not considered. The cross-sections of the toroidal LPG tanks (tanks A, B, C) are given in Fig. 3.5. The models are assumed to have uniform thickness. The analysis is carried out using a 4-node 24-degree-of-freedom shell element, although an 8-node element is also used in the validation study. Shell elements in ADINA can be used with a small displacement/small strain, large displacement/small strain, or large displacement/large strain formulation. It was found that the 4-node element is the most effective element for analysis of general shells. This element does not lock and has a high predictive capability and hence can be used for effective analysis of thin and thick shells (ADINA Theory and Modeling Guide, 2004). The speed of calculation with 4-node elements was also found much faster than with 8-node elements. The 4-node element thus is used in the buckling and collapse analysis.

Different boundary conditions are applied to the tank due to different installation requirements for LPG tanks used in vehicles. Typical boundary conditions are applied at the outer, at the inner or at the both of the equators of the tanks simultaneously. The influence of various types of boundary conditions on the toroidal LPG tanks is indicated in section 4.4.

4.3 Results of validation study

The buckling of toroidal shells with circular and elliptical cross-sections has been investigated by several researchers. Combescure and Galletly (1999) dealt with the effect of certain geometrical ratios on the buckling loads of several toroidal shells with elliptical cross-section. They used the finite difference code BOSOR5. For validation study purpose,

four of the shell cases of Combescure and Galletly (1999) are chosen. The four complete toroidal shells of elliptical cross-section were modeled in ADINA.

To determine an appropriate mesh density for obtaining stable and reliable results from ADINA, a convergence study is carried out. The study first involves 4-node-elements. Three mesh sizes 20x120, 30x180, and 40x240 are considered. The first number in each case indicates the number of elements in the meridional direction, and the second the number in the circumferential direction. The number of the elements in the three meshes is 4800, 10800, and 19200. Results are given in Table 4.1. In this table, a and b are the semi-minor and semi-major axes of the elliptical cross-section of a toroidal shell, C is the bend radius of the toroidal shell, and t is the thickness of the shell. For all four geometric cases the ratio C/b was 4.0. The comparison of the results obtained by ADINA and BOSOR5 indicates good agreement in the buckling pressures. The largest error of the results obtained by ADINA and BOSOR5 is 4.59%.

The study next involves 8-node elements (Table 4.1). For the mesh density of 30x180 (10800 elements) new results are determined by using 8-node elements. As expected, the 8-node elements with 48 degree-of-freedom (6 degree-of-freedom per node) provide faster convergence (Table 4.1). However, determining the buckling loads with 8-node elements is costly, requiring a longer computer time and a larger memory. For the intermediate size mesh density 30x180, the analysis with 8-node elements using a PC with 2.4 GHz CPU, 768MB memory requires about 1 hour. Thus in the remainder of the study 4-node elements are used.

4.4 Results of parametric study

The main purpose of this section is to determine the influence of the geometric and material parameters on the failure characteristics of the LPG tank. In the parametric study the tank size, wall thickness, boundary condition, and tank cross-section are varied. Three sizes of tanks (A, B and C) are studied. The cross-sections of the three tanks are shown in Fig. 3.5. The wall thickness is taken as 1 *mm*, 3 *mm*, and 5 *mm*. Three boundary conditions (Fig. 4.1) are applied at the tank equators (fixing of displacements at the inner equator, the outer equator, or both equators).

4.4.1 Linearized buckling analysis

Linearized buckling analysis is a typical eigenvalue problem in ADINA. Through solving the system equilibrium equations, the eigenvalues of the system, which are the buckling load factors, can be obtained. For the buckling analysis of the parametric study, the toroidal LPG tanks are subjected to internal pressure, and the material is assumed to be linear elastic, with Young's modulus of E=207 *GPa*, and Poison's ratio of μ=0.3.

Results for the buckling pressures are given in Table 4.2, with the effect of size considered first. The dimensions of the three sizes of the tanks are given in the Table 3.4. It is observed that the medium-sized tank B has the largest buckling pressure. Further results are given in the table which indicate the effect of varying the thickness in tank B. It is noted that increasing the thickness from 1 *mm* to 5 *mm*, leads to an increase in the buckling pressure by a factor of about 21.1, i.e. a nonlinear dependence on the thickness. The final results of the table indicate the influence of the boundary conditions. The results apply directly to tank B, for which a thickness of 3 *mm* is assumed. Three types of boundary

conditions are considered, corresponding to the positioning of a circumferential line of support at the inner or outer equators, or simultaneously at both equators. From the results it is seen that boundary conditions do not have a large influence on the buckling pressure of tank B. This conclusion agrees with that observed in earlier studies about the effect of the pre-buckling boundary conditions applied at toroidal tanks by Blachut and Jaiswal (2000).

The buckling mode shape of each tank is given in Figs. 4.2 - 4.4. It is observed that, for tank A, the buckling deformations occur at the top and at the bottom of the cross-section (Fig. 4.2). For tanks B and C, the shapes of their buckling modes are similar (Figs. 4.3 and 4.4); local 'spike' deformations occurred close to the top or bottom of their cross-section, i.e. the tanks have localized buckling close to the top or bottom of their cross-sections. It is clear that the elements located near the top or the bottom are compressed when the toroidal LPG tanks are subjected to internal pressures. Comparing the profiles of the cross-sections (Fig. 3.5) of tanks B and C with tank A, it is observed that the profiles of the cross-sections of tanks B and C are not entirely smooth, i.e. there are some turning points or imperfection at the geometry of the tanks. These imperfections may be the places where the buckling phenomenon arises.

Overall, the results of the buckling study given in Table 4.2 indicate that the wall thickness is the most important factor; boundary conditions do not play an important role. The results of the present work are approximations, as mathematical descriptions of the cross-sectional profiles for the various tanks were not available.

4.4.2 Collapse analysis

Nonlinear collapse analysis is considered in this section. In ADINA, a small strain, large displacement static formulation with elastic-plastic material property was used. For the material the Young's modulus is taken as $E = 207\ GPa$, the Poisson's ratio as $\mu = 0.3$, the yield point σ_{yp} of the material of the tank is 250 MPa, and the strain hardening modulus is 0. In the parametric study, the effect of the tank size, wall thickness, boundary conditions, and tank cross-section on the collapse pressure was determined. Additionally, two tanks which have similar volume to tank B, but with circular and elliptical cross-sections are analyzed.

Results from the parametric study on plastic collapse are given in Table 4.3. As expected, the collapse pressures decrease with the increment of the size of the tank, while the wall thickness is kept constant. The mode shapes for the deformed tanks are given in Figs. 4.5-4.8. Because the cross-section of tank A is different from the cross-sections of tanks B and C, the deformation of tank A is not similar to tanks B and C. Tank A has large deformations at the inner equator and relatively small deformations at the top and at the bottom (see Figs. 4.5 and 4.6), while tanks B and C have deformations mainly at the top and bottom (see Figs. 4.7 and 4.8). Comparing the cross-sections of the three tanks, it is noted that the profiles of tanks B and C are not very smooth at the top and at the bottom, and tank A does not have an entirely smooth profile at the inner equator. Thus the curvature of toroidal LPG tanks has a minor influence on the locations where the collapse deformations occur.

In the thickness study case, the collapse pressure of the LPG tank showed strong dependence on the wall thickness. Collapse pressures of the toroidal LPG tanks are approximately proportional to the thickness of the shells (see Table 4.3). The boundary

conditions do not have a significant effect on the collapse pressure (see Table 4.3). The collapse pressures of the tank under three types of boundary conditions are almost the same in the study. Figs. 4.9-4.11 show the deformed shape of the tank with different boundary conditions.

To further determine the effect of the shape of the cross-section, two tanks having a volume equal to that of tank B (Fig. 3.5b), but with circular or elliptical cross-sections (Figs. 4.12 and 4.13), were analyzed. The results, given in Table 4.3, indicate that the tank with an elliptical cross-section has a higher collapse capacity than the circular one, and the toroidal LPG tank. Thus a clear advantage for the elliptical shape is indicated.

Comparing the buckling pressures of Table 4.2 with the collapse pressures of Table 4.3, it is clear that the buckling pressures of LPG tanks are much higher than the collapse pressures. Thus, it is unlikely that LPG tanks subjected to internal pressure loading will fail by buckling. Large plastic deformations would occur prior to buckling, i.e. collapse governs the failure of practical toroidal LPG tanks.

4.5 Conclusion

The numerical solutions of the parametric study indicate that the wall thickness has the greatest influence on the buckling pressure of a toroidal LPG tank. The boundary conditions do not appear to significantly influence the buckling pressure. According to the investigation done by Blachut and Jaiswal (2000) of the toroidal shells with circular and elliptical cross-sections, failure by collapse or bifurcation depends on the magnitude of the yield point of material and on the (C/r_c) ratio. In this case, the material property in the buckling analysis

was assumed elastic; the approximated (C/r_c) ratio of this tank is very small (about 1.5). Thus, it is reasonable to assume that collapse governs the stability of a toroidal LPG tank.

Chapter 5: Impact analysis

5.1 Introduction

The problem of the impact of a flat-nosed projectile on a metallic shell is of importance in a number of engineering applications. Considerable work on shell impact has already been carried out, dealing mainly with spherical and cylindrical shells. Theoretical and/or numerical work for spherical shells has been carried out by Stolarski (1977), Lukasiewicz and Opalinski (1987), Zhong and Ruiz (1990), Wen (1997), Ning et al. (2006), Gupta et al. (2007), among others. In some contributions simple formulas are presented that serve to predict the geometric characteristics of the deformed area of the shell, or necessary properties for the piercing of the shell. In other contributions more elaborate theories are presented, serving to predict the transient behavior of the shell after impact. Experimental results have been given in a few studies. Similar studies on cylindrical shells have been carried out by Wierzbicki and Hoo Fatt (1993), Wen and Reid (1998), among others. Concerning toroidal shells, Redekop and Muhammad (2003) provided an analysis for the response under a local time-dependent loading at the extrados. In this chapter the work on impact is extended to toroidal shells.

Dynamic behavior is a very critical characteristic of many mechanisms and structures. Toroidal LPG tanks in accident conditions may be subject to dynamic loading, including impact by flat nosed projectiles. For toroidal tanks two special types of impact can be identified, that of impact on the extrados, and that of impact on the crown. (Figs. 5.1 and 5.2).

In this chapter, the elastic-plastic nonlinear FEM is used to study the impact of flat-nosed projectiles on toroidal shells. The procedure of the current study is validated by

comparing FEM results obtained for spherical shells with previously published results. Results for toroidal LPG tanks, impacted on the extrados or crown, are then presented, and these results are compared with results for equivalent spherical or cylindrical shells. Conclusions are drawn, noting the similarity in response to impact loading of the various types of shells. Details for the LS-DYNA impact analysis of shells are given in Appendix I.4.

5.2 Impact analysis using LS-DYNA

Three softwares were used in the FEM simulations of the current study. The pre-processor was FEMB (Finite Element Model Builder), and the solver was LS-DYNA 970 (LS-DYNA 1998). This package is a general-purpose explicit FEM software that has the capability to determine the nonlinear dynamic response of three-dimensional elasto-plastic structures. The post-processor was ETA/Post-Processor, which has been designed to work more integrally with LS-DYNA and has high-end graphics capabilities. In Figs. 5.1 and 5.2 are shown some sample FEM meshes for toroidal shells. In this study the 4-node 24-degree-of-freedom shell elements of the S/R Hughes-Liu shell model were used throughout (LS-DYNA Theoretical Manual, 1998).

For the material, the plastic kinematic option was selected. Isotropic, kinematic or a combination of isotropic and kinematic hardening models with strain rate dependency and failure can be considered. In LS-DYNA, isotropic and kinematic contributions may be varied by adjusting the hardening parameter β between 0 (kinematic hardening only) and 1 (isotropic hardening only). In this study, the elastic-plastic response of toroidal LPG tanks is considered. For impact problems, the hardening parameter β is set to 0 corresponding to kinematic hardening. The strain rate is accounted for by using the Cowper-Symonds model,

which scales the yield stress by the strain-rate-dependent factor. For some models a surface to surface contact element was assigned between the projectile and shell parts, leading to only minor changes in the results.

5.3 Simplified theoretical approach for impact on shells

Because of the geometrical complexity of the toroidal LPG tanks, currently there is no single mathematical expression available to depict the cross-section. Thus a theoretical derivation for the impact analysis of toroidal LPG tanks has not been carried out. The FEM method is used to build the mathematical models and to obtain the numerical results of the impact analysis.

To provide a control on the FEM results, an approximate analysis was derived to predict the maximum deflection in a spherical shell under projectile impact (Fig. 5.3). The analysis represented a simplification of the theory developed earlier by Wen and Jones (1996) and Wen and Reid (1998). The relation between the shell reactive force F and the central deflection W_o (at the impact point) was taken as:

$$F = K_m^s W_0 + F_c^s \tag{5.1}$$

The membrane stiffness K_m^s and collapse force F_c^s for the shell are defined as:

$$K_m^s = \beta_0^{\,2} K_m, \quad F_c^s = \beta_0 F_c \tag{5.2}$$

where $\beta_0 = (\varphi_0 / 2\pi)^{\frac{1}{2}}$, angle φ_0 is the angle subtended at the center of the sphere (Fig. 5.3), and K_m and F_c are respectively the membrane stiffness and collapse load for an equivalent circular plate. These values are given by:

$$K_m = 2\pi N_0 \Big/ \ln(\frac{\alpha\varphi_0 R}{d}), \quad F_c = \frac{4\pi M_0}{\sqrt{3}}\left[1+\left(1+\frac{\sqrt{3}}{2}\right)\Big/\ln(\frac{\alpha\varphi_0 R}{d})\right] \tag{5.3}$$

The plastic capacities are given by $M_0 = \sigma_y t^2/4$, $N_0 = \sigma_y t$. In the above R is the shell radius, t is the shell thickness, d is the projectile diameter, and α is an experimental parameter. The impacting of the projectile with the shell leads to stored bending strain energy E_{bm} and shear strain energy E_s given by:

$$E_{bm} = \int_0^{W_0} (K_m^s W_0 + F_c^s) dW_0 \tag{5.4}$$

$$E_s = \int_0^{\Delta} F_s d\Delta \tag{5.5}$$

The initial kinetic energy E_k of the projectile and the stored strain energy E_{se} (bending strain energy E_{bm} and shear strain energy E_s) in the shell are given by:

$$E_k = \frac{1}{2}\cdot m \cdot v^2 \tag{5.6}$$

$$E_{se} = E_{bm} + E_s \tag{5.7}$$

where m is the mass of the projectile, v is the initial velocity of the projectile. In the current study, it was found that the shear strain energy could be neglected compared with the bending strain energy E_{bm}. Therefore, Eqn. (5.7) can be simplified as:

$$E_k = E_{bm} \tag{5.8}$$

Equating the initial kinetic energy and the strain energy, and substituting Eqns. (5.4) and (5.7) into the resulting equation, the expression for the central deflection W_0 is obtained as:

$$W_0 = \left(\sqrt{F_c^{s2} + K_m^s \cdot m \cdot v^2} - F_c^s\right)\Big/ K_m^s \tag{5.9}$$

5.4 Results of validation study

Because of the absence of experimental data on the impacting of toroidal shells, the validation for the LS-DYNA software was carried out against the results for spherical shells. Results were available from two previous studies, one by Ning et al. (2006), and the other by Zhong and Ruiz (1990).

The study by Ning et al. (2006) concerned the radial impacting of a part-spherical shell by a cylindrical projectile (Fig. 5.4). The radius of the spherical shell was R=0.2212 m, the horizontal radial projection R_o=0.16 m, and the wall thickness t=1 mm. The projectile had a diameter of d=0.012 m, and a mass of 0.04 kg. The material was aluminum, having a yield point of 190 MPa, a strain rate of 4500/s and a strain rate parameter of 5. Experimental and theoretical results were presented by Ning et al. (2006). It was observed that the deformed area had a dimple shape, and results for the depth and radius of the dimple were given for a number of initial velocities of the projectile.

The experimental results given by Ning et al. (2006) for the central deflection and dimple radius are given in Tables 5.1 and 5.2. These results are compared with the results obtained by Wen's theoretical approach and LS-DYNA. It is seen that the theoretical results given by Wen's theory and LS-DYNA differ from the experimental results by almost equal amounts. The average difference between Wen's theoretical results and the experimental results of the central deflection is 16.6%, while the average error between the values obtained by LS-DYNA and the experiment is 17.3%. In the comparison for the dimple radius, the maximum error between the results given by Wen's theory and Ning et al. (2006) is 9.2%, and for the results obtained by LS-DYNA, the maximum error is 9.8%. Thus, generally close agreement between Wen's results and LS-DYNA are observed.

In Table 5.3, a comparison of the results for the central deflection of aluminum shells by Zhong and Ruiz (2003) with the current LS-DYNA results and Wen's theoretical results is given. Results were available for 8 models, representing different projectile mass and velocity, and shell thickness. It is noted that there is again close agreement between the LS-DYNA and other results.

For further validation of the reliability and stability of the calculations of LS-DYNA, a comparison between results given by Wen's theory and LS-DYNA were made for additional models. The material was again aluminum, but a different value of the radius of the spherical shell was considered. The projectile radius and diameter were 10 *mm*, and 20 *mm* respectively, and the mass was 490 *gm*. For the shell, the radius of the spherical shell was R=0.314 *m*, the projection Ro=0.314 *m*, and the wall thickness t=1 *mm*. The Young's modulus of the material was 68.9 *GPa*, while the yield stress 268 *MPa*. The results presented in Table 5.4 indicate a close agreement between the Wen's theory and LS-DYNA for this aluminum shell.

However, for steel shells, results obtained from Wen's theory did not agree well with the LS-DYNA results, and thus further models were analyzed to indicate qualitatively the accuracy of the FEM procedure. Results for the central deflection were found using LS-DYNA for spherical and cylindrical shells made of aluminum and steel. Projectiles of several mass values were considered. The results given in Table 5.5 indicate a reasonable qualitative trend relative to the experimental results of Ning et al. (2006).

5.5 Impact of projectile on extrados of toroidal shells

A parametric study was carried out to determine the effect of the LPG tank size and cross-section on the response characteristics of the impacted shells. Results were found for

the three tanks A, B and C, whose dimensions and cross-sections are given in Table 5.6 and Fig. 4.1. Also the radii of equivalent circular toroidal, cylindrical, and spherical shells (equal volume shells) are included in Table 5.6. The wall thickness was generally taken as 5 *mm*, but in the study of the effect of the wall thickness, four thicknesses ranging from 3-10 *mm* were considered. The material was assumed to be elastic-plastic, with the Young's modulus of 207 *GPa*, the Poisson's ratio of 0.3, the density of 7800 kg/m^3, the yield strength of 310 *MPa*, a hardening parameter of zero, and a tangent modulus of 763 *MPa*. The strain rate was taken as 40/*s*, the strain rate parameter as 5, and the failure strain as 0.75. The projectile was cylindrical, with a diameter of 20 *mm* and a mass of 49 *gm*.

In a preliminary analysis a check of the convergence of the solution was made. In Fig. 5.5 the convergence of the central deflection for tank B is indicated, covering mesh sizes from 1760 to 7200 elements. A check of the effect of the wall thickness on the central deflection was made for tank B. The results for central deflection, given in Fig. 5.6, indicate a very strong dependence on the wall thickness.

Results for the central deflection w_0 were computed using LS-DYNA for the three tanks A, B, C for projectile mass of 49 *gm*, and various initial velocities (see Tables 5.7-5.9). The motion of the projectile was considered parallel to the equator of the tank, and to produce impact at the extrados. Only one half of the tank was modeled, extending through a circumferential angle of 180° (Fig. 5.7), and boundaries on the vertical edges were fixed. Results were also found for equivalent circular toroidal and spherical shells. It is noted from Tables 5.7-5.9 that for each tank the three sets of results show close agreement. For tank A the LPG values are bounded by the results for the circular toroidal and the spherical shell,

while for tanks B and C the LPG values are slightly higher. Views of the impacted tanks appear in Figs. 5.7-5.9, showing in each case a dimple, similar to that in spherical shells.

5.6 Impact of projectile on crown of toroidal shell

In this section, results for the central deflection were computed by LS-DYNA for three of the shell structures of Table 5.6 (LPG tank B, circular toroidal shell, cylindrical shell). For the LPG tank and circular toroidal shell the motion of the projectile was now considered to be parallel to the axis, producing impact on the upper crown (Figs. 5.10 and 5.11). Only one half of the toroidal shell was modeled, extending through a circumferential angle of 180^{0}. A circular support line on the lower crown was now assumed. The circular toroidal shell and cylindrical shell analyzed in this section had equal volume relative to tank B.

The results for the three shells are given in Table 5.10. It is noted that the three sets of results are generally similar, with the LPG tank values generally somewhat higher than the others. The central deflections of both the toroidal shells are lower than the cylindrical shell when the impact velocity goes to 160 *m/s*. Views of the impacted LPG tank, circular toroidal shell, and cylindrical shell are shown in Figs. 5.10-5.12. Comparing the results in Tables 5.8 and 5.10, it is noted that the central deflections due to the impact at the extrados are larger than those at the crown. The difference is at least partially due to the different support conditions for the two models.

5.7 Conclusion

The results obtained from LS-DYNA for the central deflection of a shell impacted by a cylindrical projectile agree well with previously published results for the case of a spherical

shell. For toroidal geometries the results given by LS-DYNA for LPG tanks agree closely with those for equivalent spherical or cylindrical tanks.

Chapter 6: Conclusion

6.1 Vibration analysis of toroidal LPG tanks

The vibration analysis of toroidal LPG tanks using ADINA was successfully completed. In the validation study, the convergence of FEM results of the LPG tank model was quite satisfactory; the results obtained using ADINA had good agreement (maximum error is less than 7%) with previous work of other researchers. The natural frequencies and the vibration mode shapes are obtained in this study for three sizes of toroidal LPG tanks. Various shell thicknesses, boundary conditions and materials have different degree effects on the natural frequencies of the simulated model. Among those parameters, boundary conditions play the most important role. Supports on the inner-equator of a toroidal shell lead to lower natural frequencies.

6.2 Buckling and collapse analysis of toroidal LPG tanks

Wall size plays an important role in the buckling and collapse of toroidal LPG tanks subject to internal pressure as well. Thinner wall size leads to lower buckling load and collapse pressure. The buckling mode shapes for the toroidal LPG tanks subjected to internal pressure are obtained. The imperfection of toroidal LPG tanks is one factor affecting the position where buckling deformations or failure occurs. Boundary conditions do not have a significant effect on the buckling and collapse pressures for toroidal LPG shells. Buckling for a toroidal LPG tank under internal pressure is not expected, as generally collapse would occur first.

6.3 Impact analysis of toroidal LPG tanks

Wall thickness affects the impact behavior of toroidal LPG tanks the most. Results from Wen's theory and LS-DYNA had fair agreement (average error is less than 20%) against experimental data involving spherical aluminum tanks. However, large differences arose between the results obtained by Wen's theory and LS-DYNA, for steel tanks. In Wen's theory, only a few material parameters are included. Therefore, the equations of Wen's theory may have difficulties dealing with general material cases. Two special types of impact, which are the impact on the extrados and the impact on the crown, are studied. The toroidal shell shows stronger resistance to impact loadings applied on the crown than a comparable cylindrical shell.

6.4 DQM for non-smooth shells

Based on material presented in the appendix it is concluded that the DQM approach may not give satisfactory results for shells which are not smooth. For shells of revolution, the DQM approach, in its current form, gives satisfactory vibration results for circular and elliptical cross-section but not for "squarish" ones.

6.5 Suggestions for further research

The current study represents a beginning for the research on toroidal LPG tanks. Toroidal LPG tanks of non-circular cross-section can have significantly different properties from toroidal tanks with circular or elliptical cross-section.

For future study, the following research subjects could be considered:

- Appropriate geometric equations for the cross-section of the toroidal LPG tank may be an approach to improve the solutions of the DQM program for solving the vibration problem of toroidal LPG tanks.
- The simplified Wen's theory for impact may be extended to toroidal shells.
- Further parametric study could be carried out for toroidal LPG tanks with more detail (geometric imperfection, nozzle on the surface of a tank).

- Toroidal LPG tanks made of composite materials could be considered in further research.
- Propose design changes of LPG tank geometry based on the current results.
- Perform an experimental study of toroidal LPG tanks.

References

ADINA User Interface Primer, ARD-04-6, September 2004.

ADINA Theory and Modeling Guide, Volume I: ADINA, September 2004.

ADINA User's Manual, Worcester, MA, 2003.

ADINA Verification Manual, ARD2003-9, Watertown, MA, USA, 2003.

Bathe K. J., Finite Element Procedures, Prentice Hall, Upper Saddle River, New Jersey, 1995.

Blachut J., Jaiswal O.R., On the buckling of toroidal shells under external pressure, Computers and Structures, Vol. 77, 233-251, 2000.

Combescure A., Galletly G.D., Plastic buckling of complete toroidal shells of elliptical cross-section subjected to internal pressure, Thin-Walled Structures, Vol. 34, 135-146, 1999.

Corbett G.G., Reid S.R., Johnson, W., Impact loading of plates and shells by free-flying projectiles: a review, International Journal of Impact Engineering, Vol. 18, 141-230, 1996.

Dym C.L., Introduction to the Theory of Shells, Pergamon, Oxford, 1974.

Fung Y.C., Sechler E.E., Thin-Shell Structures Theory, Experiment and Design, Prentice-Hall, Inc., Englewood Cliffs, New York, 1974.

Galletly G.D., Elastic buckling of complete toroidal shells of elliptical cross-section subjected to uniform internal pressure, Thin-Walled Structures, Vol. 30, Nos. 1-4, 23-34, 1998.

Galletly G.D., Blachut J., Stability of complete circular and non-circular toroidal shells, Proceedings of the Institution of Mechanical Engineering, Part C: Journal of Mechanical Engineering Science, Vol. 209, No. 4, 245-255, 1995.

Gupta N.K., Venkatesh, Experimental and numerical studies of dynamic axial compression of thin walled spherical shells, International Journal of Impact Engineering, Vol. 30, 1225-1240, 2004.

LS-DYNA Theoretical Manual, Livermore Software Technology Corporation, May 1998.

Lukasiewicz S.A., Opalinski W., Elasto-plastic behavior of double-curved shells under a concentrated load, International Journal of Non-Linear Mechanics, Vol. 22, 391-399, 1987.

Ming R.S., Pan J., Norton M.P., Free vibrations of elastic circular toroidal shells, Applied Acoustics, Vol. 63, 513-528, 2002.

Ning J.G., Liu H.Y., Wang Y.Y., Yang G.T., Analysis of dynamic failure of plastic spherical shells under local impact, Journal of Beijing Institute of Technology, Vol. 8, No.1, 1999.

Ning J.G., Song W.D., Yang G.T., Failure analysis of plastic spherical shells impacted by a projectile, International Journal of Impact Engineering, Vol. 32, 1464-1484, 2006.

Redekop D., Vibration analysis of a torus-cylinder shell assembly, Journal of Sound and Vibration, Vol. 277, 919-930, 2004.

Redekop D., Muhammad T., Analysis of toroidal shells using the differential quadrature method, International Journal of Structural Stability and Dynamics, Vol. 3, 1-12, 2003.

Redekop D., Buckling analysis of an orthotropic thin shell of revolution using differential quadrature, International Journal of Pressure Vessels and Piping, Vol. 82, 618-624, 2005.

Shu C., Differential Quadrature and Its Application in Engineering, Springer-Verlag, London, 2000.

Sutcliffe W.J., Stress analysis of toroidal shells of elliptical cross-section, International Journal of Mechanical Science, Vol. 13, 951-958, 1971.

Soedel W., Vibration of Shells and Plates, Marcel Dekker. Inc., New York, 1981.

Sanders J.L., An improved first-approximation theory for thin shells, Langley Research Center, TR R-24, 1959.

Wang X.H., Free vibration and stability of complete orthotropic circular toroidal shells, M.A.Sc. Thesis, University of Ottawa, 2004.

Wang X.H., Redekop D., Natural frequencies and mode shapes of an orthotropic thin shell of revolution, Thin-Walled Structures, Vol. 43, 735-750, 2005.

Wen H.M., Jones N., Low-velocity perforation of punch-impact-loaded metal plates, Journal of Pressure Vessel Technology, Vol. 118, 181-187, 1996.

Wen H.M., Large plastic deformation of spherical shells under impact by blunt-ended missiles, International Journal of Pressure Vessels and Piping, Vol. 69, 147-152, 1997.

Wen H.M., Reid S.R., Deformation and perforation of cylindrical shells struck normally by blunt projectiles, International Journal of Pressure Vessels and Piping, Vol. 75, 213-219, 1998.

Wen H.M., Reid S.R. R, Deformation and perforation of spherical shells by normal impact of blunt-ended projectiles, Mechanical Structures and Machine, Vol. 26, 239-255, 1998.

Witmer E.A., Balmer H.A., Leech J.W., Pian T.H.H., Large dynamic deformations of beams, rings, plates and shells, AIAA Journal, Vol. 1, 1848-1857, 1963.

Xu B., Redekop D., Natural frequencies of an orthotropic thin toroidal shell of elliptical cross-section, Journal of Sound and Vibration, Vol. 293, 440-448, 2006.

Yamada G., Kobayashi Y., Ohta Y., Yokota S., Free vibration of a toroidal shell with elliptical cross-section, Journal of Sound and Vibration, Vol. 135, 411-425, 1989.

Zhong H.Z., Ruiz C., Assessment of damage resulting from missile impact on a spherical shell, International Journal of Impact Engineering, Vol. 9, No. 2, 223-236, 1990.

Zbigniew E.M., Roman T.N., Shells of Revolution, Elsevier, Warsaw, 1991.

Publications arising from this thesis

1. Zhan H.J., Redekop D., Vibration analysis of a toroidal LPG tank, CSME Forum 2006, Calgary, Canada, May 2006, 8 pages, published.

2. Zhan H.J., Redekop D., Buckling and collapse analysis of a toroidal LPG tank. ICAMEM 2006, Hammamet, Tunisia, Dec. 2006, 5 pages, published.

3. Zhan H.J., Redekop D., Projectile impact on a toroidal shell, ICTWS 2008, Brisbane, Australia, June 2008, submitted.

4. Zhan H.J., Redekop D., Vibration, buckling and collapse of ovaloid toroidal tanks, Thin-Walled Structures, accepted Sep. 27 2007, available on-line 26 November 2007 at www.sciencedirect.com.

Tables

Table 3.1 Convergence of FEM results for non-dimensional radial outward displacement w/r_c and bending stress $(\sigma_0 x 10^4)/E$ on the outside surface at point Φ=-9°

Mesh	Mesh density	Radial displacement w/r_c x 10^3 at point Φ=-9°	Bending stress $(\sigma_0 x 10^4)/E$ at point Φ=-9°
1	20x30	4.163	-3.963
2	40x50	4.197	-4.187
3	60x70	4.203	-4.233

Table 3.2 Comparison of FEM results for non-dimensional radial outward displacement w/r_c, and bending stress $(\sigma_0 x 10^4)/E$ on the outside surface, with value from Sutcliffe (1971)

Φ	Radial displacement w/r_c x 10^3			Bending stress $(\sigma_0 x 10^4)/E$		
	Sutcliffe	ADINA	Error (%)	Sutcliffe	ADINA	Error (%)
-90°	0.103	0.085	-17.5	0.822	0.970	18.0
-72°	0.416	0.418	0.48	0.697	0.716	2.73
-54°	1.273	1.267	-0.47	1.226	1.244	1.47
-36°	2.652	2.646	-0.23	0.567	0.792	39.7
-18°	3.998	3.990	-0.20	-3.630	-3.582	-1.32
-9°	4.207	4.197	-0.24	-4.270	-4.187	-1.94
0°	3.994	3.983	-0.28	-3.108	-3.061	-1.51
9°	3.467	3.457	-0.29	-0.999	-1.017	1.8
18°	2.819	2.812	-0.25	0.876	0.823	6.05
36°	1.785	1.783	-0.11	1.897	1.867	-1.58
54°	1.358	1.359	0.07	0.870	0.871	0.11
72°	1.262	1.265	0.24	0.171	0.162	-5.26
90°	1.251	1.250	-0.08	0.025	0.065	160

Table 3.3 Comparison of FEM results for frequency parameter λ with results from Yamada et al. (1989)

Mode	Mesh 1	Mesh 2	Mesh 3	Yamada et al. (1989)	Error (%) (Mesh 2 & Yamada et al.)
	FEM 30x90	FEM 60x180	FEM 120x360		
1	0.02371	0.02242	0.02217	0.0220	1.90
2	0.02987	0.02788	0.02751	0.0275	1.34
3	0.04187	0.03939	0.03892	0.0390	1.10
4	0.04679	0.04415	0.04364	0.0437	1.03
5	0.04938	0.04592	0.04523	0.0453	1.37
6	0.06444	0.06042	0.05959	0.0596	1.38

Table 3.4 Dimensions of the three toroidal LPG tanks

Tank	Diameter D (mm)	Height H (mm)	Volume V (l)
A	566	180	33
B	600	250	54
C	650	270	70

Table 3.5 Variation of fundamental frequency ω (rad/s) with size of tank

Mode	Natural frequency ω (rad/s)		
	Tank A	Tank B	Tank C
1	3884	2953	2185
2	5471	4577	3638
3	8898	8570	5300
4	10994	9355	7692
5	11878	10691	9179
6	12165	11160	10690

Table 3.6 Variation of natural frequency ω (rad/s) with wall thickness

Mode Number	Natural frequency ω (rad/s)		
	t =6 mm	t =8 mm	t =10 mm
1	2677	2953	3202
2	4085	4577	5025
3	7878	8570	9208
4	8056	9355	10508
5	10396	10691	10961
6	10662	11160	11480

Table 3.7 Variation of natural frequency ω (rad/s) with boundary conditions

Mode Number	Natural frequency ω (rad/s)			
	Point Contact	Line Contact 1	Line Contact 2	Surface Contact
1	2178	2953	2022	3095
2	3356	4577	3102	8887
3	5972	8570	4576	8932
4	9019	9355	5829	10297
5	9096	10691	10928	12581
6	9553	11160	11825	14277

Table 3.8 Variation of natural frequency ω with different materials

Mode Number	Natural frequency ω (*rad/s*)		
	Material-a - tank B	Material-b - tank B	Material-a - circular
1	2953	2833	4192
2	4577	4391	4964
3	8570	8222	6781
4	9355	8975	7653
5	10691	10257	9601
6	11160	10706	9630

Table 4.1 Convergence of the buckling pressure (*MPa*) for various FEM meshes for elliptical tanks, and comparison with Bosor5 values (Combescure and Galletly, 1999)

	Case 1	Case 2	Case 3	Case 4
*a/b***	1.24	2.0	1.25	2.0
b/t	50	50	100	100
20 x 120	4.57	2.63	2.35	1.31
30 x 180	4.43 4.24*	2.47 2.38*	2.10	1.17
40 x 240	4.43	2.46	2.09	1.14
BOSOR5	4.33	2.42	2.09	1.09
Error (%)	2.31	1.65	0.00	4.59

* results using 8-node elements

** *a* and *b* are the half-minor and half-major axes of the elliptical cross-section of a toroidal shell

Table 4.2 Variation of buckling loads with different parameters

Parameters	Buckling pressure (*MPa*)		
Size (t=3 *mm*)	Tank A	Tank B	Tank C
	19.29	33.29	30.30
Thickness (Tank B)	1 *mm*	3 *mm*	5 *mm*
	3.86	33.29	81.39
Boundary support (Tank B with t=3 *mm*)	Equator line support		
	Inner	Outer	Both
	33.29	33.50	33.35

Table 4.3 Parametric study for collapse analysis

Parameters	Collapse pressure (*MPa*)		
Size	Tank A	Tank B	Tank C
(t =3 *mm*)	4.51	3.26	2.65
Thickness	1*mm*	3*mm*	5*mm*
(Tank B)	0.79	3.26	6.17
Boundary support	Equator line support		
(Tank B with t=3	Inner	Outer	Bottom
mm)	3.26	3.25	3.26
Cross-sections	Circular	Elliptical	LPG
	4.23	4.88	3.26

Table 5.1 Comparison of central deflection w_0 for validation

Impact velocity	Central deflection w_0 (*mm*)			Error (%)	
(*m/s*)	Experiment	Wen	LS-DYNA	Wen	LS-DYNA
32.00	23.60	18.60	25.93	-21.2	9.9
34.75	28.80	20.80	29.11	-27.8	1.1
38.00	27.00	23.50	32.99	-13.0	22.2
43.50	35.20	28.12	39.53	-20.2	12.3
45.90	33.50	30.22	42.39	-9.9	26.5
53.40	44.00	36.70	51.79	-16.6	17.7
53.70	38.00	37.00	52.18	-2.6	37.3
55.05	45.30	38.19	53.93	-15.7	19.1
67.00	63.50	49.37	69.45	-22.2	9.37

Table 5.2 Comparison of radius of the dimple R_d for validation

Impact velocity	Radius of the dimple R_d (*mm*)			Error (%)	
(*m/s*)	Experiment	Wen	LS-DYNA	Wen	LS-DYNA
32.00	73.00	68.21	71.57	-6.6	-2.0
34.75	68.00	71.58	74.63	5.3	9.8
38.00	79.50	75.43	80.93	-5.2	1.8
43.50	89.00	81.50	86.97	-8.4	2.3
45.90	87.50	84.00	90.00	-4.0	2.9
53.40	98.00	91.37	95.72	-6.7	-2.3
53.70	92.00	91.70	98.88	-0.3	7.5
55.05	101.00	92.90	101.94	-7.9	0.9
67.00	114.00	103.5	113.05	-9.2	-0.8

Table 5.3 Comparison of results for central deflection w_0 for Zhong and Ruiz (1990) experimental models for validation

Model	Missile mass (*gm*)	Impact velocity (*m/s*)	Shell thickness (*mm*)	Deflection w_0 (*mm*)				
				Expt.	LS-DYNA	Wen	Error (%)	
							LS-DYNA	Wen
1	0.500	61.3	0.23	6.76	6.72	7.84	-0.59	16.3
2	0.509	61.6	0.22	7.62	7.12	8.19	-6.56	7.48
3	0.503	64.9	0.21	8.99	7.83	8.87	-12.9	-1.33
4	0.502	64.3	0.22	7.82	7.40	8.52	-5.37	8.95
5	0.514	66.8	0.20	8.89	8.57	9.52	-3.60	7.09
6	0.913	115	0.27	19.1	17.50	19.22	-8.38	0.63
7	0.900	118	0.28	17.6	17.30	19.27	-1.70	9.49
8	0.991	113	0.28	17.4	17.50	19.38	0.57	11.4

Table 5.4 Further comparison between LS-DYNA and Wen's theory results for a spherical aluminum shell

Velocity (*m/s*)	w_0 (*mm*)		Error (%)
	LS-DYNA	Wen's theory	
20	42.37	39.42	7.48
40	82.24	82.28	-0.05
65	137.3	135.9	1.03
72	152.1	150.9	0.80

Table 5.5 Results for central deflection w_0 in spherical and cylindrical shells of various materials

Velocity (*m/s*)	Central deflection w_0 (*mm*)				
	Sph. shell (steel) 49 *gm*	Sph. shell (steel) 490 *gm*	Ning's result (Al) 40 *gm*	Cyld. shell (steel) 49 *gm*	Cyld. shell (steel) 490 *gm*
32.0	9.62	38.1	23.6	8.09	31.9
45.9	14.2	56.5	33.5	11.6	44.0
53.7	16.5	66.5	38.0	13.3	50.4
67.0	20.9	86.9	63.5	16.6	61.0

Table 5.6 Description of toroidal LPG tanks and the equivalent shells

Tank	Diameter D (*mm*)	Height H (*mm*)	Volume V (*l*)	Radius (*mm*) of the equivalent shells		
				Circ.tor.shell	Cyld. shell	Sph. shell
A	566	180	33	96.0	94.6	281.6
B	600	250	54	104.5	118.3	313.8
C	650	270	70	117.0	130.6	338.6

Table 5.7 Effect of initial velocity on deflections w_0 at center for tank A geometry- impact at extrados

Velocity (*m/s*)	Central deflection w_0 (*mm*)		
	Circ. tor. shell	Tor. LPG tank	Spherical shell
50	0.82	0.81	1.09
60	1.05	1.22	1.47
65	1.19	1.46	1.68
72	1.41	1.75	1.99
86	1.93	2.41	2.69
90	2.10	2.62	2.92
110	3.04	3.76	4.19
160	5.89	7.13	8.85

Table 5.8 Effect of initial velocity on deflections w_0 at center for tank B geometry- impact at extrados

Velocity (*m/s*)	Central deflection w_0 (*mm*)		
	Circ. tor. shell	Tor. LPG tank	Spherical shell
50	0.97	1.13	1.09
60	1.27	1.53	1.39
65	1.47	1.76	1.55
72	1.76	2.11	1.81
86	2.43	2.90	2.43
90	2.65	3.17	2.61
110	3.87	4.62	3.74
160	7.98	8.35	7.63

Table 5.9 Effect of initial velocity on deflections w_0 at center for tank C geometry - impact at extrados

Velocity (*m/s*)	Central deflection w_0 (*mm*)		
	Circ. tor. shell	Tor. LPG tank	Spherical shell
50	0.99	1.12	1.08
60	1.29	1.53	1.43
65	1.46	1.73	1.62
72	1.72	2.04	1.89
86	2.28	2.82	2.53
90	2.46	3.08	2.72
110	3.43	4.50	4.13
160	6.49	8.36	8.27

Table 5.10 Results for the central deflection w_0 for the tank B geometry - impact at crown

Velocity (*m/s*)	Central deflection w_0 (mm)		
	Tor. LPG tank	Circ. tor. shell	Cylindrical shell
50	0.97	0.88	1.00
60	1.32	1.24	1.22
65	1.51	1.43	1.44
72	1.80	1.71	1.68
86	2.46	2.36	2.32
90	2.67	2.57	2.45
110	3.88	3.71	3.60
160	7.42	7.13	7.45

Figures

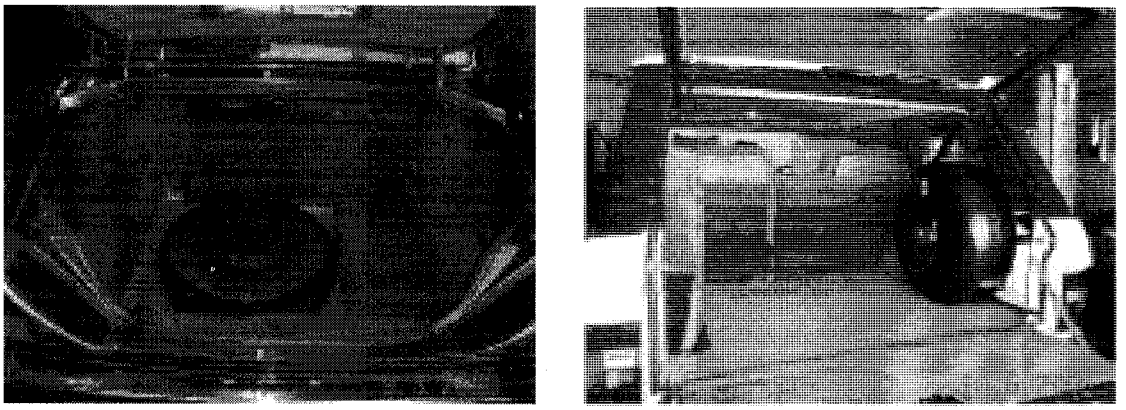

(a) (b)

Fig. 1.1 The use of toroidal LPG tanks in car trunks (a) horizontal installation (b) vertical installation

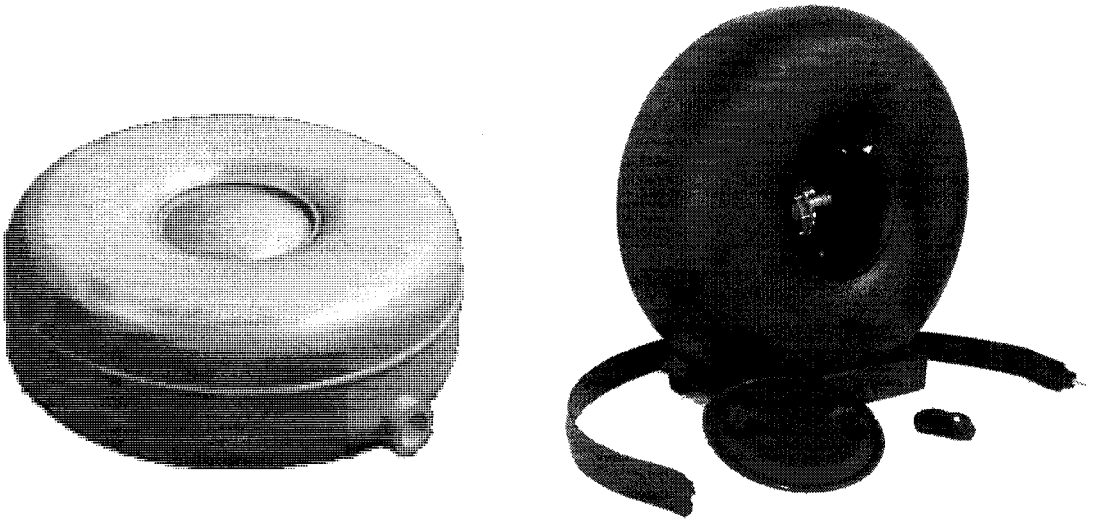

(a) (b)

Fig. 1.2 Toroidal LPG tank installation (a) horizontally (b) vertically

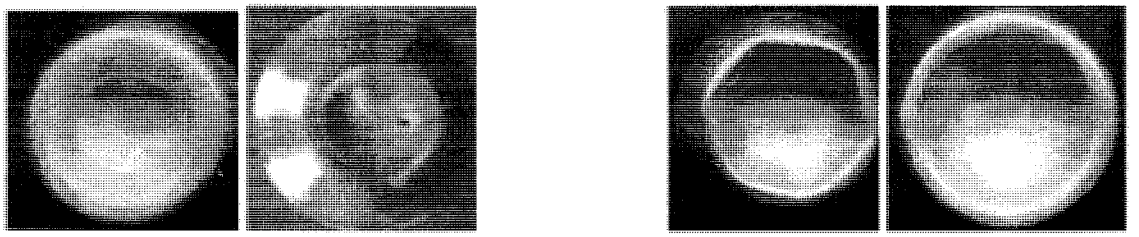

(a) (b)

Fig. 2.1 Deformed shapes for impacted spherical shells (a) axisymmetric (b) non-axisymmetric (Gupta and Venkatesh, 2004)

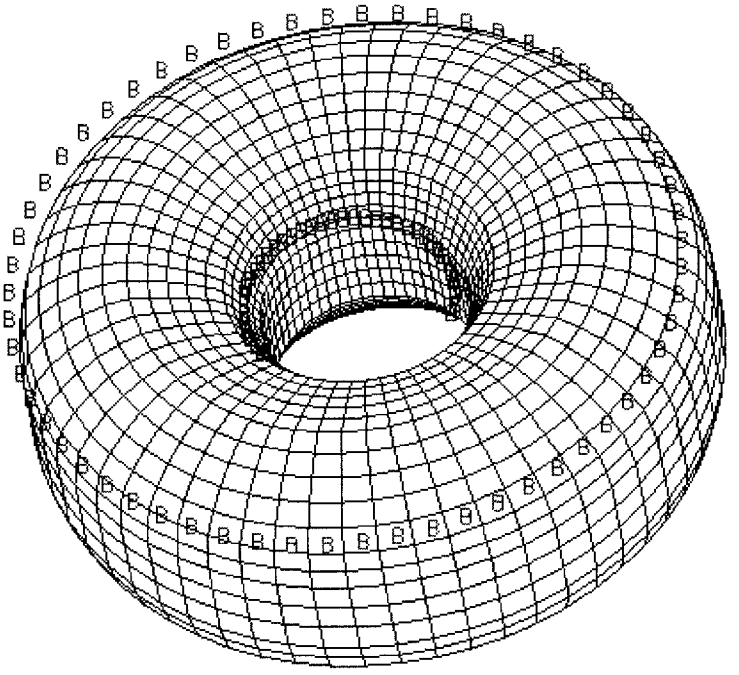

(a)

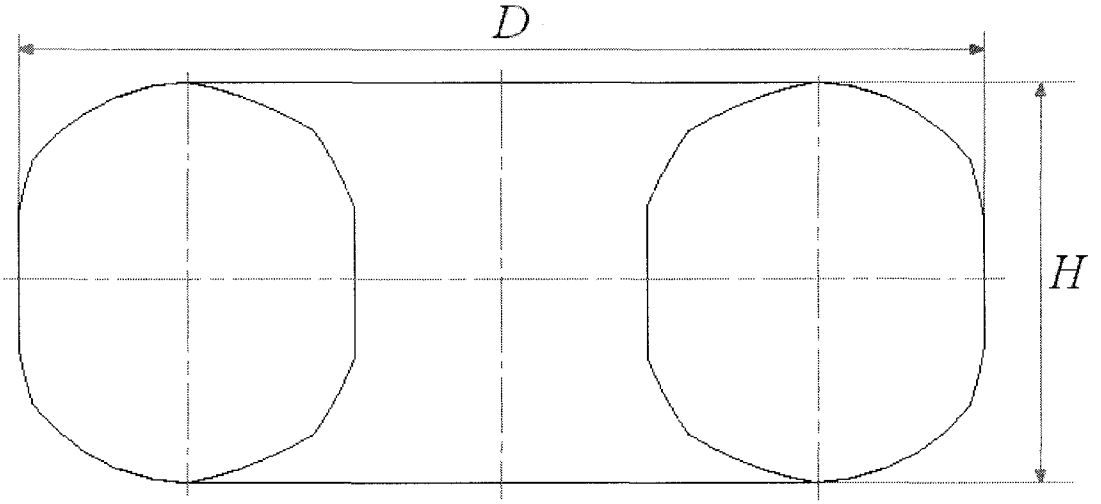

(b)

Fig. 3.1 Toroidal LPG tank, (a) finite element model, (b) cross-section

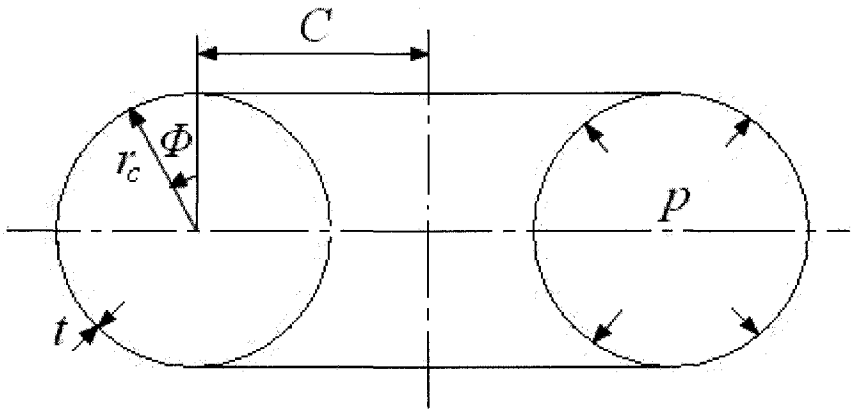

Fig. 3.2 Circular toroidal shell (section on a plane through the axis)

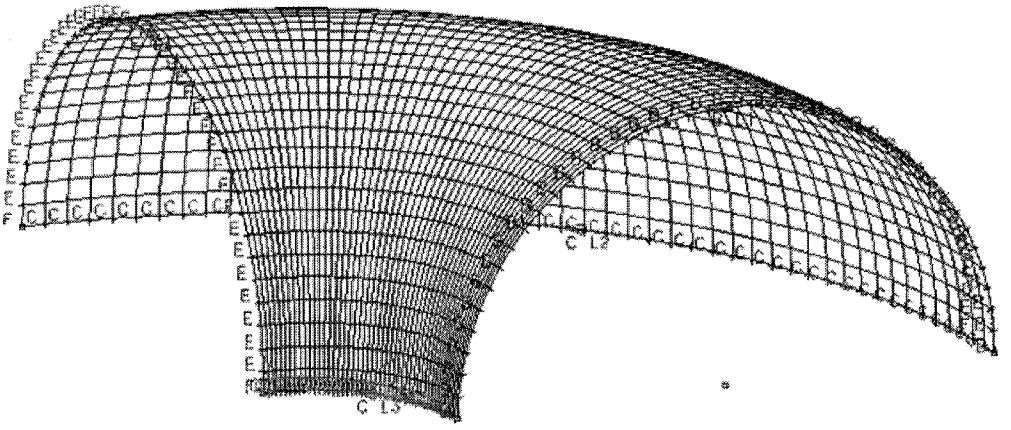

Fig. 3.3 The 1/8th finite element model in stress analysis for validation

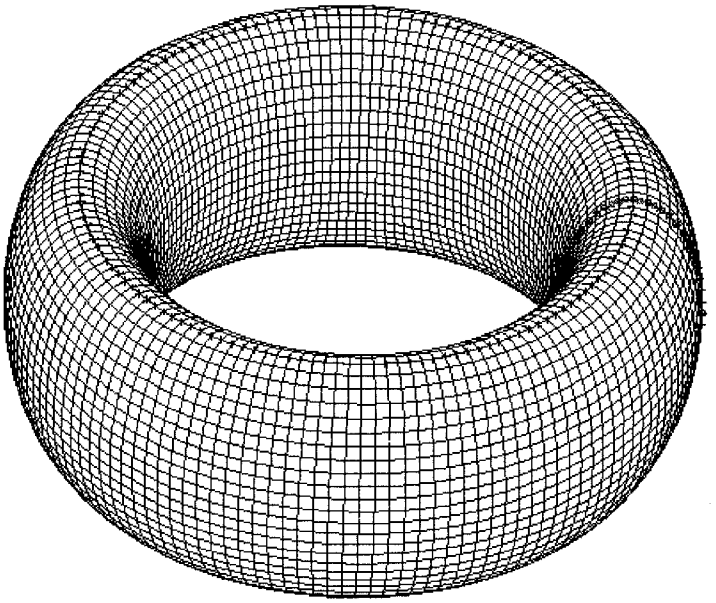

Fig. 3.4 The FE model of an elliptical toroidal shell for validation

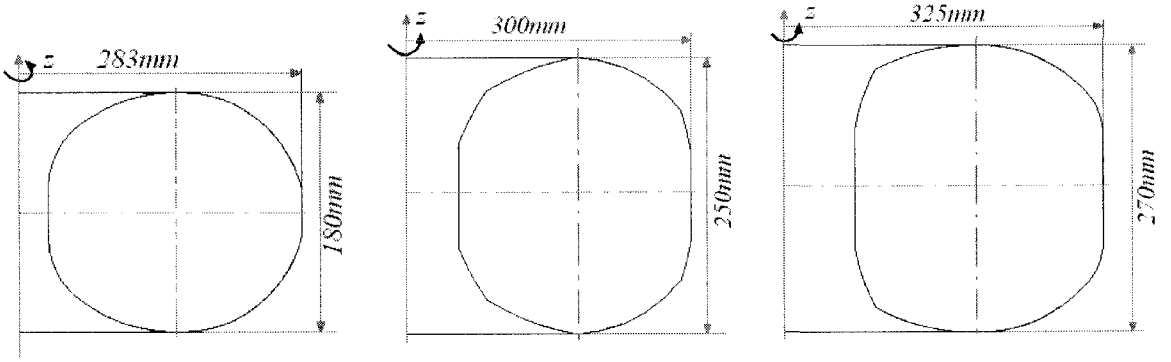

(a) (b) (c)

Fig. 3.5 The cross-section of tanks A, B, C

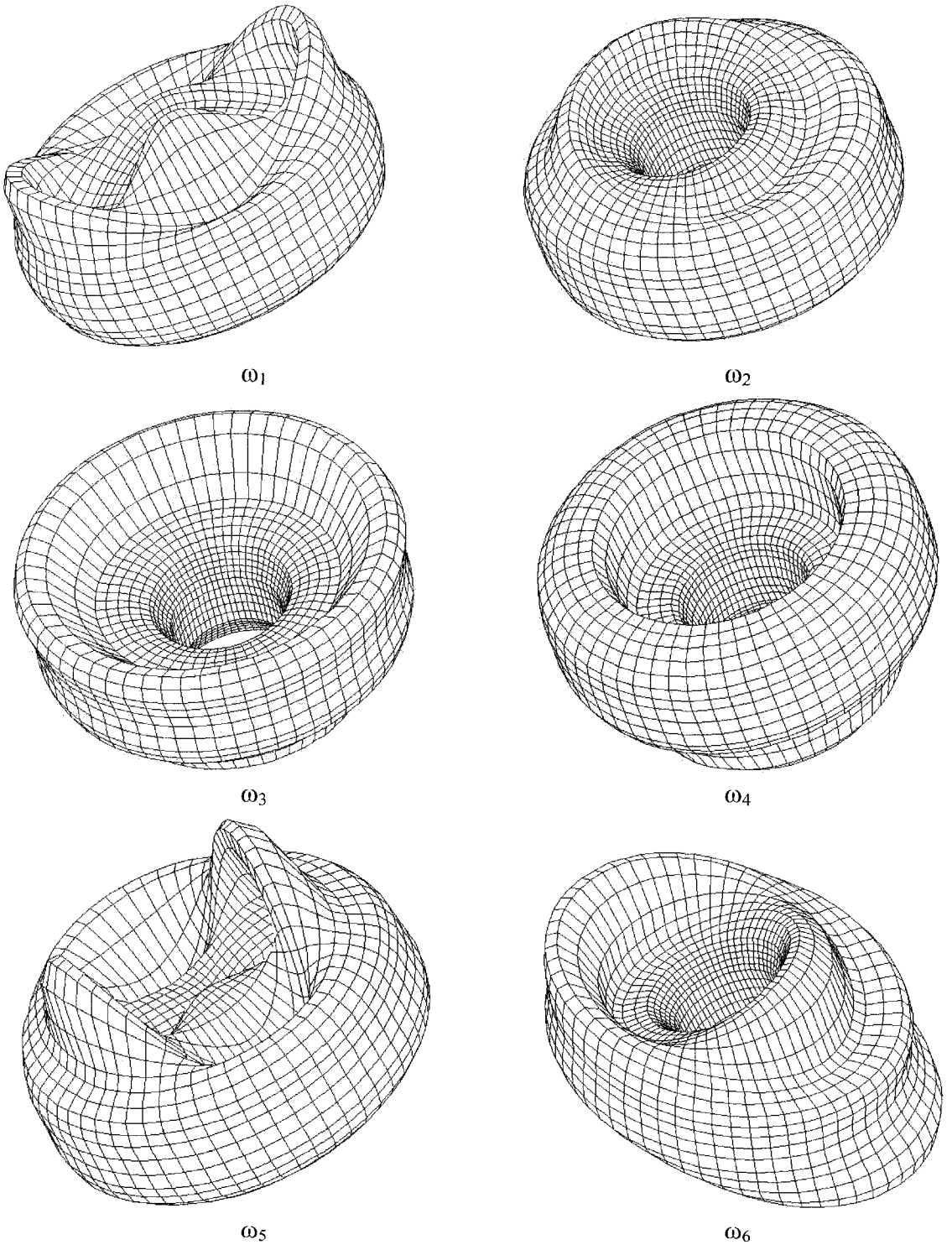

Fig. 3.6 Vibration mode shapes 1-6 of LPG tank B

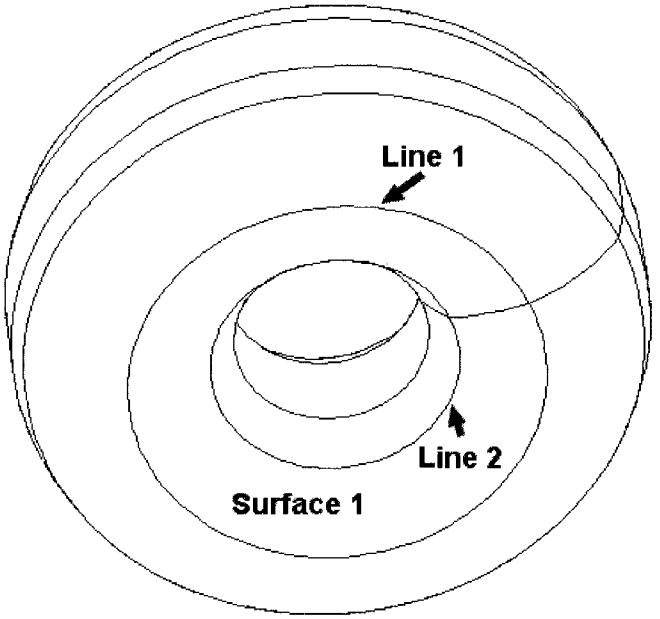

Fig. 3.7 Various boundary conditions for toroidal tanks

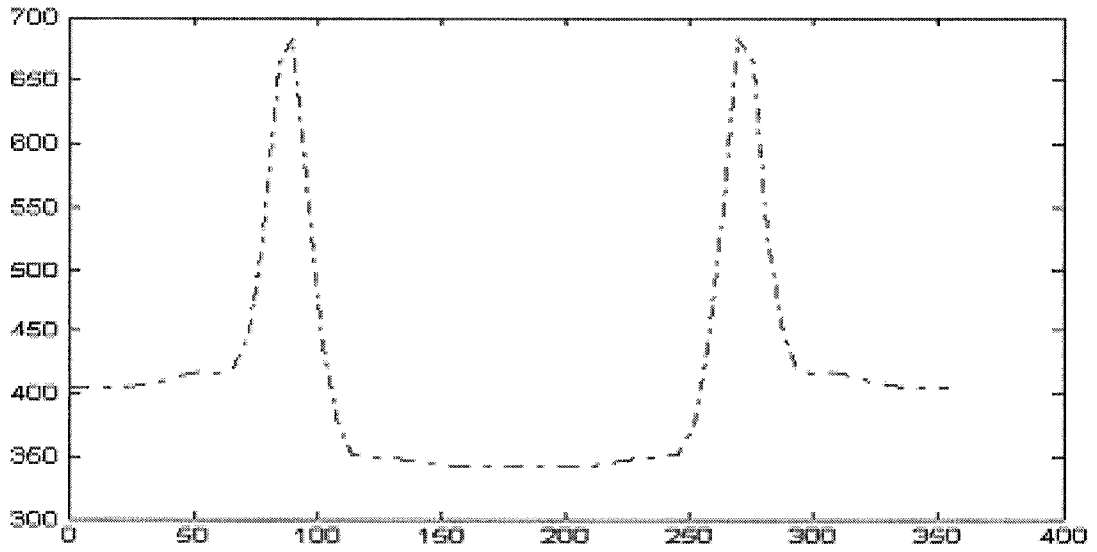

Fig. 3.8 Variation for a toroidal shell of circular cross-section of the fundamental frequency ω (*rad/s*) with angular position θ of a circumferential boundary support line

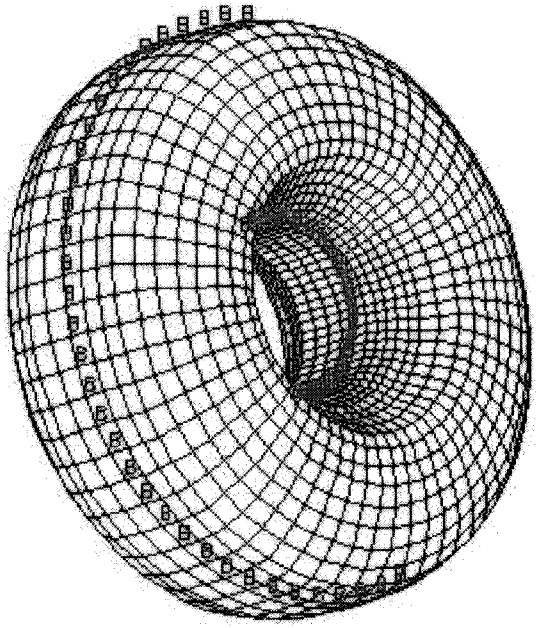

Fig. 4.1 Support lines along extrados and intrados of a toroidal LPG tank

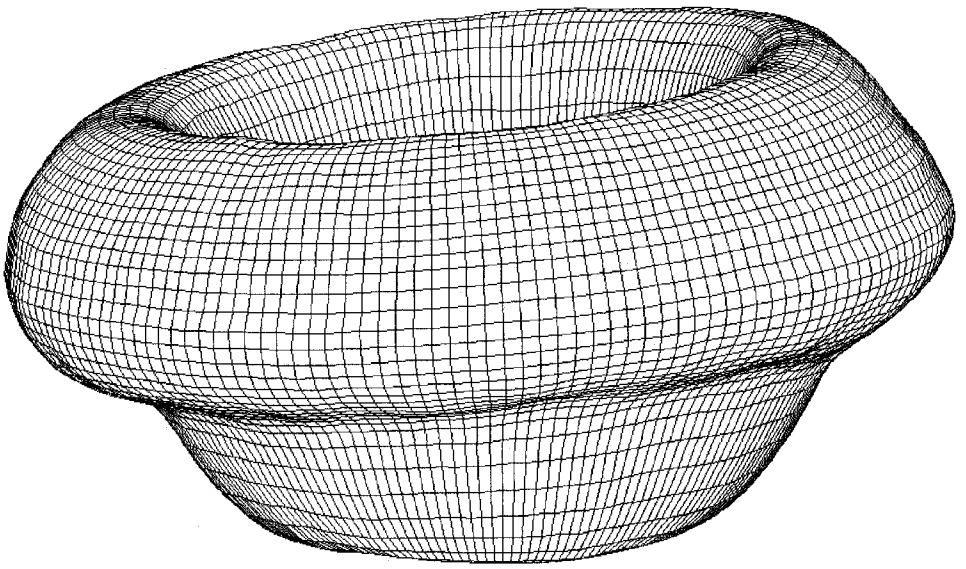

(a)

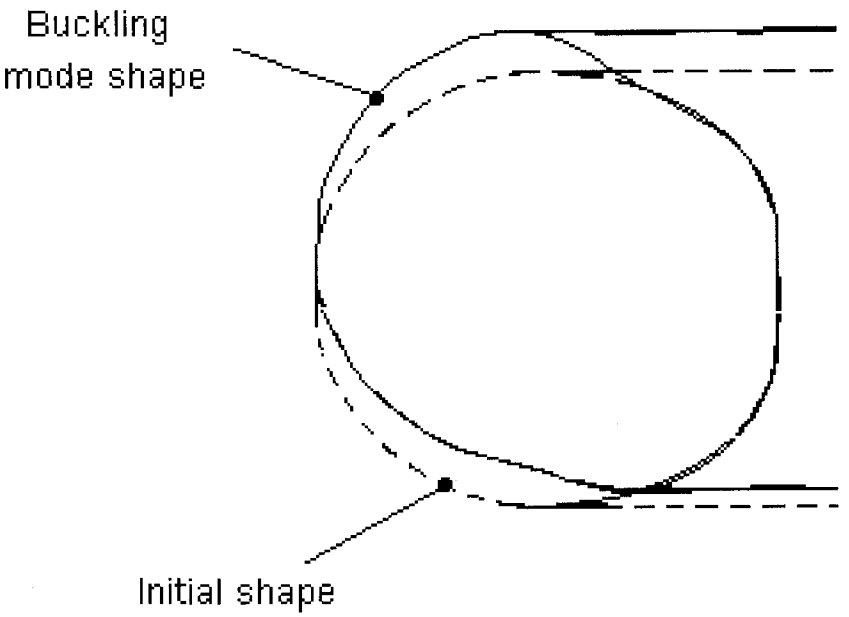

(b)

Fig. 4.2 The first buckling mode of tank A (constraint on inner equator), (a) buckling mode shape, (b) cross-section

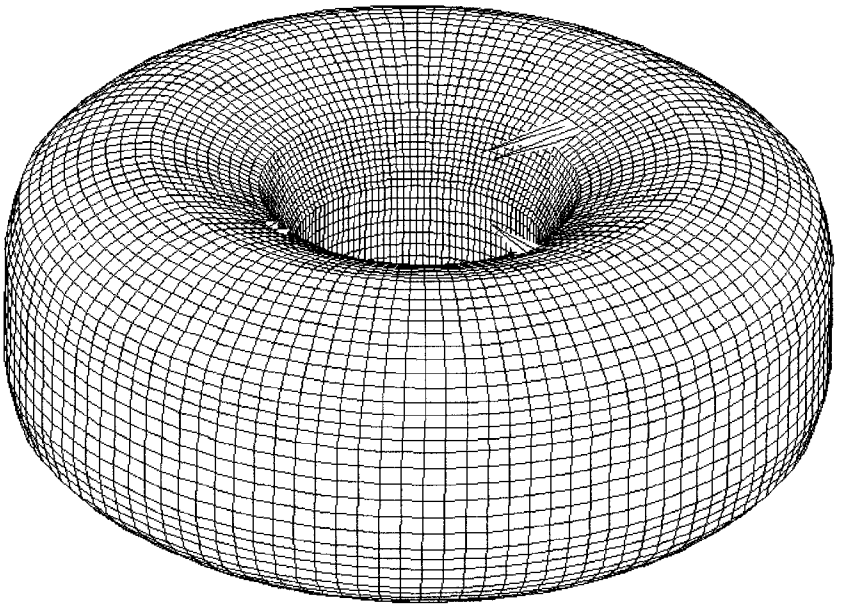

Fig. 4.3 The buckling mode of tank B (constraint on inner equator)

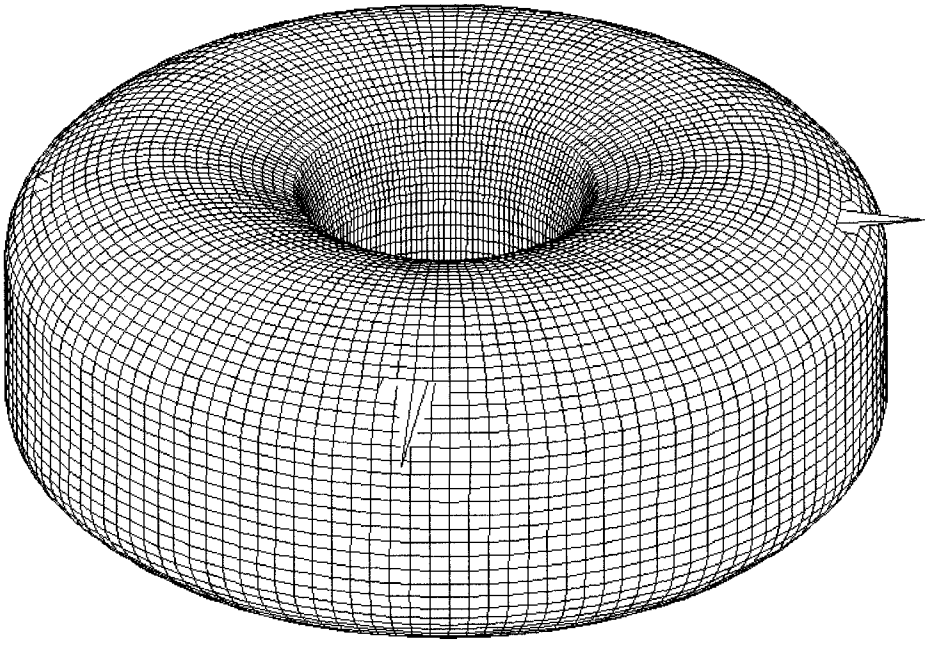

Fig. 4.4 The buckling mode of tank C (constraint on inner equator)

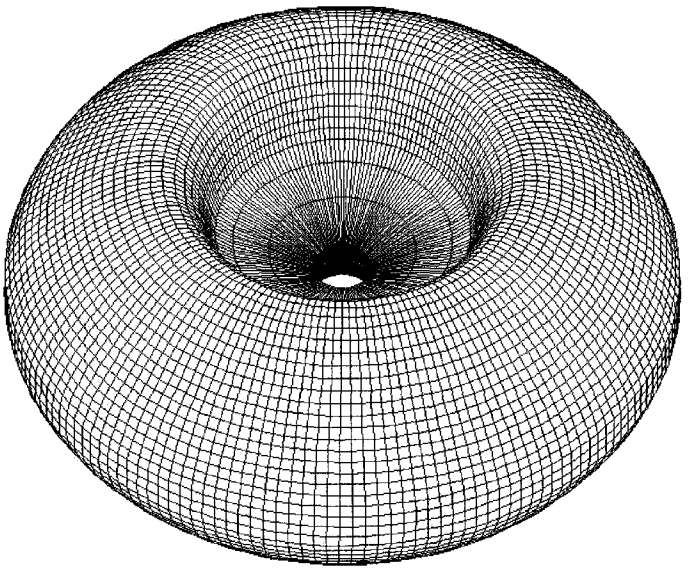

Fig. 4.5 The deformed shape in collapse analysis of tank A (3D model)

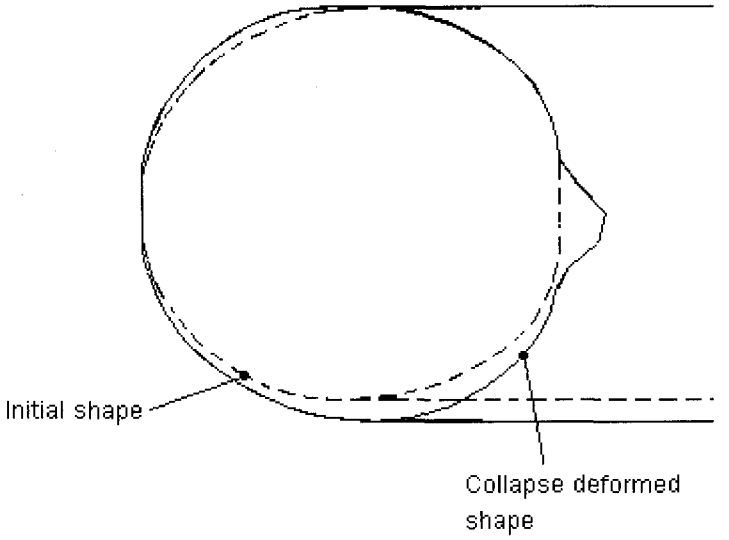

Fig. 4.6 The deformed shape of tank A in collapse analysis (cross-section)

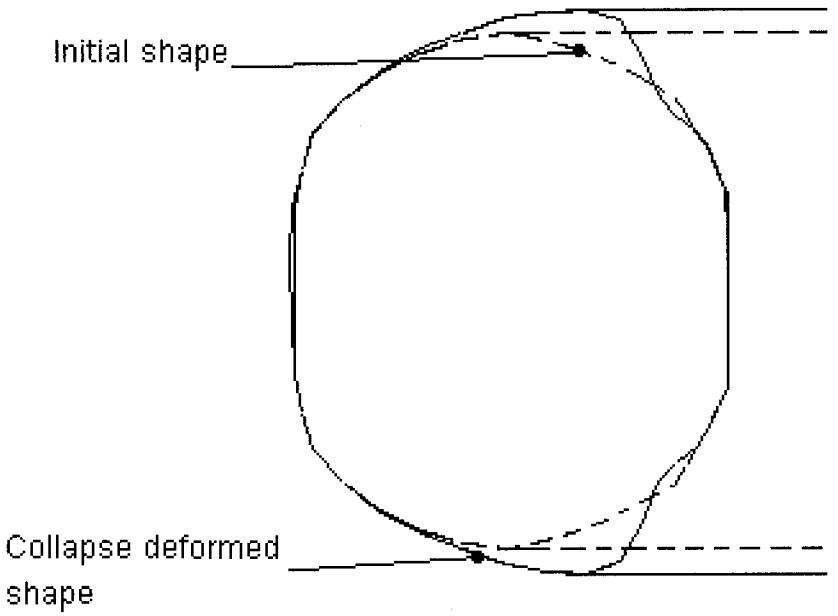

Fig. 4.7 The deformed shape of tank B in collapse analysis (cross-section)

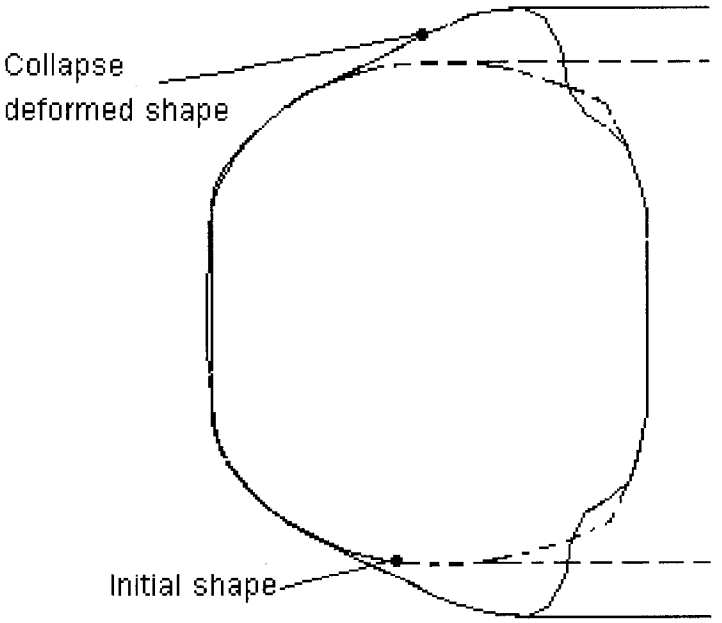

Fig. 4.8 The deformed shape of tank C in collapse analysis (cross-section)

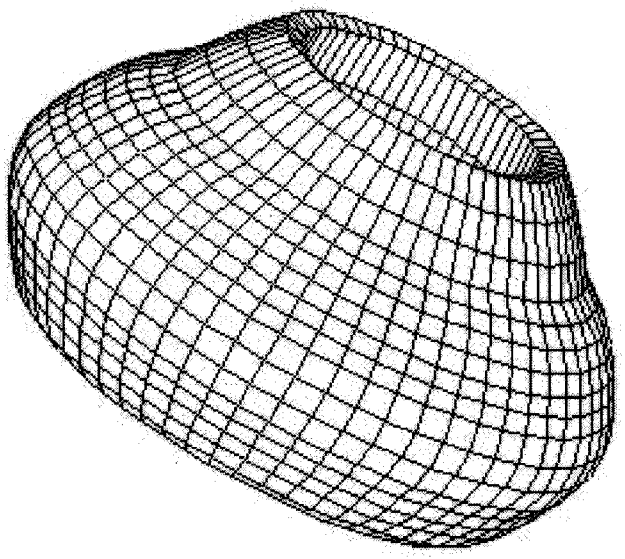

Fig. 4.9 The deformed shape of tank B in collapse analysis (support applied at the bottom of the tank)

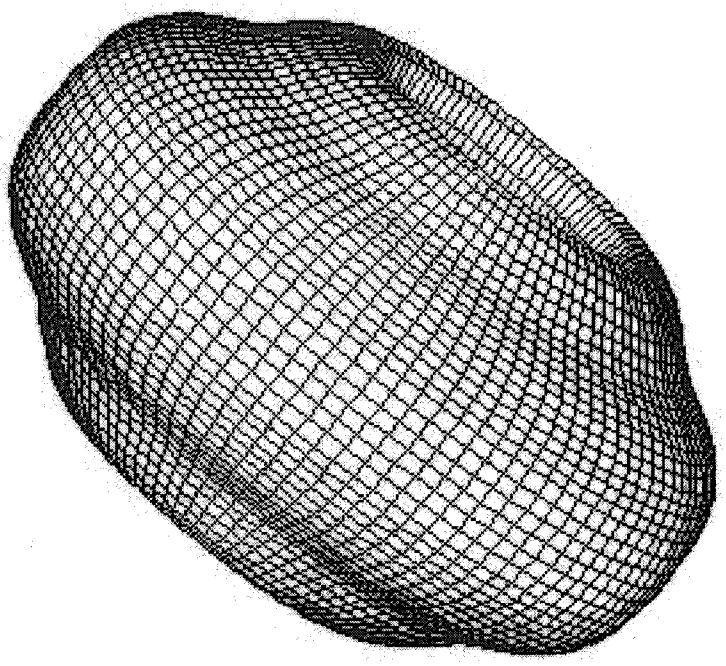

Fig. 4.10 The deformed shape of tank B in collapse analysis (support applied at the inner equator of the tank)

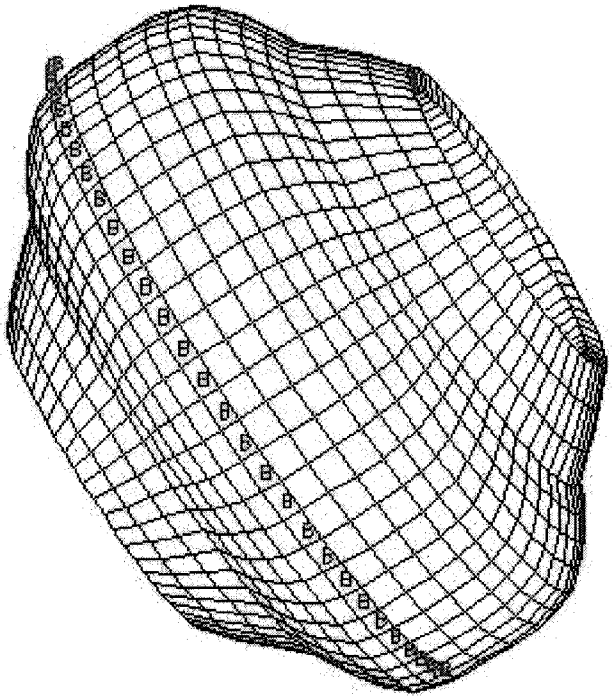

Fig. 4.11 The deformed shape of tank B in collapse analysis (support applied at the outer equator of the tank)

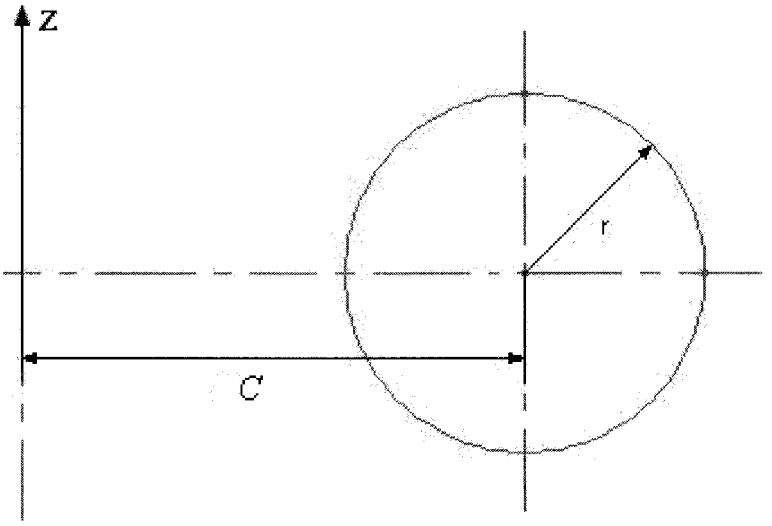

Fig. 4.12 Cross-section of a circular toroidal shell

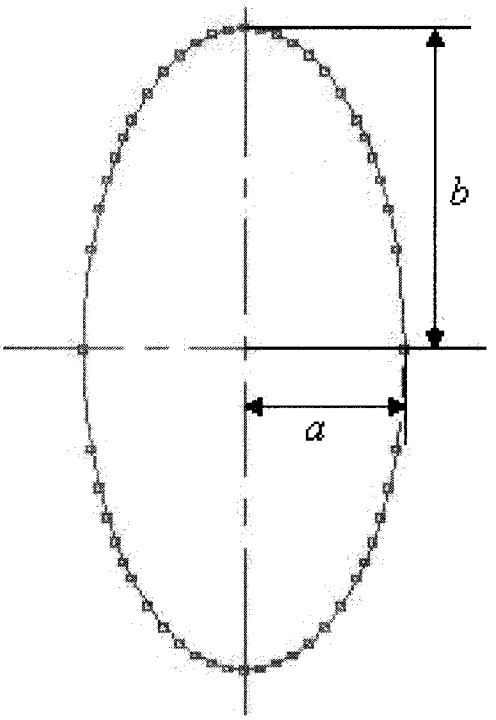

Fig. 4.13 Cross-section of an elliptical toroidal shell

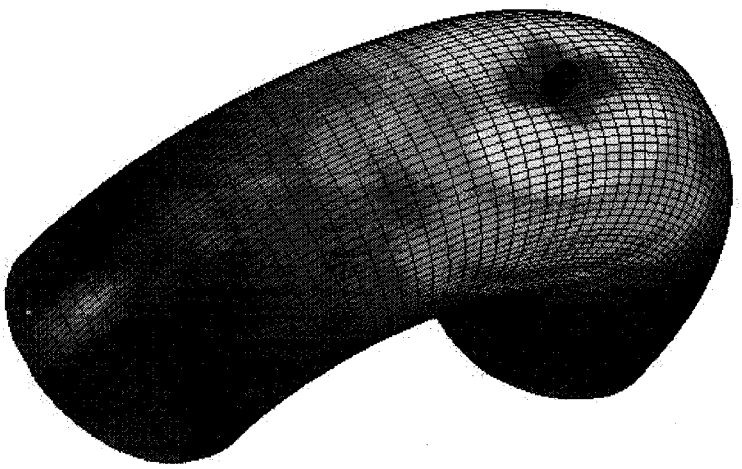

Fig. 5.1 Impact on extrados

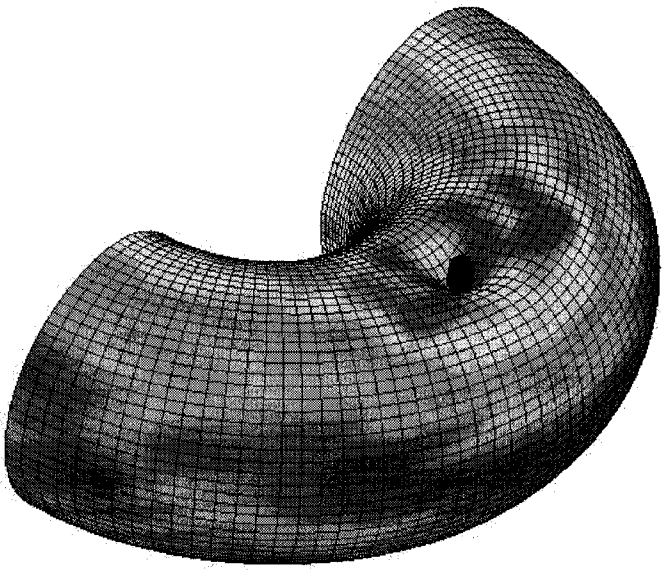

Fig. 5.2 Impact on crown

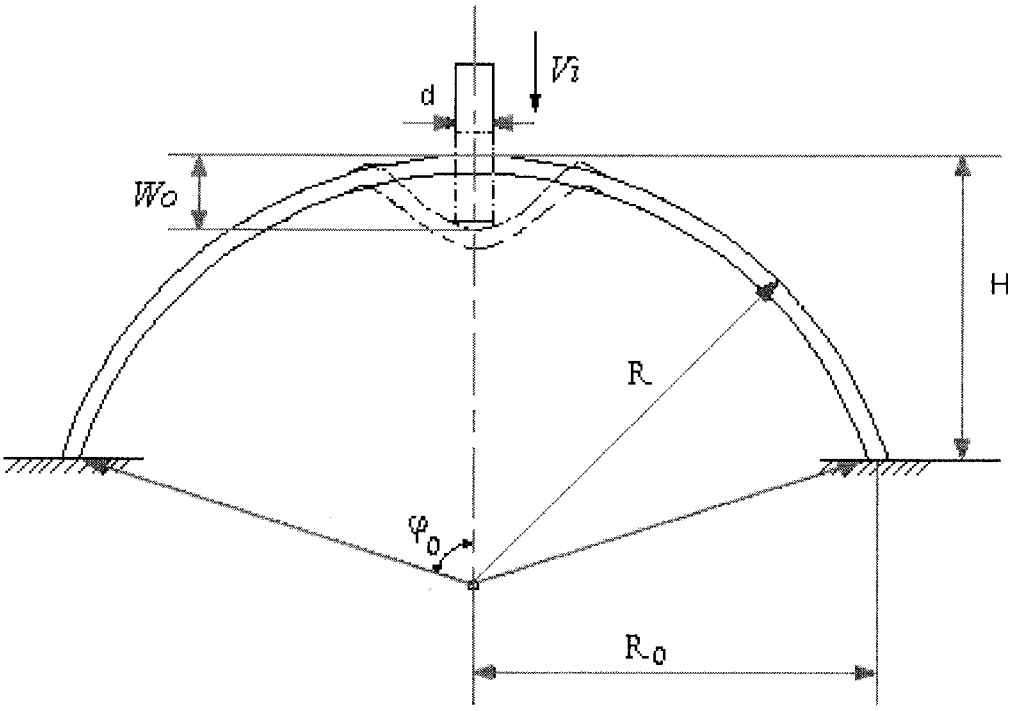

Fig. 5.3 Geometry for part-spherical shell impacted by a projectile

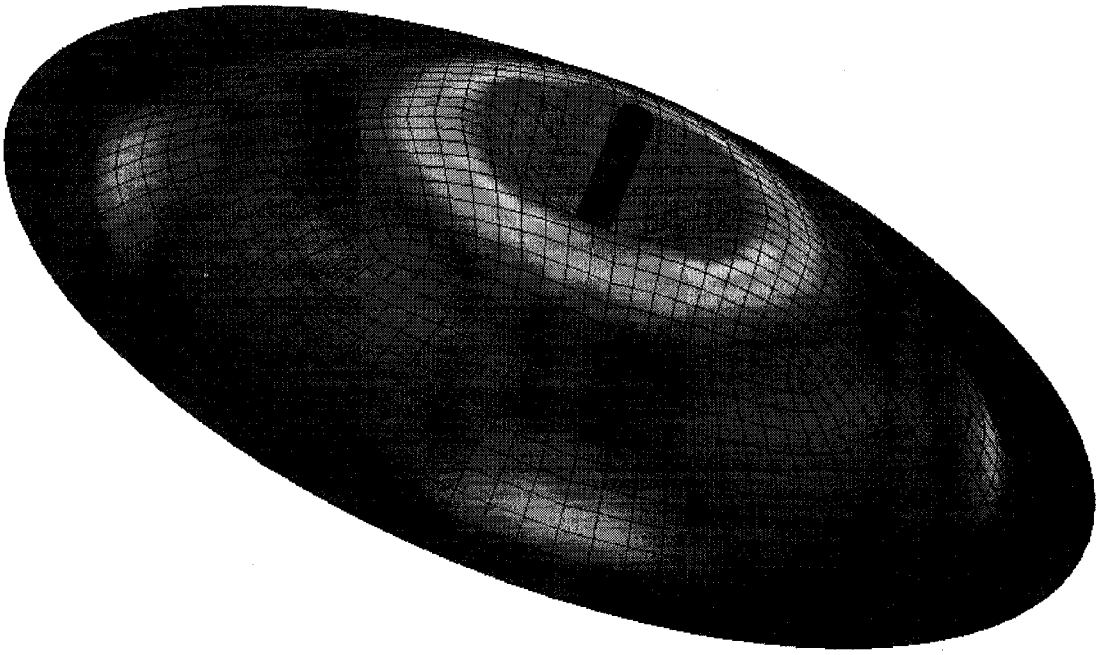

Fig. 5.4 FEM mesh for part-spherical shell impacted by a cylindrical projectile

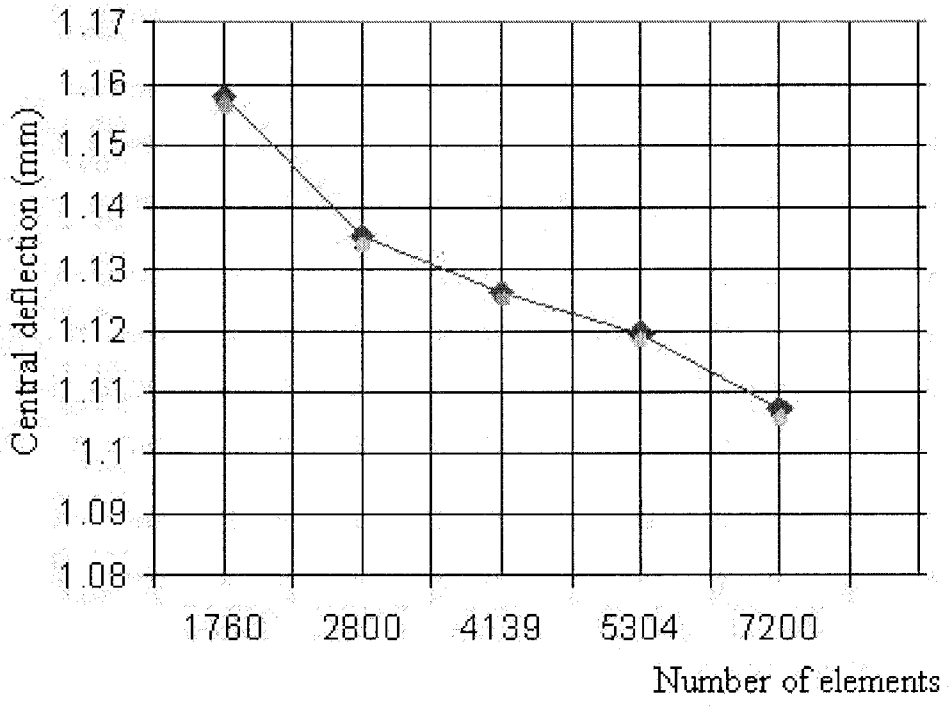

Fig. 5.5 Convergence of solution given by LS-DYNA

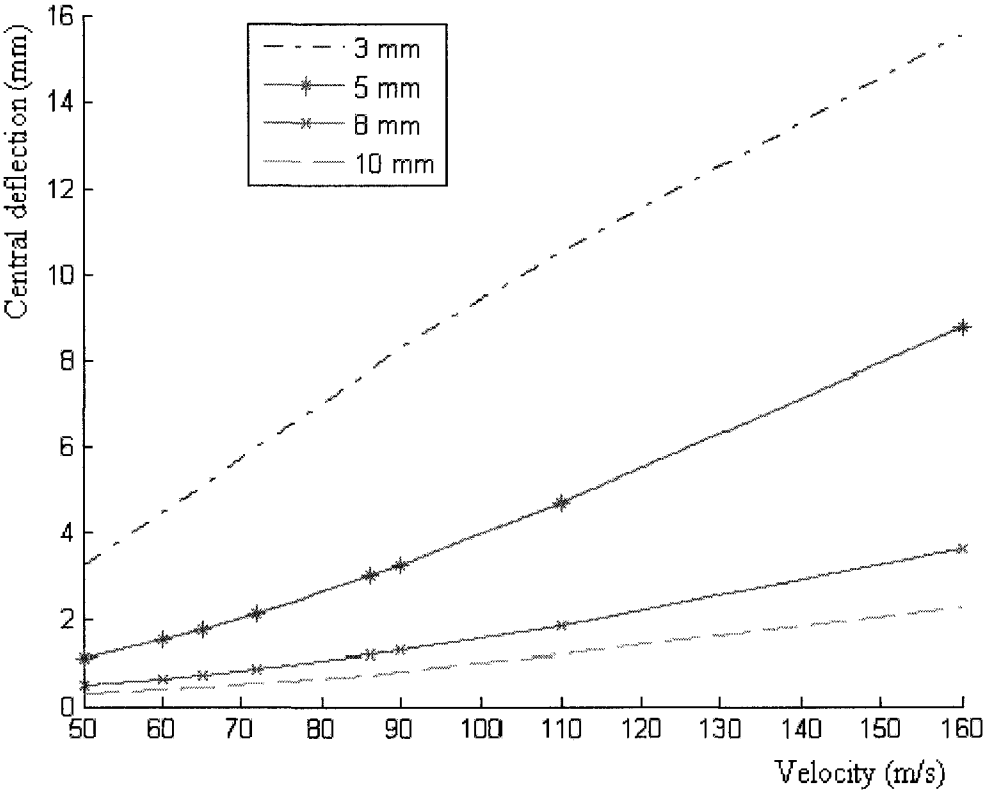

Fig. 5.6 Effect of the wall thickness on tank B impacted by a cylindrical projectile on the extrados given by LS-DYNA

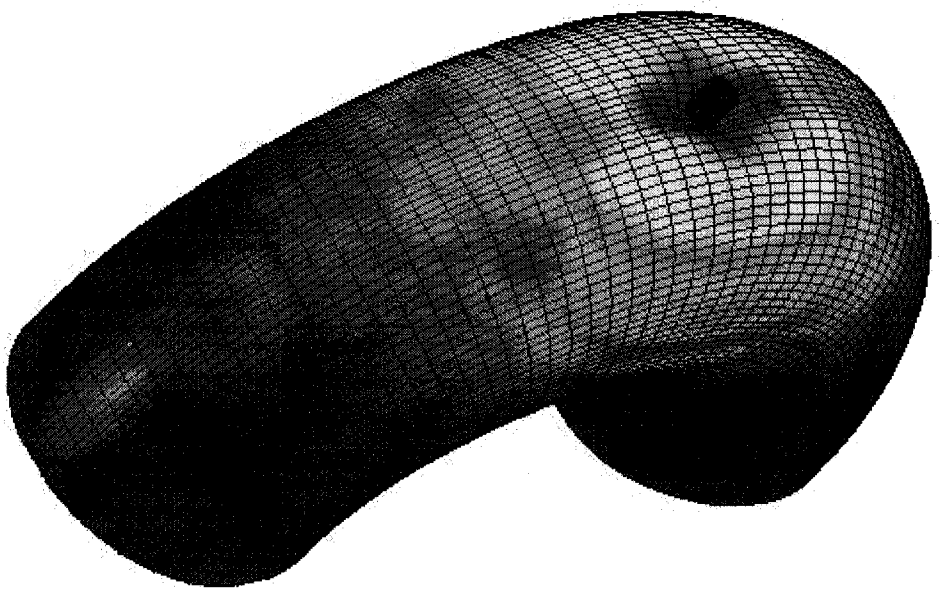

Fig. 5.7 Deformed shape of tank A impacted at the extrados

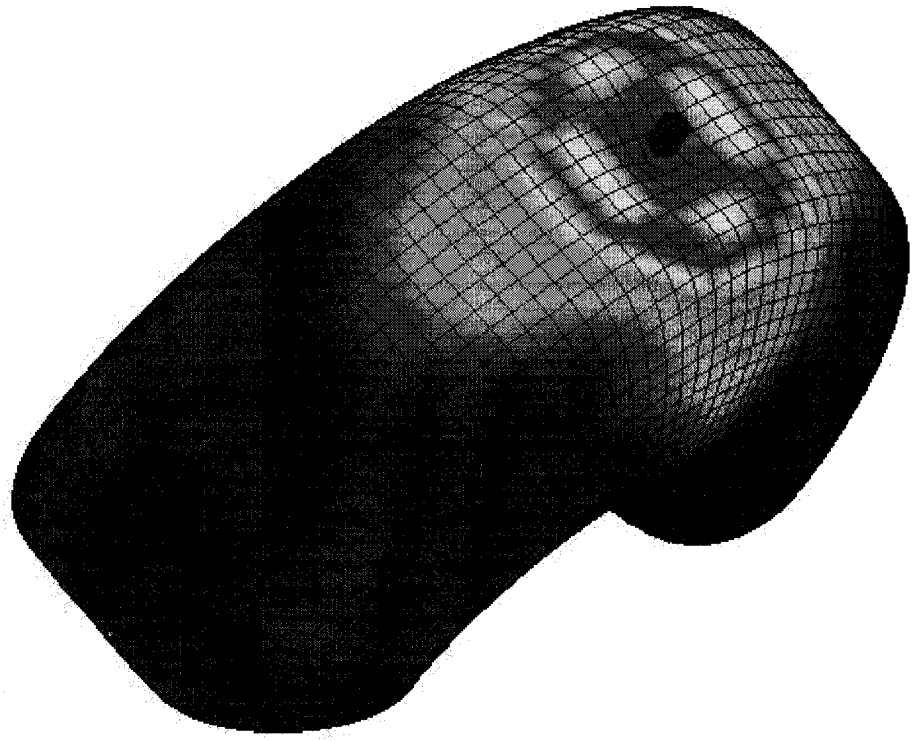

Fig. 5.8 Deformed shape of tank B impacted at the extrados

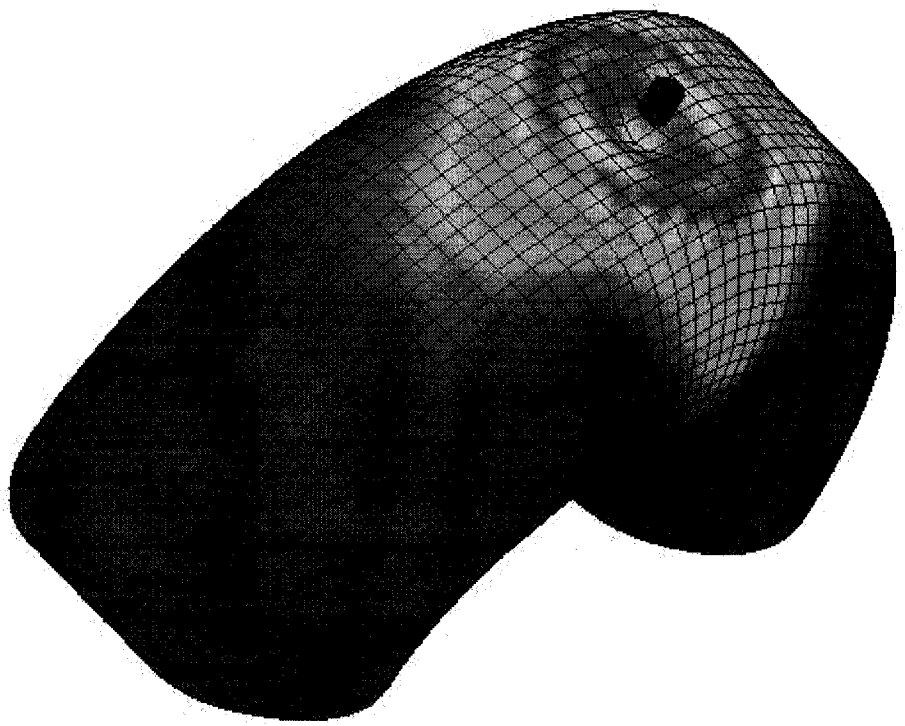

Fig. 5.9 Deformed shape of tank C impacted at the extrados

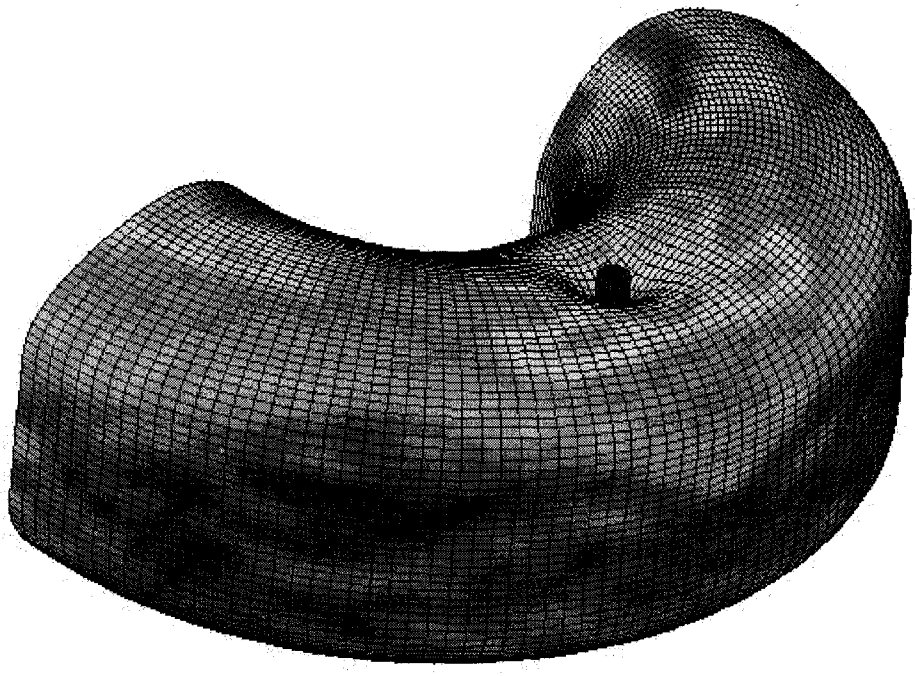

Fig. 5.10 Deformed shape of tank B impacted at the crown

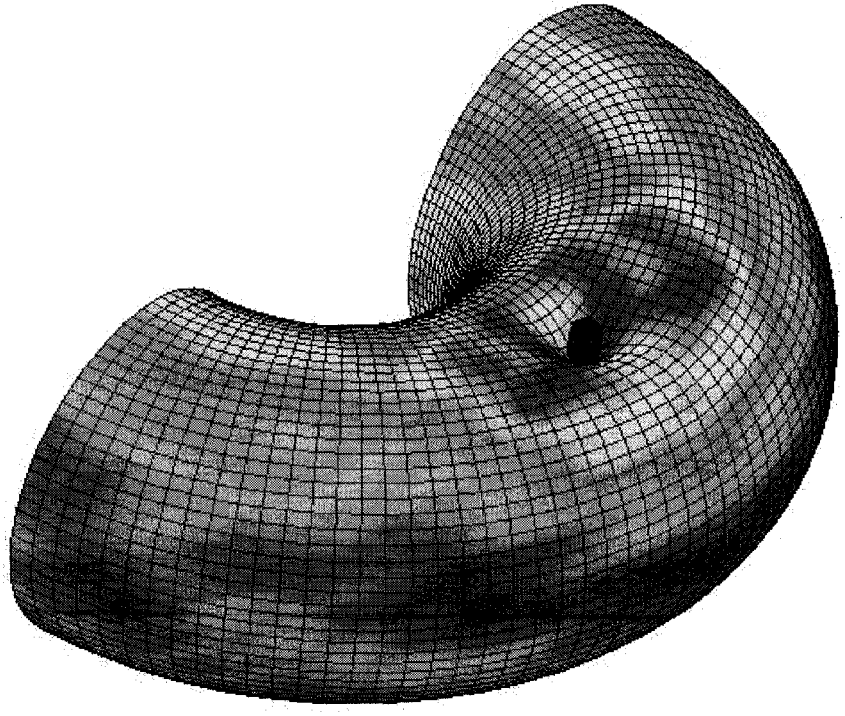

Fig. 5.11 Deformed shape of the circular toroidal shell impacted at the crown

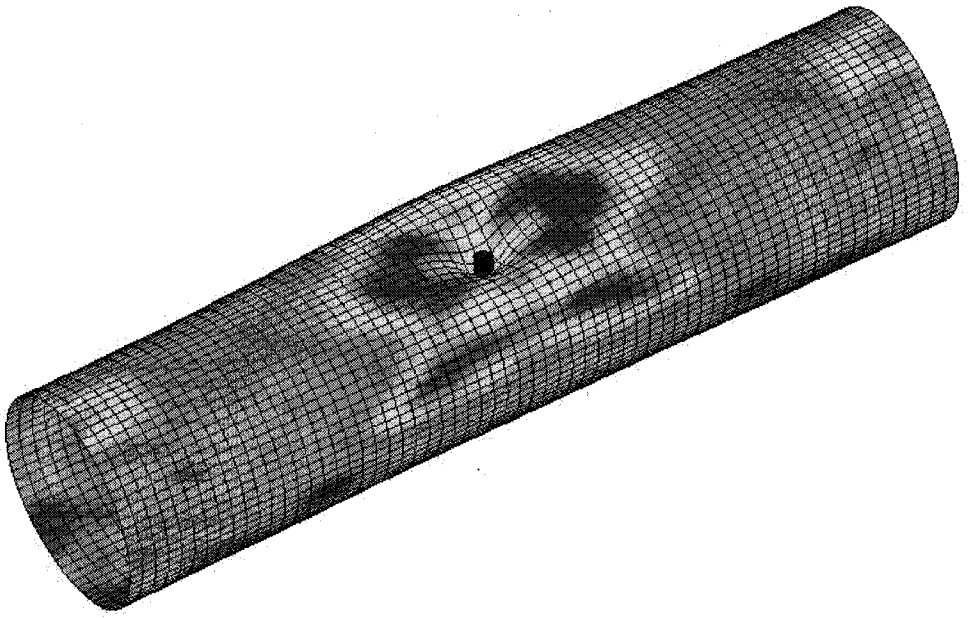

Fig. 5.12 Deformed shape of the cylindrical shell impacted at the crown

Appendix I: Software instructions

I.1 Free vibration analysis of a toroidal shell with circular cross-section

ADINA-AUI---
Control-Analysis Assumption-Kinematics:
Check-Displacement/Rotation-Large

A. Model building

Point #	X1	X2	X3
1	0.192	0.0	0.0
2	0.192	0.119	0.0
3	0.073	0.0	0.0

Geometry-Lines-Define-Add-Type: Circle
Defined by: Centre P1 P3
Centre:1, P1:2, P2:3
-ok-

Geometry-Surfaces-Define-Add-Type: Revolved
Initial Line: 1
Angle of Rotation: 360
Number of: 1
Axis of Revolution
Axis: Y
-ok-

Geometry-Surfaces-Thickness

Surfaces #	Thickness
1	0.003

-ok-

Model-Materials-Plastic-bilinear-Add
Yong's Modulus: 0.207e12
Poisson Ratio: 0.3
Initial Yield Stress: 0.25e9
Density: 7800
-ok-

Meshing-Element Groups-Add
Group Number: 1 Type: Shell
-ok-
Meshing-Mesh Density-Surface
Method: Use number of divisions
Number of subdivisions: 40 for u, 100 for v.

Meshing-Create Mesh-Surface
Type: Shell
Element Group: 1
Node per Element: 4
Surface #: 1

-ok-

B. Choosing the type of the analysis

Analysis type: Frequencies/Modes
Analysis options-
Frequencies/Mode shapes:
Number of Frequencies/Mode shapes: 12
-ok-

C. Running the program

Solution-datefile/run
File name: Freevib –ok-

D: Post processing

ADINA-Plot- yes
File-open- Freevib.por -open-
List-Value List-Zone:
Variables to List-Frequencies/Mode-Natural frequencies

I.2 Buckling analysis of a toroidal shell with circular cross-section

ADINA-AUI---
Control-Analysis Assumption-Kinematics:
Check-Displacement/Rotation-Large

A. Model building

Point #	X1	X2	X3
1	0.192	0.0	0.0
2	0.192	0.119	0.0
3	0.073	0.0	0.0

Geometry-Lines-Define-Add-Type: Circle
Defined by: Centre P1 P3
Centre:1, P1:2, P2:3
-ok-

Geometry-Surfaces-Define-Add-Type: Revolved
Initial Line:1
Angle of : 360
Number of : 1
Axis of Revolution
Axis: Y

-ok-

Geometry-Surfaces-Thickness
Surfaces # - Thickness
1 0.003
-ok-

Model-Materials-Elastic-Add
Yong's Modulus: 0.207e12
Poisson Ratio: 0.3
Density: 7800
-ok-

Meshing-Element Groups-Add
Group Number: 1 Type: Shell
Kinematic Formulation -- Displacement: Large

-ok-

Model-Boundary Condition-Apply Fixity-Apply to: Lines

Line #	Fixity
2	All

Meshing-Mesh Density-Surface
Method: Use number of divisions
Number of subdivisions: 40 for u, 100 for v.
-ok-

Meshing-Create Mesh-Surface
Type: Shell
Element Group: 1
Node per Element: 4
Surface #: 1

-ok-

B. Input the loading

Model-Loading-Apply
Load type: Pressure
Load number: Define-Add-Pressure number: 1
Magnitude: 1 -ok-
Apply to: Surface
Surface #: 1
-ok-

C. Choosing the type of the analysis

Linearized Buckling
Analysis options-
Number of Buckling: 2
Number of Buckling to be: 2
-ok-

D. Running the program

Solution-datefile/run
File name: buck –ok-
After program running –ok- -close- -close-

E: Post processing

ADINA-Plot- yes
File-open- buck.por -open-
Display-Load plot-User Default (to see the buckling pressure)

I.3 Collapse analysis of a toroidal shell with circular cross-section

ADINA-AUI---
Control-Analysis Assumption-Kinematics:
Check-Displacement/Rotation-Large

A. Model building

Point #	X1	X2	X3
1	0.192	0.0	0.0
2	0.192	0.119	0.0
3	0.073	0.0	0.0

Geometry-Lines-Define-Add-Type: Circle
Defined by: Centre P1 P3
Centre:1, P1:2, P2:3
-ok-

Geometry-Surfaces-Define-Add-Type: Revolved
Initial Line:1
Angle of Rotation: 360
Number of : 1
Axis of Revolution
Axis: Y
-ok-

Geometry-Surfaces-Thickness

Surfaces #	Thickness
1	0.003

-ok-

Model-Materials-Plastic-bilinear-Add
Yong's Modulus: 0.207e12
Poisson Ratio: 0.3
Initial Yield Stress: 0.25e9
Density: 7800
-ok-

Meshing-Element Groups-Add
Group Number: 1 Type: Shell
Kinematic Formulation -- Displacement: Large

-ok-

Model-Boundary Condition-Apply Fixity-Apply to: Lines

Line #	Fixity
2	All

Meshing-Mesh Density-Surface
Method: Use number of divisions
Number of subdivisions: 40 for u, 100 for v.
-ok-

Meshing-Create Mesh-Surface
Type: Shell
Element Group: 1
Node per Element: 4
Surface #: 1

-ok-

B. Input the loading

Model-Loading-Apply
Load type: Pressure
Load number: Define-Add-Pressure number: 1
Magnitude: 3e6 -ok-
Apply to: Surface
Surface #: 1
-ok-

Control-Time step
Number of step: 10
Control-Time function

Time	Value
0	1
1	1.05
2	1.1
3	1.15
4	1.2
6	1.25
7	1.3
8	1.35
9	1.4
10	1.45

-ok-

C. Choosing the type of the analysis

Analysis type: Static

D. Running the program

Solution-datefile/run

File name: collapse –ok-
(ADINA runs)- The running of program is cancelled at time step 9 (the number here may be not the exact one in the real program).
Then use the value of load at step 9 and the value at the last step 8 as the end and beginning value of the next trial to get more accurate result.

E: Post processing

The collapse factor for the toroidal tank is the mean of value at stop step and the value at the last step.

ADINA-Plot- yes
File-open- collapse.por -open-
Push the "mesh plot" icon
View of deformed shape:
Display - Geometry/Mesh plot - Modify - Model Depiction
Select - Defined by: Max displacement - 8 - ok
Click the 'boundary plot' icon and the 'load plot' icon, etc.

I.4 Impact analysis of a toroidal shell with circular cross-section by using LS-DYNA

A. Building model

Build a toroidal shell model in Solidworks
Import the model into FEMB

B. Meshing

Element-Plate/Solid Mesh-Topology Mesh-By Region
Select all the surfaces of the toroidal shell.
Apply
Enter 5 in the element size blank of the following message box.
ok-Yes-Yes

Element-Plate/Solid Mesh-Tetra Mesh-By Region
Select 4-Node
Select the body of the cylindrical projectile
Apply
ok-Yes-Yes

C. Material

Material-Create-Structural-3.1*Mat_Plastic_Kinematic
Mass Density: 4900
Young's Modulus: 6.89e+10
Poisson's Ratio: 3.0e-01
Yield Stress: 2.68e+08
Plastic Hardening Modulus: 0
Hardening Parameter: 0
ok

Material-Create-Structural-20.1*Mat_Rigid
Mass Density: 7800
Young's Modulus: 2.01e11
Poisson's Ratio: 3.0e-01
ok

Material-Assign-1. M-1->Shell->Apply
Material-Assign-1. M-2->Projectile->Apply

D. Element property

Property-Create-Shells
1.1

ELFORM: S/R Hughes-Liu
SHRF: 1.0
NIP: 5
PROPT 0
QR/IRID: 0
ICOMP: 0
SETYP: 1
2.1
T1~T4 : 0.001
NLOC: Mid Surface

Property-Create-Solids
1.1
ELFORM: Constant Stress Solid Element
ok

Property-ASSIGN
P-1-Shell-Apply

Property-ASSIGN
P-2-Solid-Apply

E. Contact

Contact-Create-3 Dimensions-*Contact_Automatic_Surface_To_Surface-Next
2.1
SSID: 1
MSID: 2
SSTYP: 3
MSTYP: 3
3.1
FS: 5.0e-02
FD: 5.0e-02

F. Boundary conditions

BC-Initial Conditions-Create-Rigid Body
PID: Select the body of the projectile
VY: -60
ok

BC-Constraint
Select all the nodes at the bottom of the toroidal shell
DOF: 1
VAD: 2
LCID: 2

SF: 1.0
ok

Create Node Sets
Set-Node-Create
Select the nodes at the bottom of the toroidal shell, named "Shell BC"

BC-Boundary-SPC
Create-Shell BC
2.1
DOFX: 1
DOFY: 1
DOFZ: 1
DOFRX: 1
DOFRY: 1
DOFRZ: 1
ok

G. Post processing

Export LS-DYNA file
File-export-LS-DYNA(*.dyn)
Named "impact.dyn"

Solving (LS-DYNA 970)
Solvers-start analysis-Input File-Browse
Select impact .dyn
RUN.

Post-Processor (POST GL 1.0)
File-open
Select the d3plot file generated by LS-DYNA, and then results can be viewed in the post-processor.

Appendix II: Equations for DQM program

II.1 Introduction

In the current study, it was intended that the differential quadrature method (DQM) be used as an alternate means to obtain numerical results for the vibration analysis. An existing DQM program developed by Wang and Redekop (2005) was modified to determine the natural frequencies of toroidal LPG tanks, and then the results obtained by the modified DQM program were to be compared with the finite element results. Since the cross-section of a toroidal LPG tank is difficult to describe using a mathematical expression, two geometries similar to those of the toroidal LPG tanks were defined. Both were analyzed using the modified DQM program and ADINA.

After considerable effort it was found that the solutions obtained by the modified DQM program were unsatisfactory. Thus the discussion and conclusion that are made in this appendix relate to the reason that the unacceptable DQM results were obtained.

II.2 Shell theory

II.2.1 DQM program

To determine the vibration characteristics of the toroidal shells the first-order linear version of the Sanders-Budiansky (Sanders, 1959) (Budiansky, 1968) shell theory is used, in conjunction with the D'Alembert principle. Wang and Redekop (2005) developed a DQM program to determine the natural frequencies and mode shapes for general shells of revolution. The program has already been applied successfully to toroidal shells with circular and elliptical cross-section. The equations of motion in their program are in terms of the Lamé parameters, the curvatures, the material properties. Thus for solving the vibration

problem of the toroidal shells by using the modified DQM program, the main task is to determine the Lamé parameters, curvatures and their derivatives for the specific toroidal shell that is to be considered.

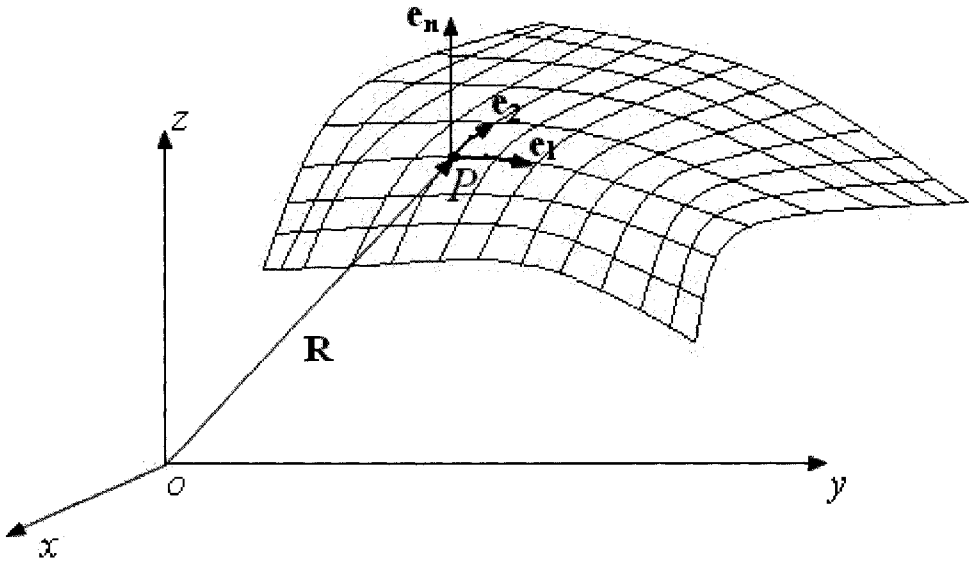

Fig. II.2.1

II.2.2 Shell geometry

A thin shell of constant thickness has a neutral surface (Fig. II.2.1). Locations on the neutral surface can be defined by two-dimensional curvilinear surface coordinates q_1 and q_2. The Cartesian coordinates x, y, z of a point P on the neutral surface in Cartesian space is related to the location of the point in surface coordinate by $x=f_1(q_1, q_2)$, $y=f_2(q_1,q_2)$, $z=f_3(q_1, q_2)$. The location of P on the neutral surface can also be expressed by a radius vector $\mathbf{R} = \mathbf{R}(q_1, q_2)$, given by:

$$\mathbf{R} = f_1(q_1,q_2)\cdot\mathbf{i} + f_2(q_1,q_2)\cdot\mathbf{j} + f_3(q_1,q_2)\cdot\mathbf{k} \qquad \text{(II.2.1)}$$

where **i**, **j**, **k** are unit vectors forming a base in the Cartesian x, y, z coordinate system, vectors $\mathbf{e}_1$ and $\mathbf{e}_2$ are the tangent vectors along q_1 and q_2 respectively (Fung and Sechler,

1974). The Lamé parameters of the shell are depicted by α_1 and α_2, and the curvatures by k_1 and k_2. For a shell of revolution the radius vector takes the form:

$$\mathbf{R} = r \cdot \sin\phi \cdot \mathbf{i} + r \cdot \cos\phi \cdot \mathbf{j} + z \cdot \mathbf{k} \qquad \text{(II.2.2)}$$

where $q_1 = \phi$ is the circumferential angle (see Fig. II.2.2), $r = r(q_2), z = z(q_2)$ (Dym, 1974).

The geometric parameters for a specific shell of revolution may readily be derived from the radius vector (Soedel, 1981). For example, for a toroidal shell of circular cross-section (Fig. II.2.2) the parameters are given by: $q_1 = \phi$; $q_2 = \theta$; $\alpha_1 = C + r_c \cdot \cos\theta$; $\alpha_2 = r_c$; $k_1 = \dfrac{\cos\theta}{C + r_c \cos\theta}$; $k_2 = \dfrac{1}{r_c}$, where ϕ is the circumferential angle, and θ is the meridional angle, measured clockwise from the positive horizontal, C is the bend radius, r_c is the radius of the circular cross-section, and $r = r(\theta) = C + r_c \cdot \cos\theta$, $z = z(\theta) = r_c \cdot \cos\theta$.

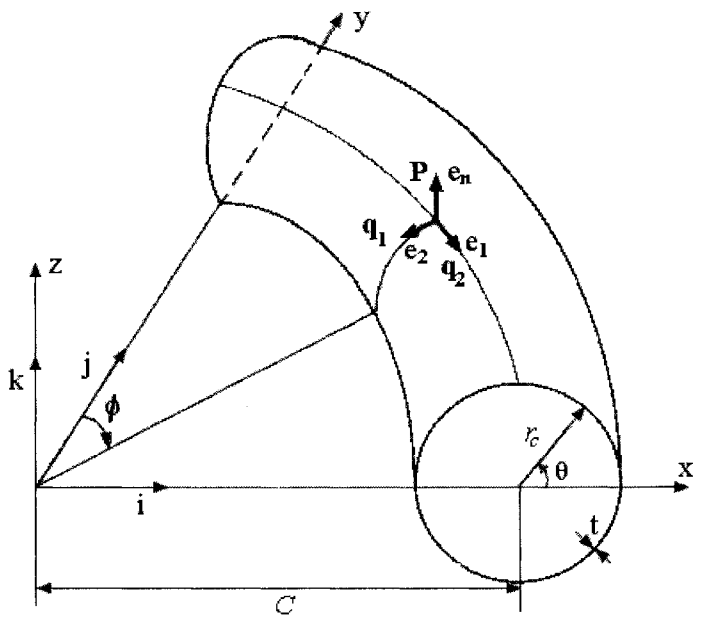

Fig. II.2.2 Coordinate system for thin circular toroidal shell

For an arbitrary shell, the equations of the Lamé parameters and the curvatures are given by:

$$\alpha_1 = \sqrt{\frac{\partial \mathbf{R}}{\partial q_1} \cdot \frac{\partial \mathbf{R}}{\partial q_1}} \qquad \text{(II.2.3)}$$

$$\alpha_2 = \sqrt{\frac{\partial \mathbf{R}}{\partial q_2} \cdot \frac{\partial \mathbf{R}}{\partial q_2}} \tag{II.2.4}$$

$$k_1 = -\frac{L}{\alpha_1^{\,2}} \tag{II.2.5}$$

$$k_2 = -\frac{N}{\alpha_2^{\,2}} \tag{II.2.6}$$

where $L = \frac{\partial \mathbf{e}_n}{\partial q_1} \cdot \frac{\partial \mathbf{R}}{\partial q_1}$, $N = \frac{\partial \mathbf{e}_n}{\partial q_2} \cdot \frac{\partial \mathbf{R}}{\partial q_2}$; $\mathbf{e}_1$, $\mathbf{e}_2$ and $\mathbf{e}_n$ form an orthogonal basis for an arbitrary point on the shell surface (Fig. II.2.2), and $\mathbf{e}_1$ and $\mathbf{e}_2$ are the tangent vectors along q_1 and q_2, $\mathbf{e}_n$ is the unit vector normal to $\mathbf{e}_1$ and $\mathbf{e}_2$. The unit vectors are given by:

$$\mathbf{e}_1 = \frac{1}{\alpha_1} \cdot \frac{\partial \mathbf{R}}{\partial q_1} \tag{II.2.7}$$

$$\mathbf{e}_2 = \frac{1}{\alpha_2} \cdot \frac{\partial \mathbf{R}}{\partial q_2} \tag{II.2.8}$$

$$\mathbf{e}_n = \mathbf{e}_1 \times \mathbf{e}_2 \tag{II.2.9}$$

II.3 Squarish toroidal shell A

II.3.1 Geometry

The cross-sectional geometry of a toroidal LPG tank has a geometric configuration similar to that defined by a "squarish" curve (Figs. II.3.1 and II.3.2).

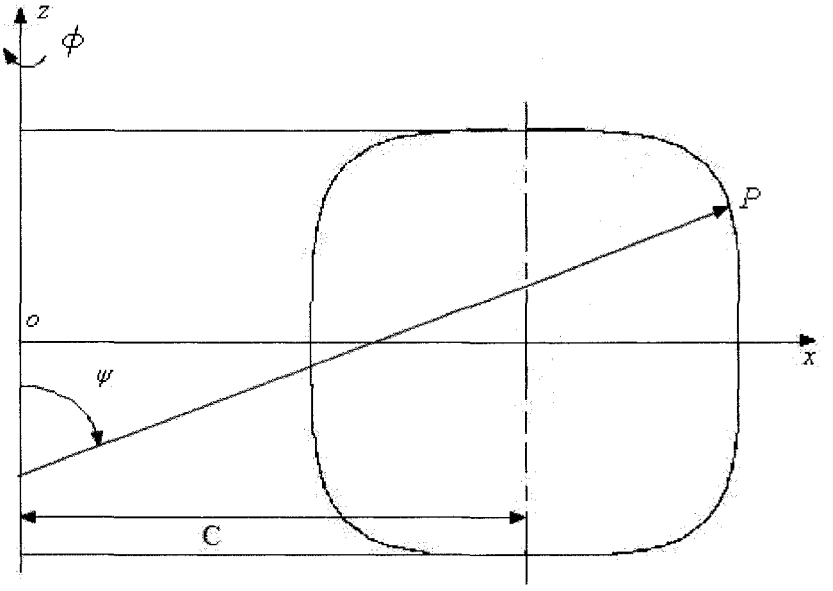

Fig. II.3.1 Cross-section view of squarish toroidal shell A

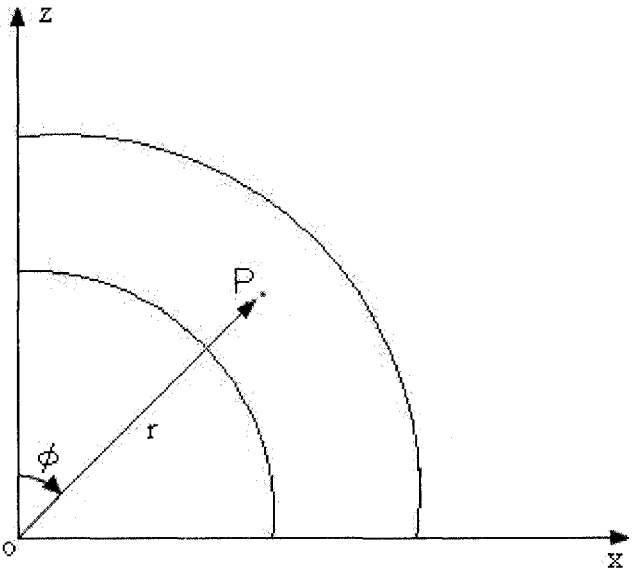

Fig. II.3.2 Top view of squarish toroidal shell A

The "squarish" curve is mathematically defined by:

$$(\frac{r-C}{b})^{2n}+(\frac{z}{a})^{2n}=1 \qquad \text{(II.3.1)}$$

where r is the radius of an arbitrary point P about the z-axis, C is the bend radius; z is the Cartesian coordinate, n is a positive integer (for squarish toroidal shell A, n=2), a and b are half of the elliptic lengths in the x and y directions respectively. It is noted that when n=1 the equation defines a conventional ellipse, and when n=1, a=b a circle is defined.

For the cross-section of squarish toroidal shell A, the angular coordinates are $q_1 = \phi$ and $q_2 = \psi$, where ϕ and ψ are defined in Figs. II.3.1 and II.3.2. The radius r can be expressed in terms of ψ as:

$$r = r(\psi) = b \cdot f_2 / G + C \tag{II.3.2}$$

$$z = z(\psi) = \pm a \cdot \left[1 - \left(\frac{r - C}{b} \right)^{2n} \right]^{\frac{1}{2n}} \tag{II.3.3}$$

where $f_1 = (a \cdot \cos\psi)^{\frac{1}{2n-1}}$; $f_2 = (b \cdot \sin\psi)^{\frac{1}{2n-1}}$; $G = \left(f_1^{2n} + f_2^{2n} \right)^{\frac{1}{2n}}$; $H = G^{2n} = f_1^{2n} + f_2^{2n}$.

II.3.2 The Lamé parameters and curvatures

Inserting Eqns. (II.3.2) and (II.3.3) into Eqn. (II.2.2), the radius vector **R** for the squarish toroidal shell A becomes:

$$\mathbf{R} = r(\psi) \cdot \sin\phi \cdot \mathbf{i} + r(\psi) \cdot \cos\phi \cdot \mathbf{j} + z(\psi) \cdot \mathbf{k} \tag{II.3.4}$$

Then inserting Eqn. (II.3.4) into Eqns. (II.2.3) and (II.2.4), the Lamé parameters are given by:

$$\alpha_1 = r \tag{II.3.5}$$

$$\alpha_2 = r' \sec\psi \tag{II.3.6}$$

where r' is the 1st derivative of r with regard to ψ. From the expressions of α_1 and α_2, it is noted that at a given point α_1 represents the radius of a point on the shell surface about z-axis, and α_2 is the radius of the squarish cross-section.

Inserting Eqn. (II.3.4) into Eqns. (II.2.7) and (II.2.8), the unit vectors are expressed by:

$$\mathbf{e}_1 = \frac{1}{\alpha_1} \cdot \frac{\partial \mathbf{R}}{\partial \varphi} = \cos\varphi \cdot \mathbf{i} - \sin\varphi \cdot \mathbf{j} \tag{II.3.7}$$

$$\mathbf{e}_2 = \frac{1}{\alpha_1} \cdot \frac{\partial \mathbf{R}}{\partial \psi} = \cos\psi \cdot \sin\varphi \cdot \mathbf{i} + \cos\psi \cdot \cos\varphi \cdot \mathbf{j} - \sin\psi \cdot \mathbf{k} \tag{II.3.8}$$

$$\mathbf{e}_n = \mathbf{e}_1 \times \mathbf{e}_2 = \sin\varphi \cdot \sin\psi \cdot \mathbf{i} + \cos\varphi \cdot \sin\psi \cdot \mathbf{j} + \cos\psi \cdot \mathbf{k} \tag{II.3.9}$$

Then inserting Eqns. (II.3.7) - (II.3.9) into Eqns. (II.2.5) and (II.2.6), the curvatures are obtained as:

$$k_1 = \sin\psi / r \tag{II.3.10}$$

$$k_2 = \cos\psi / r' \tag{II.3.11}$$

II.3.3 The derivatives of the Lamé parameters and principle curvatures

The expressions of the derivatives of the Lamé parameters α_1, α_2 and the principle curvatures k_1, k_2 for squarish toroidal shell A are listed in the following. Once these expressions are available the modified DQM program for the squarish toroidal shell A can be written.

For convenience, the notations $()' = \frac{\partial}{\partial \psi}$ and $\dot{()} = \frac{\partial}{\partial \phi}$ are defined. These notations are used throughout in Appendix II.

$$\alpha_1' = b \cdot f_2' \cdot H^{\frac{-1}{2n}} - \frac{b}{2 \cdot n} \cdot f_2 \cdot H' \cdot H^{\frac{-1-2n}{2n}}$$

$$\alpha_1'' = b\cdot f_2''\cdot H^{\frac{-1}{2n}} - \frac{2\cdot b}{2\cdot n}\cdot f_2'\cdot H'\cdot H^{\frac{-1-2n}{2n}} - b\cdot f_2\cdot\left[\frac{1+2\cdot n}{4\cdot n^2}\cdot H'^2\cdot H^{\frac{-1-4n}{2n}} - \frac{1}{2\cdot n}\cdot H''\cdot H^{\frac{-1-2n}{2n}}\right]$$

$$\alpha_1''' = b\cdot f_2'''\cdot H^{\frac{-1}{2n}} - \frac{3\cdot b}{2\cdot n}\cdot f_2''\cdot H'\cdot H^{\frac{-1-2n}{2n}} + b\cdot f_2'\cdot\left[\frac{3\cdot(1+2\cdot n)}{4\cdot n^2}\cdot H'^2\cdot H^{\frac{-1-4n}{2n}} - \frac{3}{2\cdot n}\cdot H''\cdot H^{\frac{-1-2n}{2n}}\right]$$
$$- b\cdot f_2\cdot\left[\frac{(1+2\cdot n)\cdot(1+4\cdot n)}{8\cdot n^3}\cdot H^{\frac{-1-6n}{2n}}\cdot H'^3 - \frac{3\cdot(1+2\cdot n)}{4\cdot n^2}\cdot H^{\frac{-1-4n}{2n}}\cdot H'\cdot H'' + \frac{1}{2\cdot n}\cdot H^{\frac{-1-2n}{2n}}\cdot H'''\right]$$

$$\alpha_1'''' = b\cdot f_2''''\cdot H^{\frac{-1}{2n}} - \frac{4\cdot b}{2\cdot n}\cdot f_2'''\cdot H'\cdot H^{\frac{-1-2n}{2n}} + b\cdot f_2''\cdot\left[\frac{6\cdot(1+2\cdot n)}{4\cdot n^2}\cdot H'^2\cdot H^{\frac{-1-4n}{2n}} - \frac{6}{2\cdot n}\cdot H''\cdot H^{\frac{-1-2n}{2n}}\right]$$
$$- b\cdot f_2'\cdot\left[\frac{4\cdot(1+2\cdot n)\cdot(1+4\cdot n)}{8\cdot n^3}\cdot H^{\frac{-1-6n}{2n}}\cdot H'^3 - \frac{12\cdot(1+2\cdot n)}{4\cdot n^2}\cdot H^{\frac{-1-4n}{2n}}\cdot H'\cdot H'' + \frac{4}{2\cdot n}\cdot H^{\frac{-1-2n}{2n}}\cdot H'''\right]$$
$$+ b\cdot f_2\cdot\left[\begin{array}{l}\frac{(1+2\cdot n)\cdot(1+4\cdot n)\cdot(1+6\cdot n)}{16\cdot n^4}\cdot H^{\frac{-1-8n}{2n}}\cdot H'^4 - \frac{6\cdot(1+2\cdot n)\cdot(1+4\cdot n)}{8\cdot n^3}\cdot H^{\frac{-1-6n}{2n}}\cdot H'^2\cdot H'' \\ + \frac{1+2\cdot n}{4\cdot n^2}\cdot H^{\frac{-1-4n}{2n}}\cdot\left(3\cdot H''^2 + 4\cdot H'\cdot H'''\right) - \frac{1}{2\cdot n}\cdot H^{\frac{-1-2n}{2n}}\cdot H''''\end{array}\right]$$

$$\alpha_2' = r''\cdot\sec\psi + r'\cdot\sin\psi/\cos^2\psi$$

$$\alpha_2'' = r'''\cdot\sec\psi + 2\cdot r''\cdot\sin\psi/\cos^2\psi + r'\cdot\left(2\cdot\sec^3\psi - \sec\psi\right)$$

$$\alpha_2''' = r''''\cdot\sec\psi + 3\cdot r'''\cdot\sin\psi/\cos^2\psi + r''\cdot\left(6/\cos^3\psi - 3/\cos\psi\right) + r'\cdot\left(6\cdot\sin\psi/\cos^4\psi - \sin\psi/\cos^2\psi\right)$$

$$k_1' = \cos\psi/r - \sin\psi\cdot r'/r^2$$

$$k_1'' = -\sin\psi/r - 2\cos\psi\cdot r'/r^2 + 2\sin\psi\cdot r'^2/r^3 - \sin\psi\cdot r''/r^2$$

$$k_1''' = \cos\psi\cdot\left(-1/r + 6\cdot r'^2/r^3 - 3\cdot r''/r^2\right) + \sin\psi\cdot\left(3\cdot r'/r^2 - 6\cdot r'^3/r^4 + 6\cdot r''\cdot r'/r^3 - r'''/r^2\right)$$

$$k_2' = -\sin\psi/r' - \cos\psi\cdot r''/r'^2$$

$$k_2'' = \cos\psi\left(-1/r' + 2\cdot\sin\psi\cdot r''/r'^2 - r'''/r'^2\right) + 2\sin\psi\cdot r''/r'^2$$

$$k_2''' = \cos\psi\cdot\left(-3\cdot r''/r'^2 - 6\cdot r''^3/r'^4 + 6\cdot r''\cdot r'''/r'^3 - r''''/r'^2\right) + \sin\psi\cdot\left(1/r' - 6\cdot r''^2/r'^3 + 3\cdot r'''/r'^2\right)$$

$$r' = \alpha_1', \quad r'' = \alpha_1'', \quad r''' = \alpha_1''', \quad r'''' = \alpha_1''''$$

$$\dot{\alpha}_1 = \ddot{\alpha}_1 = \dddot{\alpha}_1 = 0, \quad \dot{\alpha}_2 = \ddot{\alpha}_2 = \dddot{\alpha}_2 = 0, \quad \dot{k}_1 = \ddot{k}_1 = \dddot{k}_1 = 0, \quad \dot{k}_2 = \ddot{k}_2 = \dddot{k}_2 = 0$$

$$H' = 2 \cdot n \cdot \left({f_1}^{2n-1} \cdot f_1' + {f_2}^{2n-1} \cdot f_2' \right)$$

$$H'' = 2 \cdot n \cdot (2 \cdot n - 1) \cdot \left({f_1}^{2n-2} \cdot f_1'^2 + {f_2}^{2n-2} \cdot f_2'^2 \right) + 2 \cdot n \cdot \left({f_1}^{2n-1} \cdot f_1'' + {f_2}^{2n-1} \cdot f_2'' \right)$$

$$H''' = 2 \cdot n \cdot (2 \cdot n - 1) \cdot (2 \cdot n - 2) \cdot \left({f_1}^{2n-3} \cdot f_1'^3 + {f_2}^{2n-3} \cdot f_2'^3 \right) + 6 \cdot (2 \cdot n - 1) \cdot \left({f_1}^{2n-2} \cdot f_1' \cdot f_1'' + {f_2}^{2n-2} \cdot f_2' \cdot f_2'' \right)$$
$$+ 2 \cdot n \cdot \left({f_1}^{2n-1} \cdot f_1''' + {f_2}^{2n-1} \cdot f_2''' \right)$$

$$H'''' = 2 \cdot n \cdot (2 \cdot n - 1) \cdot (2 \cdot n - 2) \cdot (2 \cdot n - 3) \cdot \left({f_1}^{2n-4} \cdot f_1'^4 + {f_2}^{2n-4} \cdot f_2'^4 \right)$$
$$+ 12 \cdot n \cdot (2 \cdot n - 1) \cdot (2 \cdot n - 2) \cdot \left({f_1}^{2n-3} \cdot f_1'^2 \cdot f_1'' + {f_2}^{2n-3} \cdot f_2'^2 \cdot f_2'' \right) + 6 \cdot (2 \cdot n - 1) \cdot \left({f_1}^{2n-2} \cdot f_1''^2 + {f_2}^{2n-2} \cdot f_2''^2 \right)$$
$$+ 8 \cdot n \cdot (2 \cdot n - 1) \cdot \left({f_1}^{2n-2} \cdot f_1' \cdot f_1''' + {f_2}^{2n-2} \cdot f_2' \cdot f_2''' \right) + 2 \cdot n \cdot \left({f_1}^{2n-1} \cdot f_1'''' + {f_2}^{2n-1} \cdot f_2'''' \right)$$

$$f_1' = -a \cdot \sin\psi \cdot {f_1}^{2-2n} / (2 \cdot n - 1)$$

$$f_1'' = \frac{-f_1}{(2 \cdot n - 1)^2} + \frac{a^2 \cdot (2 - 2 \cdot n) \cdot {f_1}^{3-4n}}{(2 \cdot n - 1)^2}$$

$$f_1''' = \frac{a \cdot \sin\psi \cdot {f_1}^{2-2n}}{(2 \cdot n - 1)^3} - \frac{a^3 \cdot \sin\psi \cdot (2 - 2 \cdot n) \cdot (3 - 4 \cdot n) \cdot {f_1}^{4-6n}}{(2 \cdot n - 1)^3}$$

$$f_1'''' = \frac{f_1}{(2 \cdot n - 1)^4} - \frac{a^2 \cdot (2 - 2 \cdot n) \cdot \left[1 + (3 - 4 \cdot n)^2 \right] \cdot {f_1}^{3-4n}}{(2 \cdot n - 1)^4} + \frac{a^4 \cdot (2 - 2 \cdot n) \cdot (3 - 4 \cdot n) \cdot (4 - 6 \cdot n) \cdot {f_1}^{5-8n}}{(2 \cdot n - 1)^4}$$

$$f_2' = b \cdot \cos\psi \cdot {f_2}^{2-2n} / (2 \cdot n - 1)$$

$$f_2'' = \frac{-f_2}{(2 \cdot n - 1)^2} + \frac{b^2 \cdot (2 - 2 \cdot n) \cdot {f_2}^{3-4n}}{(2 \cdot n - 1)^2}$$

$$f_2''' = -\frac{b \cdot \cos\psi \cdot {f_2}^{2-2n}}{(2 \cdot n - 1)^3} + \frac{b^3 \cdot \cos\psi \cdot (2 - 2 \cdot n) \cdot (3 - 4 \cdot n) \cdot {f_2}^{4-6n}}{(2 \cdot n - 1)^3}$$

$$f_2'''' = \frac{f_2}{(2\cdot n-1)^4} - \frac{b^2\cdot(2-2\cdot n)\cdot\left[1+(3-4\cdot n)^2\right]\cdot f_2^{\,3-4n}}{(2\cdot n-1)^4} + \frac{b^4\cdot(2-2\cdot n)\cdot(3-4\cdot n)\cdot(4-6\cdot n)\cdot f_1^{\,5-8n}}{(2\cdot n-1)^4}$$

II.3.4 Figures of the Lamé parameters, curvatures, and their derivatives

The following figures show the variation of the Lamé parameters, the curvatures, and their derivatives with the angle position ψ (Fig. II.3.1) for squarish toroidal shell A. It is observed that smooth curves are not obtained in all cases. In fact discontinuities occur, despite the fact that the squarish cross-sectional curve appears continuous. It is contended that these discontinuities lead to the unsatisfactory results obtained in the application of the modified DQM program.

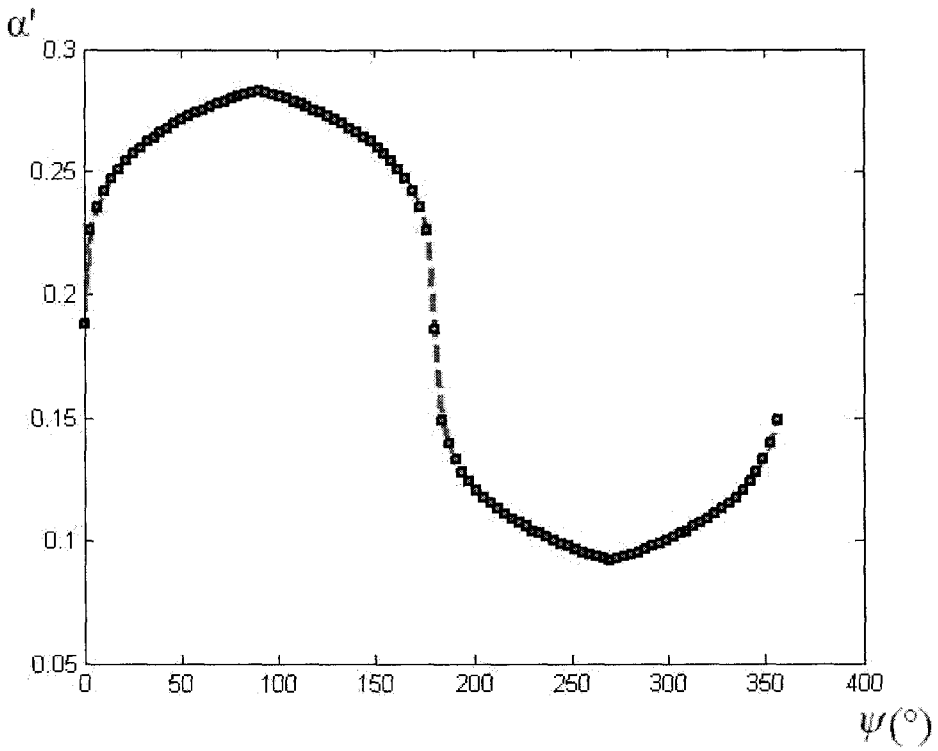

Fig. II.3.3 Lamé parameter α_1 for squarish toroidal shell A

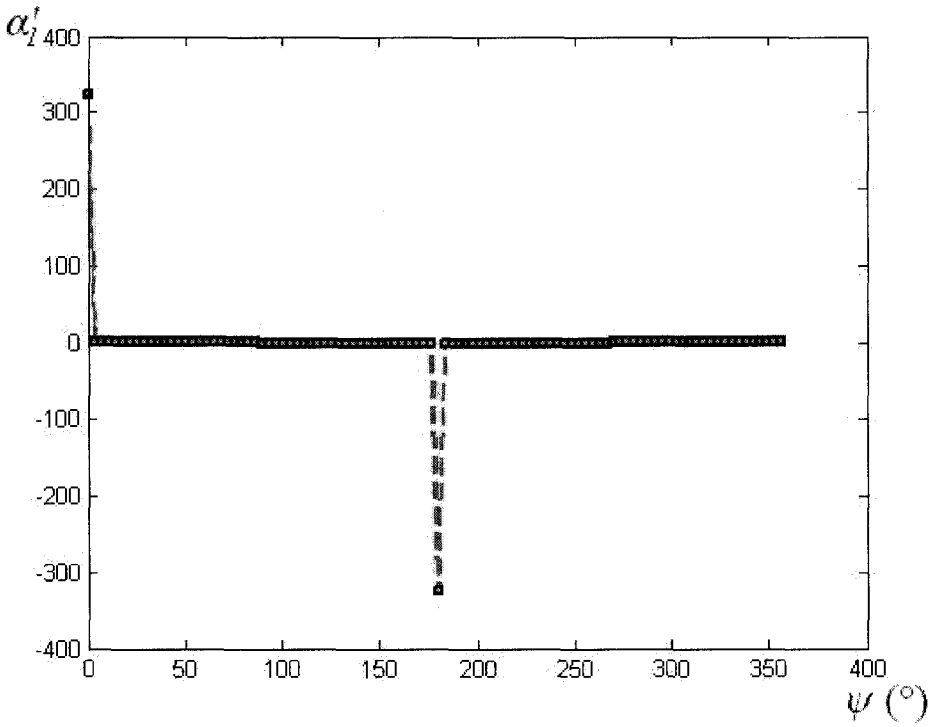

Fig. II.3.4 1st derivative of Lamé parameter α_1 for squarish toroidal shell A

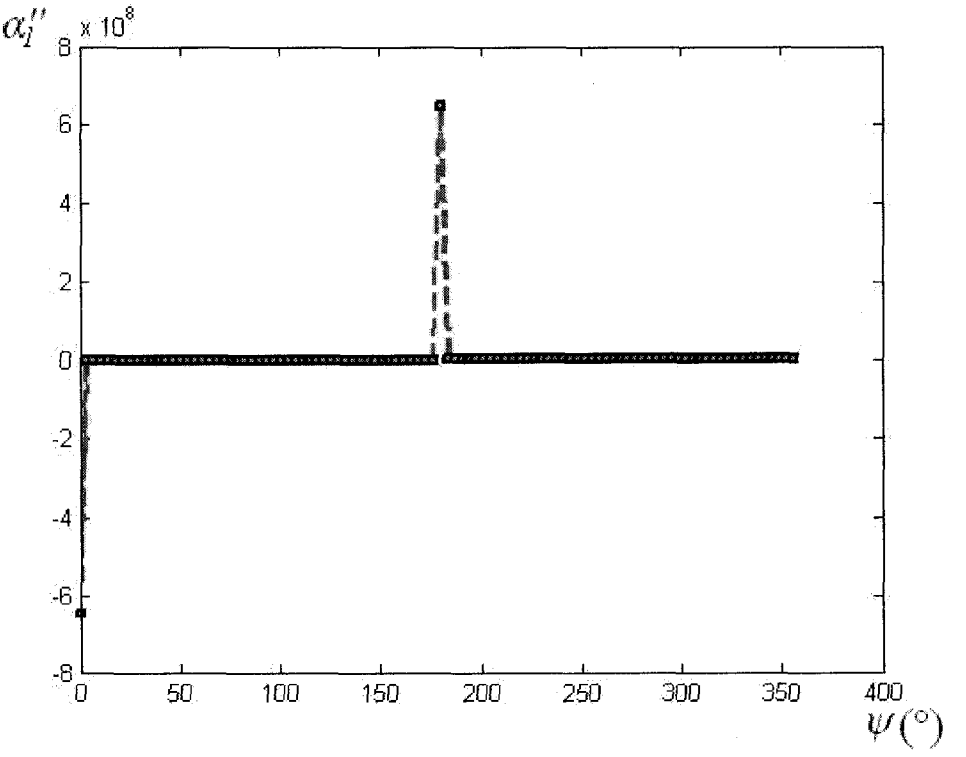

Fig. II.3.5 2nd derivative of Lamé parameter α_1 for squarish toroidal shell A

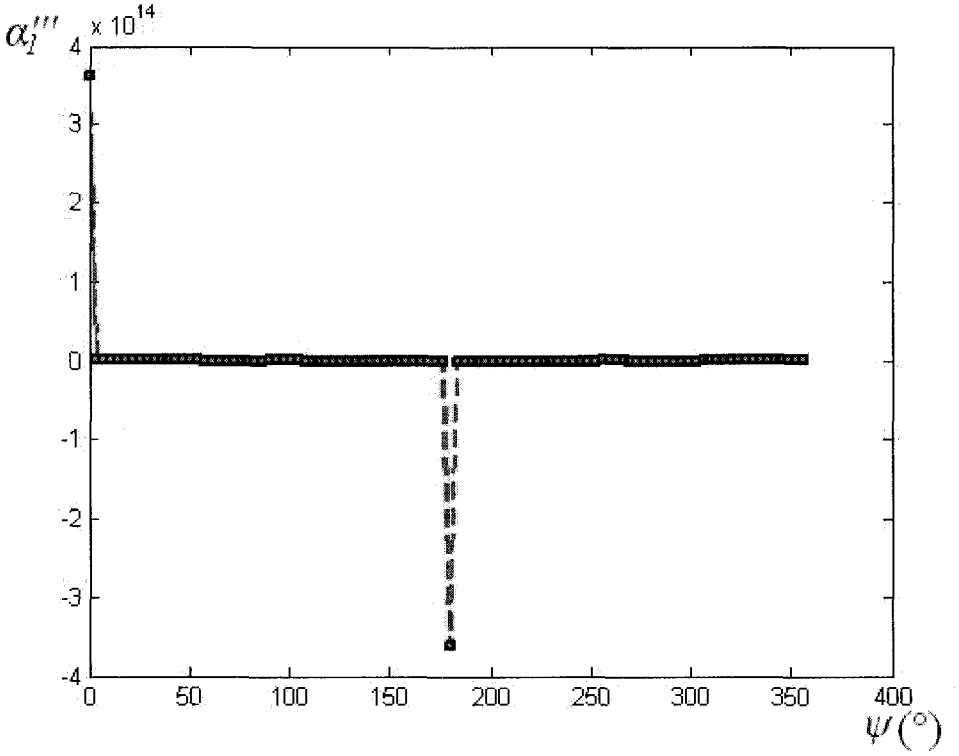

Fig. II.3.6 3rd derivative of Lamé parameter α_1 for squarish toroidal shell A

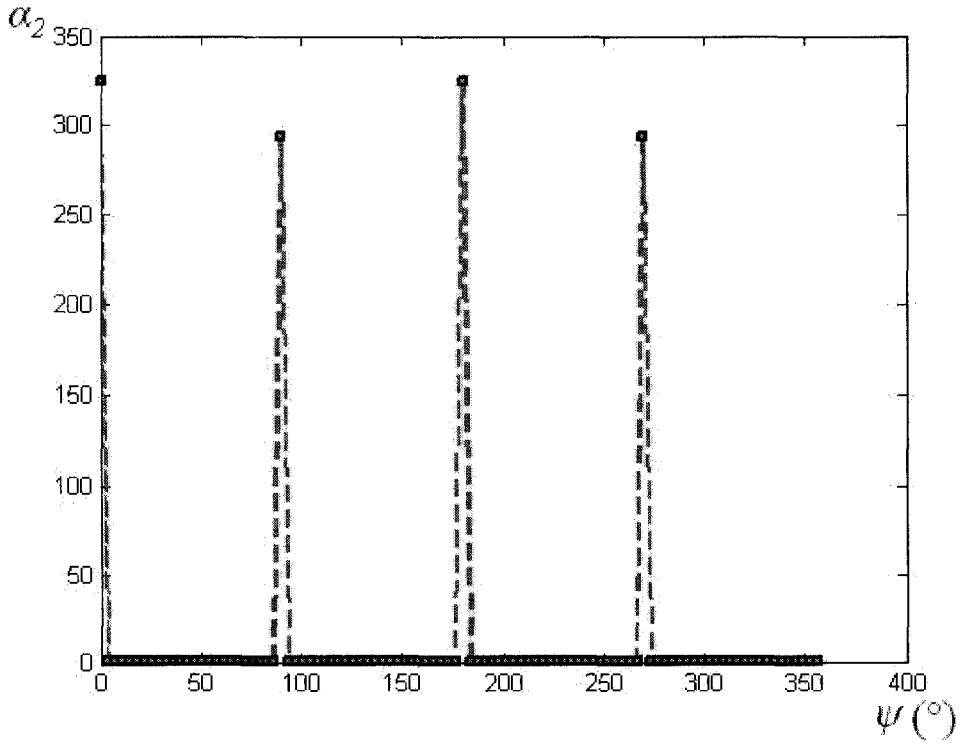

Fig. II.3.7 Lamé parameter α_2 for squarish toroidal shell A

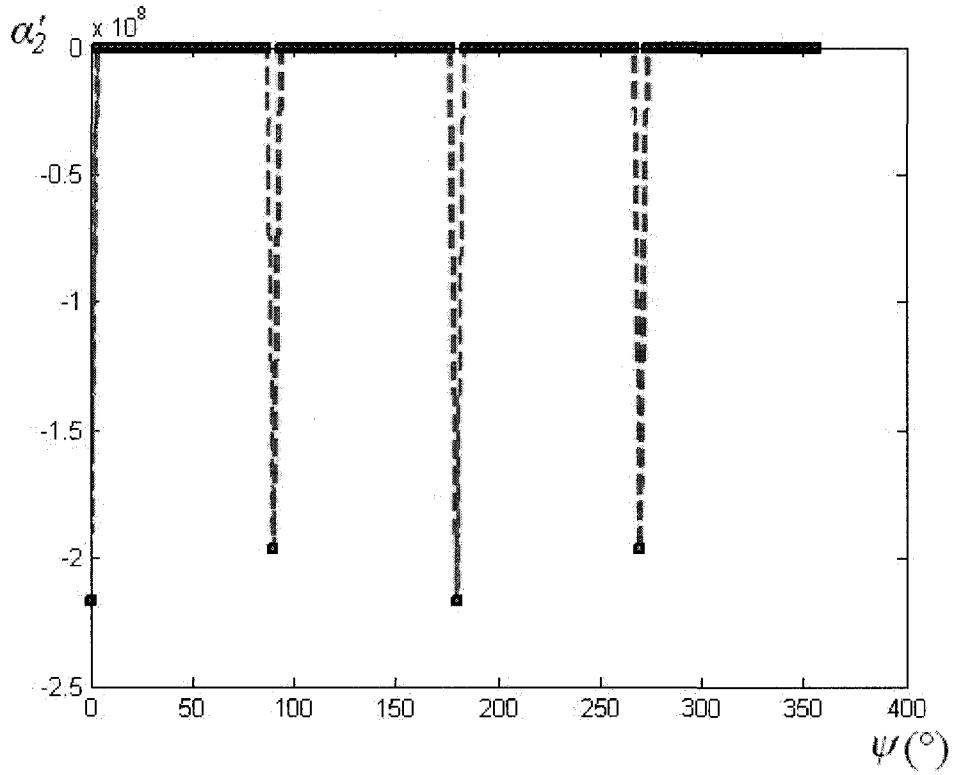

Fig. II.3.8 1st derivative of Lamé parameter α_2 for squarish toroidal shell A

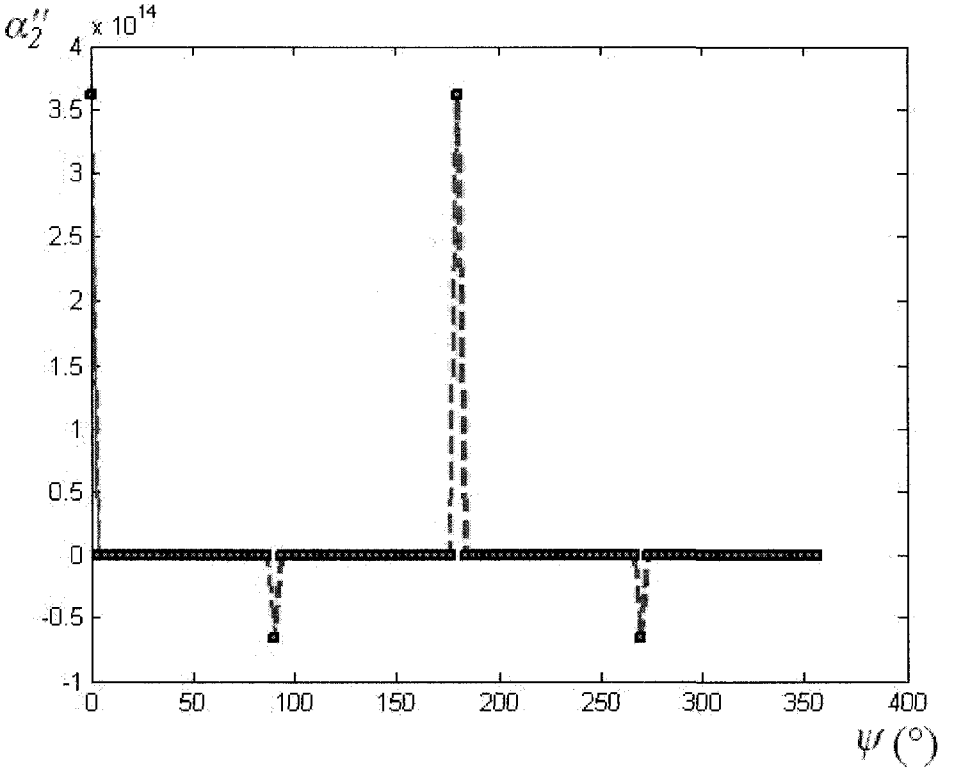

Fig. II.3.9 2nd derivative of Lamé parameter α_2 for squarish toroidal shell A

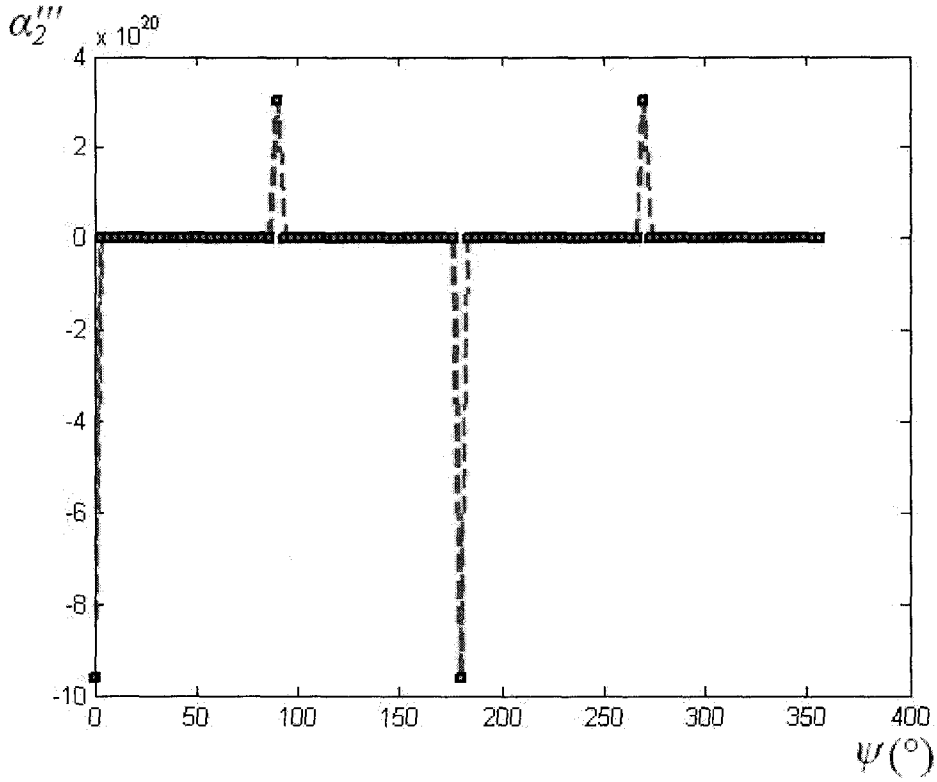

Fig. II.3.10 3rd derivative of Lamé parameter α_2 for squarish toroidal shell A

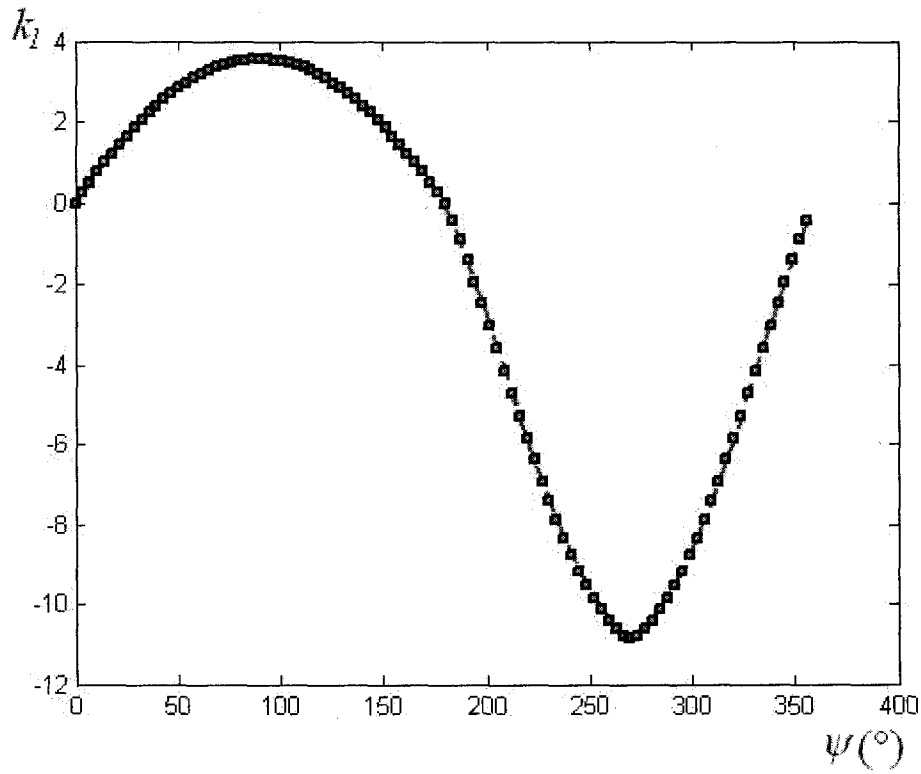

Fig. II.3.11 Curvature k_1 for squarish toroidal shell A

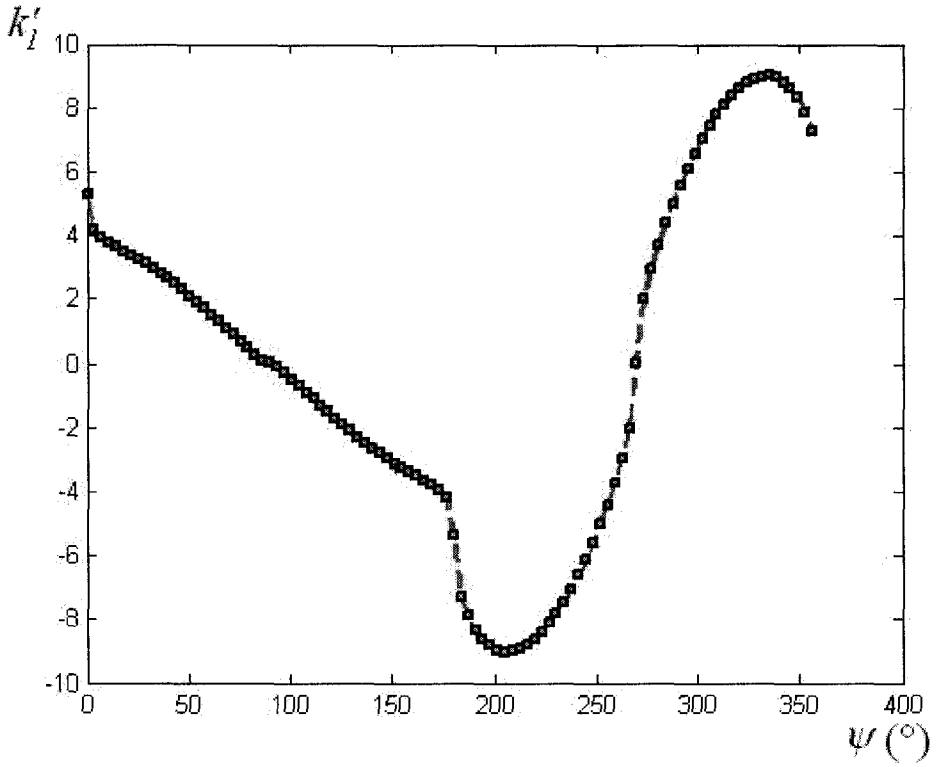

Fig. II.3.12 1st derivative of curvature k_1 for squarish toroidal shell A

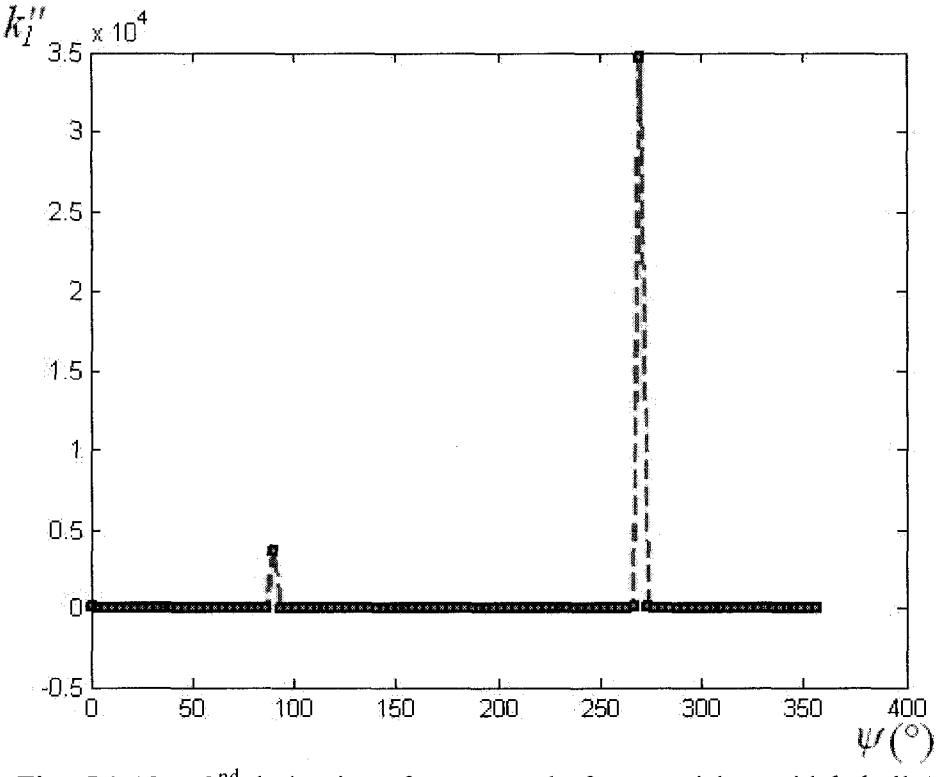

Fig. II.3.13 2nd derivative of curvature k_1 for squarish toroidal shell A

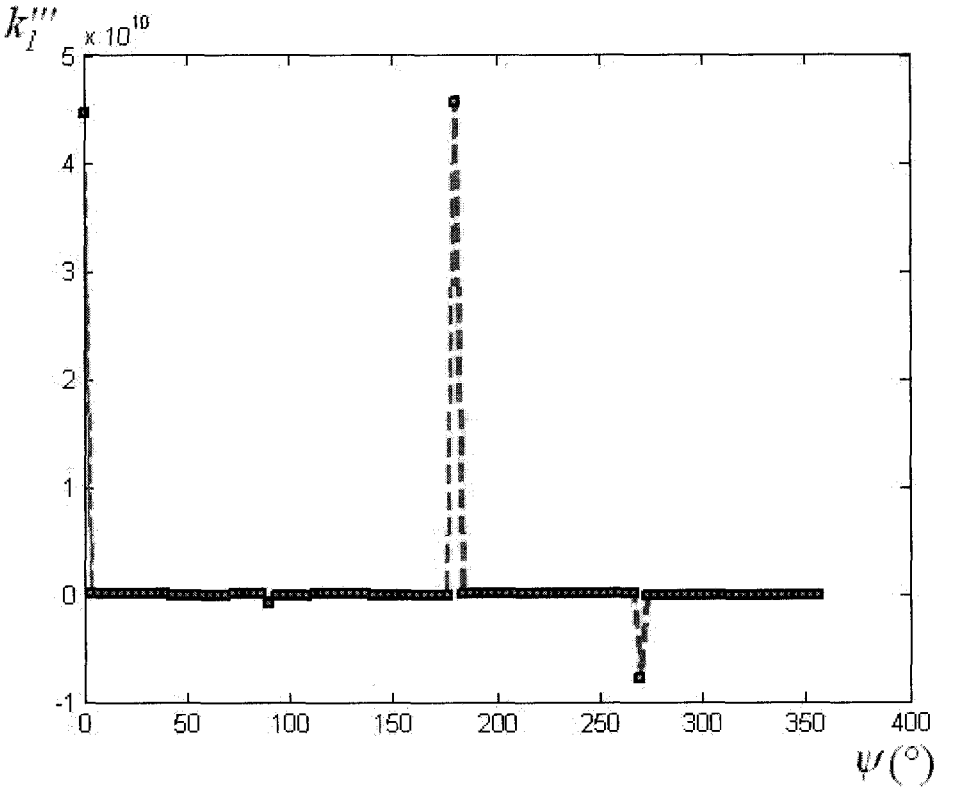

Fig. II.3.14 3rd derivative of curvature k_1 for squarish toroidal shell A

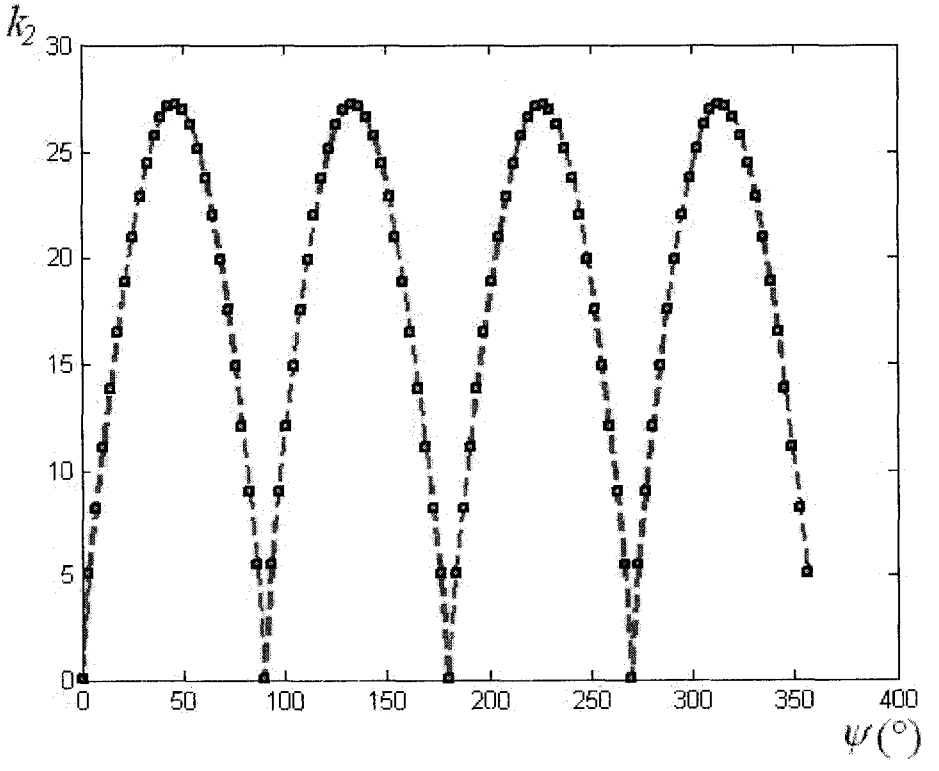

Fig. II.15 Curvature k_2 for squarish toroidal shell A

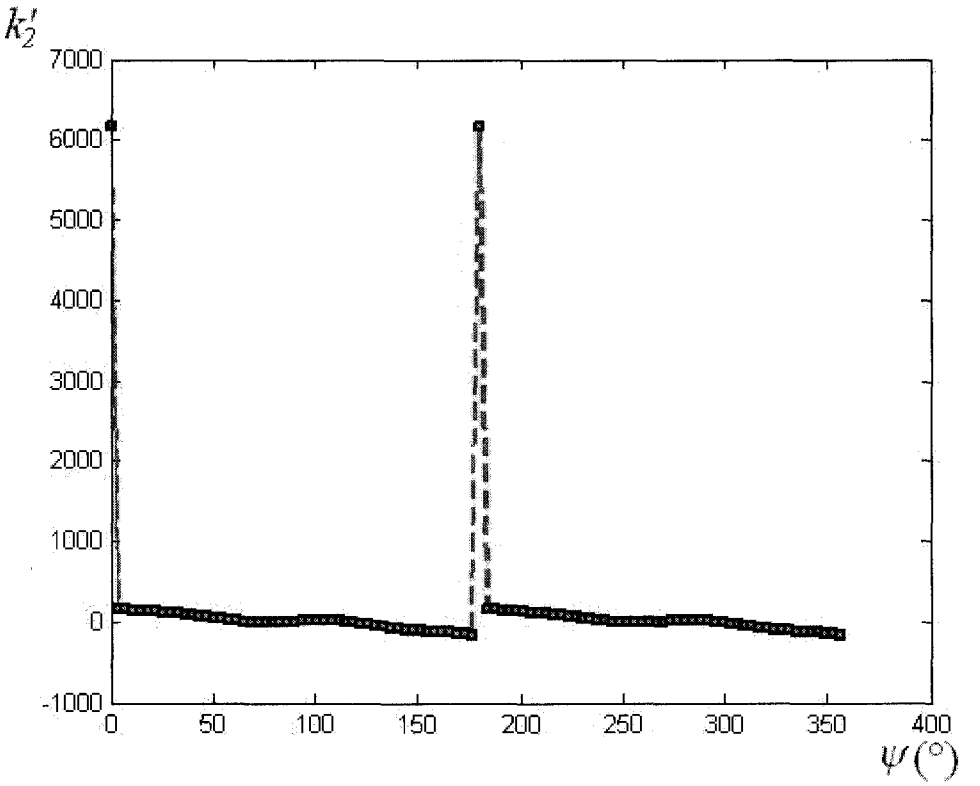

Fig. II.16 1st derivative of curvature k_2 for squarish toroidal shell A

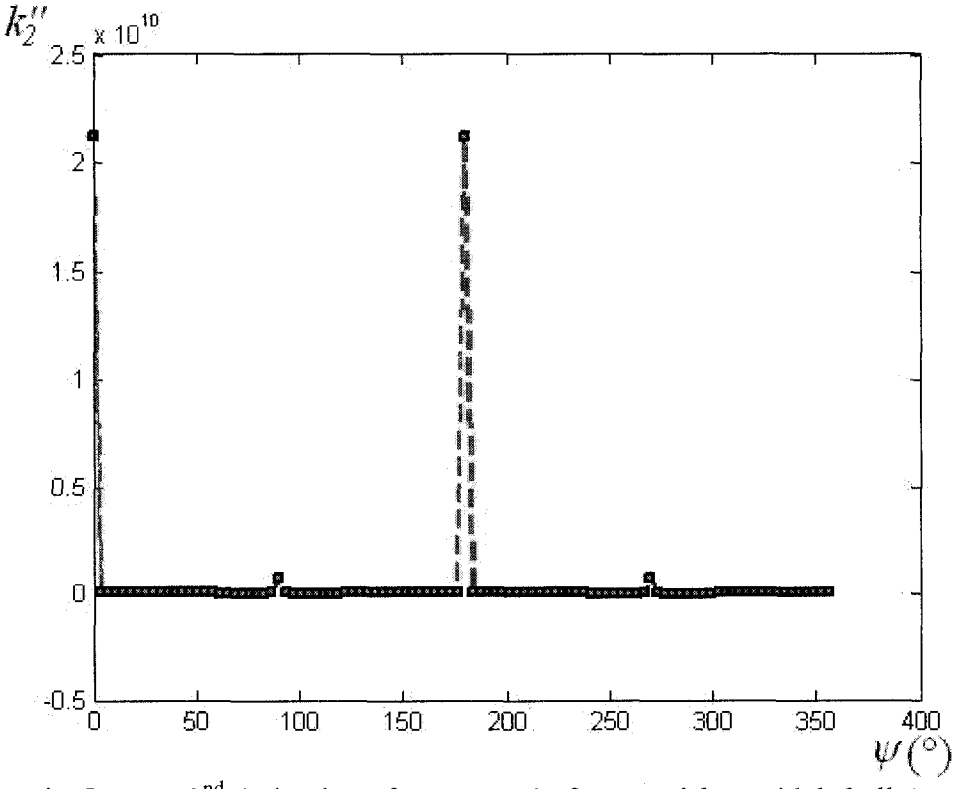

Fig. II.17 2nd derivative of curvature k_2 for squarish toroidal shell A

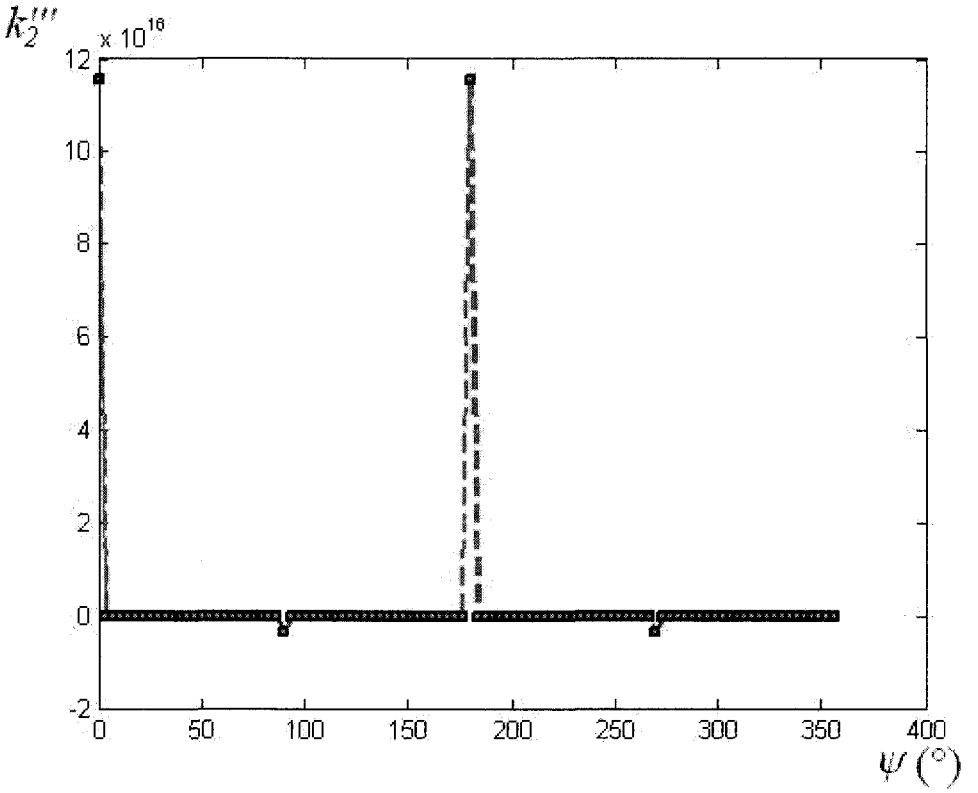

Fig.II.18 3rd derivative of curvature k_2 for squarish toroidal shell A

II.4 Squarish cross-section B

II.4.1 Geometry

The geometry of the squarish toroidal shell B is shown in Fig. II.4.1. The squarish toroidal shell B is of four-lobed cross-section. R_2 is the radius at the lobed corners, while r_2 is defined separately in each lobe, as indicated in the following. A general point P on the shell mid-surface is defined by circumferential and meridional angles ϕ and θ, which are defined in Fig. II.4.1. Therefore, the angular coordinates for this toroidal shell are $q_1 = \phi$, $q_2 = \theta$.

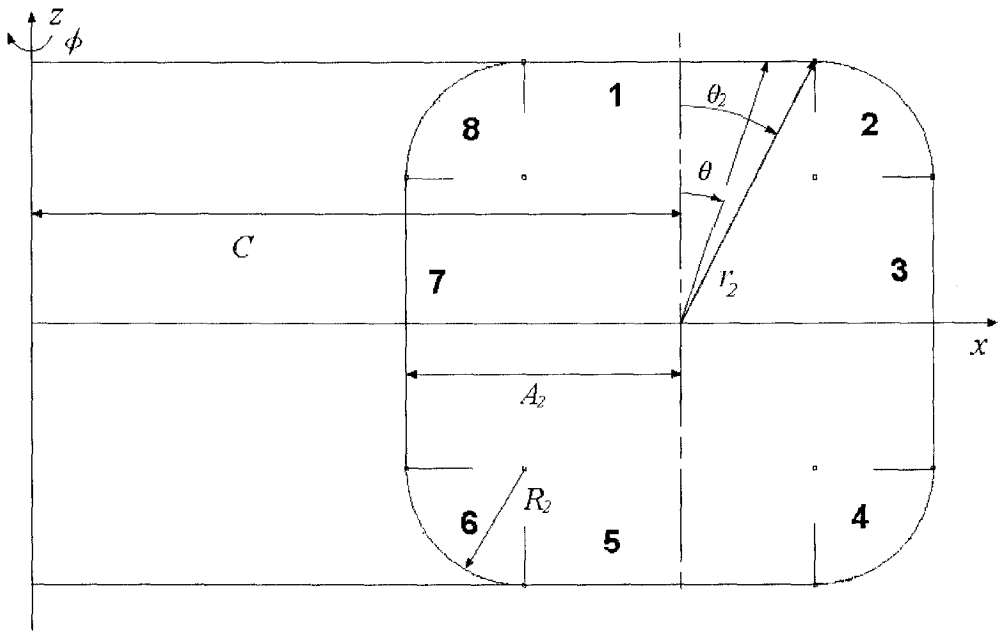

Fig. II.4.1 Cross-section view of the squarish toroidal shell

The profile of the cross-section can be divided into eight parts (Fig. II.4.1), and in these parts r_2 is defined by:

Part 1 (Straight line):

$$r_2 = A_2 \cdot \sec\theta,\ 360^\circ - \theta_2 < \theta < 360^\circ,\ 0 < \theta < \theta_2 \tag{II.4.1}$$

Part 2 (Curved line):

$$r_2 = (A_2 - R_2)(\sin\theta + \cos\theta) + \sqrt{R_2^2 - (A_2 - R_2)^2(1 - \sin 2\theta)},\ \ \theta_2 < \theta < 90^\circ - \theta_2 \tag{II.4.2}$$

Part 3 (Straight line):

$$r_2 = A_2 \cdot \operatorname{cosec}\theta,\ \ 90^\circ - \theta_2 < \theta < 90^\circ + \theta_2 \tag{II.4.3}$$

Part 4 (Curved line):

$$r_2 = (A_2 - R_2)(-\cos\theta + \sin\theta) + \sqrt{R_2^2 - (A_2 - R_2)^2(1 + \sin 2\theta)},\ \ 90^\circ + \theta_2 < \theta < 180^\circ - \theta_2$$

(II.4.4)

Part 5 (Straight line):

$$r_2 = -A_2 \cdot \sec\theta, \quad 180^\circ - \theta_2 < \theta < 180^\circ + \theta_2 \tag{II.4.5}$$

Part 6 (Curved line):

$$r_2 = (A_2 - R_2)(-\sin\theta - \cos\theta) + \sqrt{R_2^2 - (A_2 - R_2)^2(1 - \sin 2\theta)}, \quad 180^\circ + \theta_2 < \theta < 270^\circ - \theta_2$$

(II.4.6)

Part 7 (Straight line):

$$r_2 = -A_2 \cdot \mathrm{cosec}\,\theta, \quad 270^\circ - \theta_2 < \theta < 270^\circ + \theta_2 \tag{II.4.7}$$

Part 8 (Curved line):

$$r_2 = (A_2 - R_2)(-\sin\theta + \cos\theta) + \sqrt{R_2^2 - (A_2 - R_2)^2(1 + \sin 2\theta)}, \quad 270^\circ + \theta_2 < \theta < 360^\circ - \theta_2$$

(II.4.8)

II.4.2 The Lamé parameters and curvatures

The radius vector of squarish toroidal shell B is written as:

$$\mathbf{R} = (C + r_2 \sin\theta)\sin\varphi \cdot \mathbf{i} + (C + r_2 \sin\theta)\cos\varphi \cdot \mathbf{j} + r_2 \cos\theta \cdot \mathbf{k} \tag{II.4.9}$$

Inserting Eqn. (II.4.9) into Eqns. (II.2.3) and (II.2.4), the Lamé parameters are obtained as:

$$\alpha_1 = C + r_2 \cdot \sin\theta \tag{II.4.10}$$

$$\alpha_2 = \sqrt{r_2'^2 + r_2^2} \tag{II.4.11}$$

where r_2' is the 1st derivative of r_2 with regard to the angle θ. α_1 for squarish toroidal shell B actually is the radius of the point P about the z-axis.

Inserting Eqn. (II.4.9) into Eqns. (II.2.5) and (II.2.6), the unit vectors are obtained as:

$$\mathbf{e}_1 = \cos\varphi \cdot \mathbf{i} - \sin\varphi \cdot \mathbf{j} \tag{II.4.12}$$

$$\mathbf{e}_2 = \frac{1}{\alpha_2} \cdot \left[\left(r_2' \cdot \sin\theta + r_2 \cdot \cos\theta \right) \cdot \sin\varphi \cdot \mathbf{i} + \left(r_2' \cdot \sin\theta + r_2 \cdot \cos\theta \right) \cdot \cos\varphi \cdot \mathbf{j} - \left(r_2' \cdot \cos\theta - r_2 \cdot \sin\theta \right) \cdot \mathbf{k} \right] \tag{II.4.13}$$

$$\mathbf{e}_n = \frac{1}{\alpha_2} \left[\left(r_2 \cdot \sin\theta - r_2' \cdot \cos\theta \right) \cdot \sin\varphi \cdot \mathbf{i} + \left(r_2 \cdot \sin\theta - r_2' \cdot \cos\varphi \right) \cdot \cos\varphi \cdot \mathbf{j} + \left(r_2 \cdot \cos\theta + r_2' \cdot \sin\theta \right) \cdot \mathbf{k} \right] \tag{II.4.14}$$

Insert Eqn. (II.4.14) into Eqns. (II.2.5) and (II.2.6), the curvatures are obtained as:

$$k_1 = \frac{J}{\alpha_2} \tag{II.4.15}$$

$$k_2 = \frac{M}{\alpha_2^3} \tag{II.4.16}$$

where $J = \dfrac{r \cdot \sin\theta - r' \cdot \cos\theta}{C + r \cdot \sin\theta}$ and $M = r^2 - r \cdot r'' + 2 \cdot r'^2$.

II.4.3 The derivatives of the Lamé parameters and curvatures

The expressions of the derivatives of the Lamé parameters α_1, α_2 and principle curvatures k_1, k_2 for squarish toroidal shell B are listed in the following.

$\alpha_1' = r_2' \cdot \sin\theta + r_2 \cdot \cos\theta$; $\alpha_1'' = r_2'' \cdot \sin\theta + 2 \cdot r_2' \cdot \cos\theta - r_2 \cdot \sin\theta$;

$\alpha_1''' = r_2''' \cdot \sin\theta + 3 \cdot r_2'' \cdot \cos\theta - 3 \cdot r_2' \cdot \sin\theta - r_2 \cdot \cos\theta$

$\alpha_2' = \dfrac{1}{2} \cdot \left(r_2'^2 + r_2^2 \right)^{\frac{-1}{2}} \cdot \left(2 \cdot r_2' \cdot r_2'' + 2 \cdot r_2 \cdot r_2' \right)$

$\alpha_2'' = -\dfrac{1}{4} \cdot \left(r_2'^2 + r^2 \right)^{\frac{-3}{2}} \cdot \left(2 \cdot r_2' \cdot r_2'' + 2 \cdot r_2 \cdot r_2' \right)^2 + \dfrac{1}{2} \cdot \left(r'^2 + r^2 \right)^{-\frac{1}{2}} \cdot \left(2 \cdot r_2''^2 + 2 \cdot r_2' \cdot r_2''' + 2 \cdot r_2'^2 + 2 \cdot r_2 \cdot r_2'' \right)$

$$\alpha_2''' = -\frac{3}{8}\cdot\left(r_2'^2+r_2^2\right)^{\frac{-5}{2}}\cdot\left(2\cdot r_2'\cdot r_2''+2\cdot r_2\cdot r_2'\right)^3-\frac{3}{4}\cdot\left(r_2'^2+r_2^2\right)^{-\frac{3}{2}}\cdot\left(2\cdot r_2'\cdot r_2''+2\cdot r_2\cdot r_2'\right)\cdot\begin{pmatrix}2\cdot r''^2+2\cdot r_2'\cdot r_2'''\\+2\cdot r_2'^2+2\cdot r_2\cdot r_2''\end{pmatrix}$$

$$+\frac{1}{2}\cdot\left(r_2'^2+r_2^2\right)^{\frac{-1}{2}}\cdot\left(6\cdot r_2''\cdot r_2'''+2\cdot r_2'\cdot r_2''''+6\cdot r_2'\cdot r_2''+2\cdot r_2\cdot r_2'''\right)$$

$$k_1' = \frac{J'}{\alpha_2}-\frac{J\cdot\alpha_2'}{\alpha_2^2}$$

$$k_1'' = \frac{J''}{\alpha_2}-\frac{2\cdot J'\cdot\alpha_2'}{\alpha_2^2}-\frac{J\cdot\alpha_2''}{\alpha_2^2}+\frac{2\cdot J\cdot\alpha_2'^2}{\alpha_2^3}$$

$$k_1''' = \frac{J'''}{\alpha_2}-\frac{3\cdot J''\cdot\alpha_2'}{\alpha_2^2}-\frac{3\cdot J'\cdot\alpha_2''}{\alpha_2^2}+\frac{6\cdot J'\cdot\alpha_2'^2}{\alpha_2^3}-\frac{J\cdot\alpha_2'''}{\alpha_2^2}+\frac{6\cdot J\cdot\alpha_2'\cdot\alpha_2''}{\alpha_2^3}-\frac{6\cdot J\cdot\alpha_2'^3}{\alpha_2^4}$$

$$k_2' = \frac{M'}{\alpha_2^3}-\frac{3\cdot M\cdot\alpha_2'}{\alpha_2^4}$$

$$k_2'' = \frac{M''}{\alpha_2^3}-\frac{6\cdot M'\cdot\alpha_2'}{\alpha_2^4}-\frac{3\cdot M\cdot\alpha_2''}{\alpha_2^4}+\frac{12\cdot M\cdot\alpha_2'^2}{\alpha_2^5}$$

$$k_2''' = \frac{M'''}{\alpha_2^3}-\frac{9\cdot M''\cdot\alpha_2'}{\alpha_2^4}-\frac{9\cdot M'\cdot\alpha_2''}{\alpha_2^4}+\frac{36\cdot M'\cdot\alpha_2'^2}{\alpha_2^5}-\frac{3\cdot M\cdot\alpha_2'''}{\alpha_2^4}+\frac{36\cdot M\cdot\alpha_2'\cdot\alpha_2''}{\alpha_2^5}-\frac{60\cdot M\cdot\alpha_2'^3}{\alpha_2^6}$$

The derivatives of the Lamé parameters and curvatures for the eight parts of the cross-section of squarish toroidal shell B are listed in the following.

First, for the parts of the straight lines:

Part 1 (Straight line):

$$\alpha_1' = \frac{A_2}{\cos^2\theta} \qquad \alpha_1'' = \frac{2\cdot A_2\cdot\sin\theta}{\cos^3\theta} \qquad \alpha_1''' = \frac{6\cdot A_2}{\cos^4\theta}-\frac{4\cdot A_2}{\cos^2\theta}$$

$$\alpha_2' = \frac{2\cdot A_2\cdot\sin\theta}{\cos^3\theta} \qquad \alpha_2'' = \frac{6\cdot A_2}{\cos^4\theta}-\frac{4\cdot A_2}{\cos^2\theta} \qquad \alpha_2''' = \frac{24\cdot A_2\cdot\sin\theta}{\cos^5\theta}-\frac{8\cdot A_2\cdot\sin\theta}{\cos^3\theta}$$

$$k_1 = k_1' = k_1'' = k_1''' = 0$$

$$k_2 = k_2' = k_2'' = k_2''' = 0$$

Part 3 (Straight line):

$$\alpha_1' = \alpha_1'' = \alpha_1''' = 0$$

$$\alpha_2' = -\frac{2 \cdot A_2 \cdot \cos\theta}{\sin^3\theta} \qquad \alpha_2'' = \frac{6 \cdot A_2}{\sin^4\theta} - \frac{4 \cdot A_2}{\sin^2\theta} \qquad \alpha_2''' = -\frac{24 \cdot A_2 \cdot \cos\theta}{\sin^5\theta} + \frac{8 \cdot A_2 \cdot \cos\theta}{\sin^3\theta}$$

$$k_1 = \frac{1}{C + A_2} \qquad k_1' = k_1'' = k_1''' = 0$$

$$k_2 = k_2' = k_2'' = k_2''' = 0$$

Part 5 (Straight line):

$$\alpha_1' = -\frac{A_2}{\cos^2\theta} \qquad \alpha_1'' = -\frac{2 \cdot A_2 \cdot \sin\theta}{\cos^3\theta} \qquad \alpha_1''' = -\frac{6 \cdot A_2}{\cos^4\theta} + \frac{4 \cdot A_2}{\cos^2\theta}$$

$$\alpha_2' = \frac{2 \cdot A_2 \cdot \sin\theta}{\cos^3\theta} \qquad \alpha_2'' = \frac{6 \cdot A_2}{\cos^4\theta} - \frac{4 \cdot A_2}{\cos^2\theta} \qquad \alpha_2''' = \frac{24 \cdot A_2 \cdot \sin\theta}{\cos^5\theta} - \frac{8 \cdot A_2 \cdot \sin\theta}{\cos^3\theta}$$

$$k_1 = k_1' = k_1'' = k_1''' = 0$$

$$k_2 = k_2' = k_2'' = k_2''' = 0$$

Part 7 (Straight line):

$$\alpha_1' = \alpha_1'' = \alpha_1''' = 0$$

$$\alpha_2' = -\frac{2 \cdot A_2 \cdot \cos\theta}{\sin^3\theta} \qquad \alpha_2'' = \frac{6 \cdot A_2}{\sin^4\theta} - \frac{4 \cdot A_2}{\sin^2\theta} \qquad \alpha_2''' = -\frac{24 \cdot A_2 \cdot \cos\theta}{\sin^5\theta} + \frac{8 \cdot A_2 \cdot \cos\theta}{\sin^3\theta}$$

$$k_1 = \frac{1}{C + A_2} \qquad k_1' = k_1'' = k_1''' = 0$$

$$k_2 = k_2' = k_2'' = k_2''' = 0$$

Second, for the parts of curved lines:

Define that:

$$r_2 = V + H^{\frac{1}{2}},$$

$$r_2' = V' + \frac{1}{2} \cdot H^{\frac{-1}{2}} \cdot H',$$

$$r_2'' = V'' - \frac{1}{4} \cdot H^{\frac{-3}{2}} \cdot H'^2 + \frac{1}{2} \cdot H^{\frac{-1}{2}} \cdot H'',$$

$$r_2''' = V''' + \frac{3}{8} \cdot H^{\frac{-5}{2}} \cdot H'^3 - \frac{3}{4} \cdot H^{\frac{-3}{2}} \cdot H' \cdot H'' + \frac{1}{2} \cdot H^{\frac{-1}{2}} \cdot H''',$$

$$r_2'''' = V'''' - \frac{15}{16} \cdot H^{\frac{-7}{2}} \cdot H'^4 + \frac{9}{4} \cdot H^{\frac{-5}{2}} \cdot H'^2 \cdot H'' - \frac{3}{4} \cdot H^{\frac{-3}{2}} \cdot H''^2 - H^{\frac{-3}{2}} \cdot H' \cdot H''' + \frac{1}{2} \cdot H^{\frac{-1}{2}} \cdot H'''',$$

$$r_2''''' = V''''' + \frac{105}{32} \cdot H^{\frac{-9}{2}} \cdot H'^5 - \frac{150}{16} \cdot H^{\frac{-7}{2}} \cdot H'^3 \cdot H'' + \frac{45}{8} \cdot H^{\frac{-5}{2}} \cdot H' \cdot H''^2 + \frac{15}{4} \cdot H^{\frac{-5}{2}} \cdot H'^2 \cdot H''' - \frac{5}{2} \cdot H^{\frac{-3}{2}} \cdot H'' \cdot H'''$$
$$- \frac{5}{4} \cdot H^{\frac{-3}{2}} \cdot H' \cdot H'''' + \frac{1}{2} \cdot H^{\frac{-1}{2}} \cdot H'''''$$

Part 2 (Curved line):

$V = (A_2 - R_2)(\sin\theta + \cos\theta)$ $\qquad$ $H = R_2^2 - (A_2 - R_2)^2(1 - \sin 2\theta)$

$V' = (A_2 - R_2)(\cos\theta - \sin\theta)$ $\qquad$ $H' = 2 \cdot (A_2 - R_2)^2 \cdot \cos 2\theta$

$V'' = (A_2 - R_2)(-\sin\theta - \cos\theta)$ $\qquad$ $H'' = -4 \cdot (A_2 - R_2)^2 \cdot \sin 2\theta$

$V''' = (A_2 - R_2)(-\cos\theta + \sin\theta)$ $\qquad$ $H''' = -8 \cdot (A_2 - R_2)^2 \cdot \cos 2\theta$

$V'''' = (A_2 - R_2)(\sin\theta + \cos\theta)$ $\qquad$ $H'''' = 16 \cdot (A_2 - R_2)^2 \cdot \sin 2\theta$

$V''''' = (A_2 - R_2)(\cos\theta - \sin\theta)$ $\qquad$ $H''''' = 32 \cdot (A_2 - R_2)^2 \cdot \cos 2\theta$

Part 4 (Curved line):

$V = (A_2 - R_2)(-\cos\theta + \sin\theta)$ $\quad H = R_2^2 - (A_2 - R_2)^2(1 + \sin 2\theta)$

$V' = (A_2 - R_2)(\sin\theta + \cos\theta)$ $\quad H' = -2 \cdot (A_2 - R_2)^2 \cdot \cos 2\theta$

$V'' = (A_2 - R_2)(\cos\theta - \sin\theta)$ $\quad H'' = 4 \cdot (A_2 - R_2)^2 \cdot \sin 2\theta$

$V''' = (A_2 - R_2)(-\sin\theta - \cos\theta)$ $\quad H''' = 8 \cdot (A_2 - R_2)^2 \cdot \cos 2\theta$

$V'''' = (A_2 - R_2)(-\cos\theta + \sin\theta)$ $\quad H'''' = -16 \cdot (A_2 - R_2)^2 \cdot \sin 2\theta$

$V''''' = (A_2 - R_2)(\sin\theta + \cos\theta)$ $\quad H''''' = -32 \cdot (A_2 - R_2)^2 \cdot \cos 2\theta$

Part 6 (Curved line):

$V = (A_2 - R_2)(-\sin\theta - \cos\theta)$ $\quad H = R_2^2 - (A_2 - R_2)^2(1 - \sin 2\theta)$

$V' = (A_2 - R_2)(-\cos\theta + \sin\theta)$ $\quad H' = 2 \cdot (A_2 - R_2)^2 \cdot \cos 2\theta$

$V'' = (A_2 - R_2)(\sin\theta + \cos\theta)$ $\quad H'' = -4 \cdot (A_2 - R_2)^2 \cdot \sin 2\theta$

$V''' = (A_2 - R_2)(\cos\theta - \sin\theta)$ $\quad H''' = -8 \cdot (A_2 - R_2)^2 \cdot \cos 2\theta$

$V'''' = (A_2 - R_2)(-\sin\theta - \cos\theta)$ $\quad H'''' = 16 \cdot (A_2 - R_2)^2 \cdot \sin 2\theta$

$V''''' = (A_2 - R_2)(-\cos\theta + \sin\theta)$ $\quad H''''' = 32 \cdot (A_2 - R_2)^2 \cdot \cos 2\theta$

Part 8 (Curved line):

$V = (A_2 - R_2)(-\sin\theta + \cos\theta)$ $\quad H = R_2^2 - (A_2 - R_2)^2(1 + \sin 2\theta)$

$V' = (A_2 - R_2)(-\cos\theta - \sin\theta)$ $\quad H' = -2 \cdot (A_2 - R_2)^2 \cdot \cos 2\theta$

$V'' = (A_2 - R_2)(\sin\theta - \cos\theta)$ $\quad H'' = 4 \cdot (A_2 - R_2)^2 \cdot \sin 2\theta$

$V''' = (A_2 - R_2)(\cos\theta + \sin\theta)$ $\quad H''' = 8 \cdot (A_2 - R_2)^2 \cdot \cos 2\theta$

$$V''''=(A_2-R_2)(-\sin\theta+\cos\theta) \qquad H''''=-16\cdot(A_2-R_2)^2\cdot\sin 2\theta$$

$$V'''''=(A_2-R_2)(-\cos\theta-\sin\theta) \qquad H'''''=-32\cdot(A_2-R_2)^2\cdot\cos 2\theta$$

II.4.4 Figures of the Lamé parameters, curvatures, and their derivatives

The following figures show the variation of the Lamé parameters, the curvatures, and their derivatives with the angular position θ for squarish toroidal shell B. Again discontinuities arise in the plots, which cause difficulties in the DQM approach.

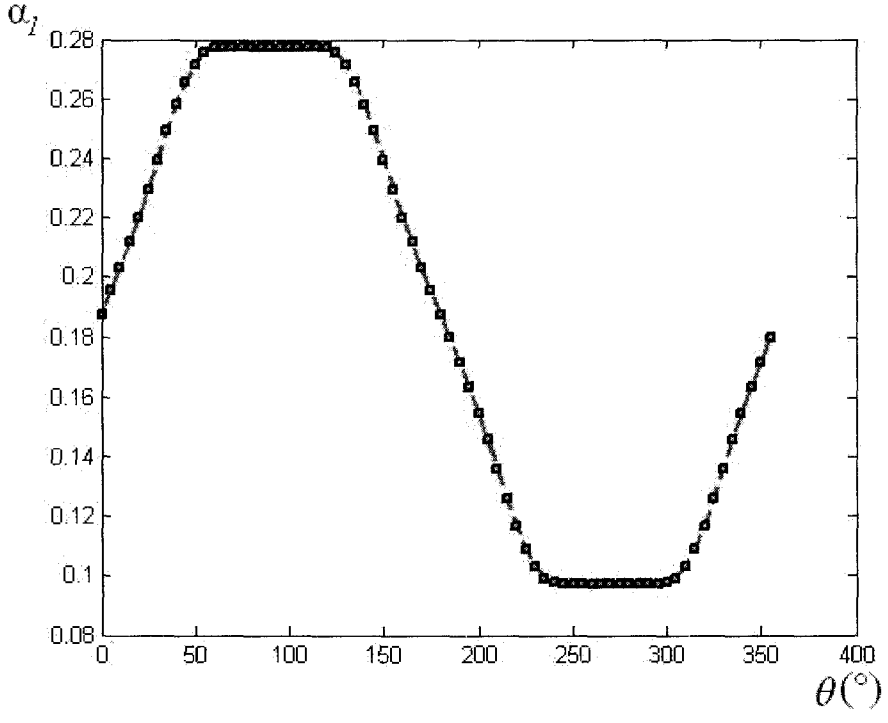

Fig. II.4.2 Lamé parameter α_1 for squarish toroidal shell B

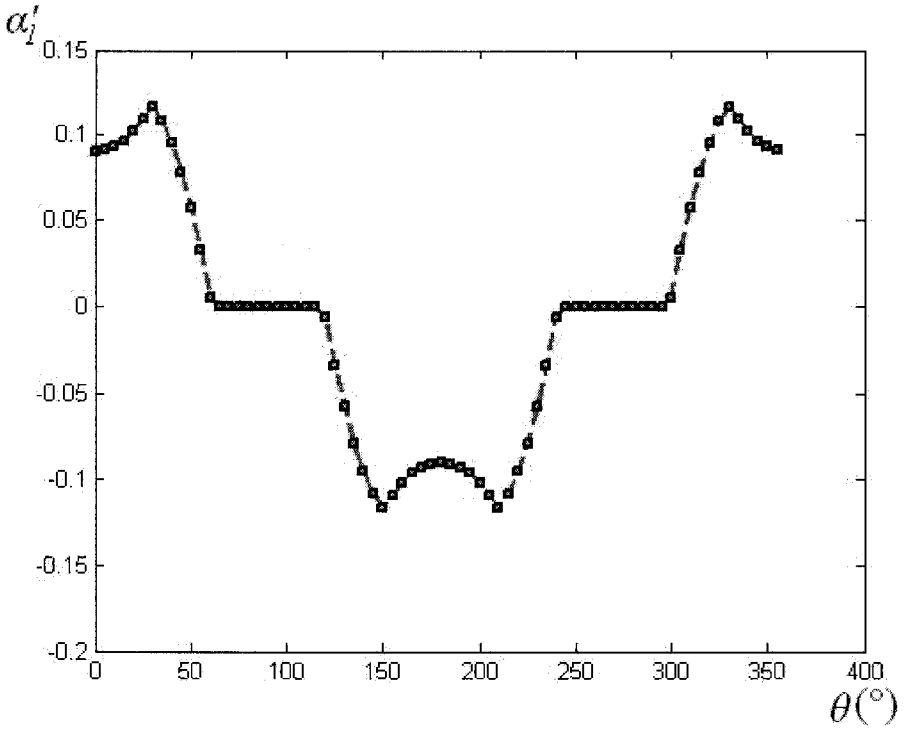

Fig. II.4.3 1st derivative of Lamé parameter α_1 for squarish toroidal shell B

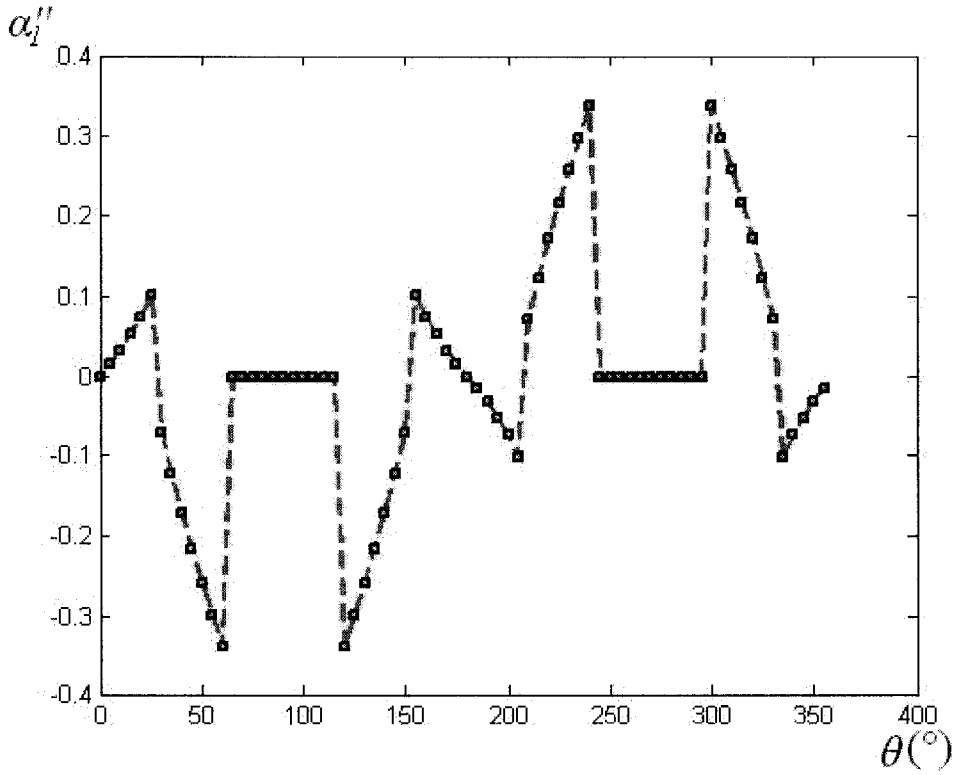

Fig. II.4.4 2nd derivative of Lamé parameter α_1 for squarish toroidal shell B

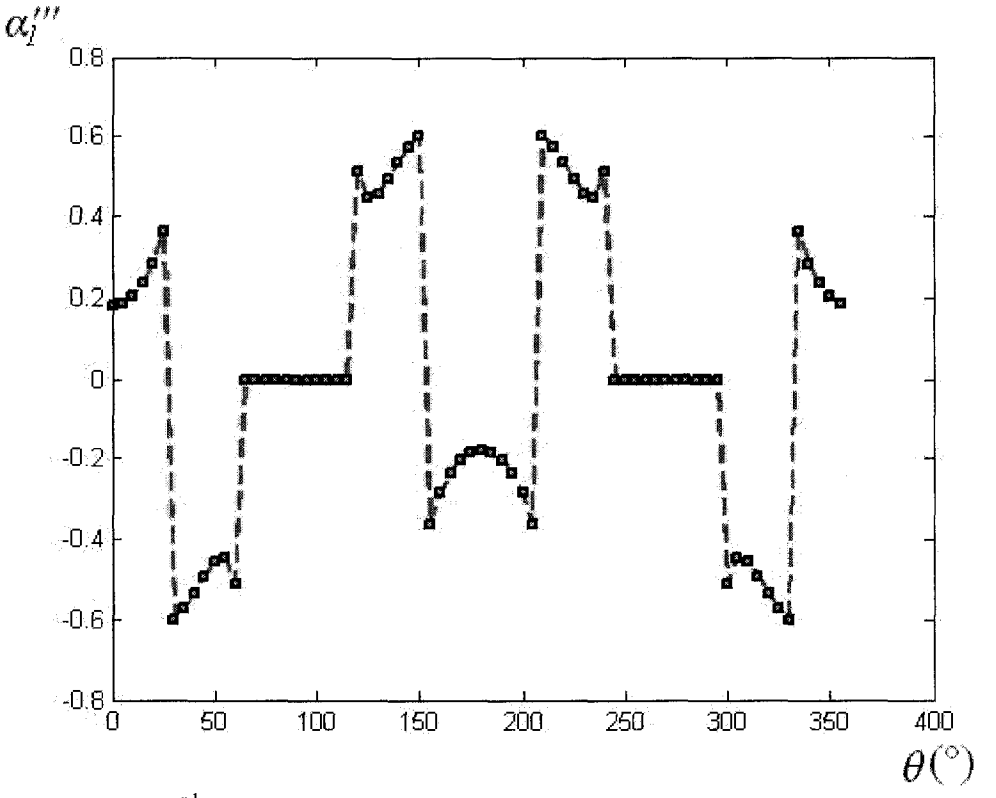

Fig. II.4.5 3rd derivative of Lamé parameter α_1 for squarish toroidal shell B

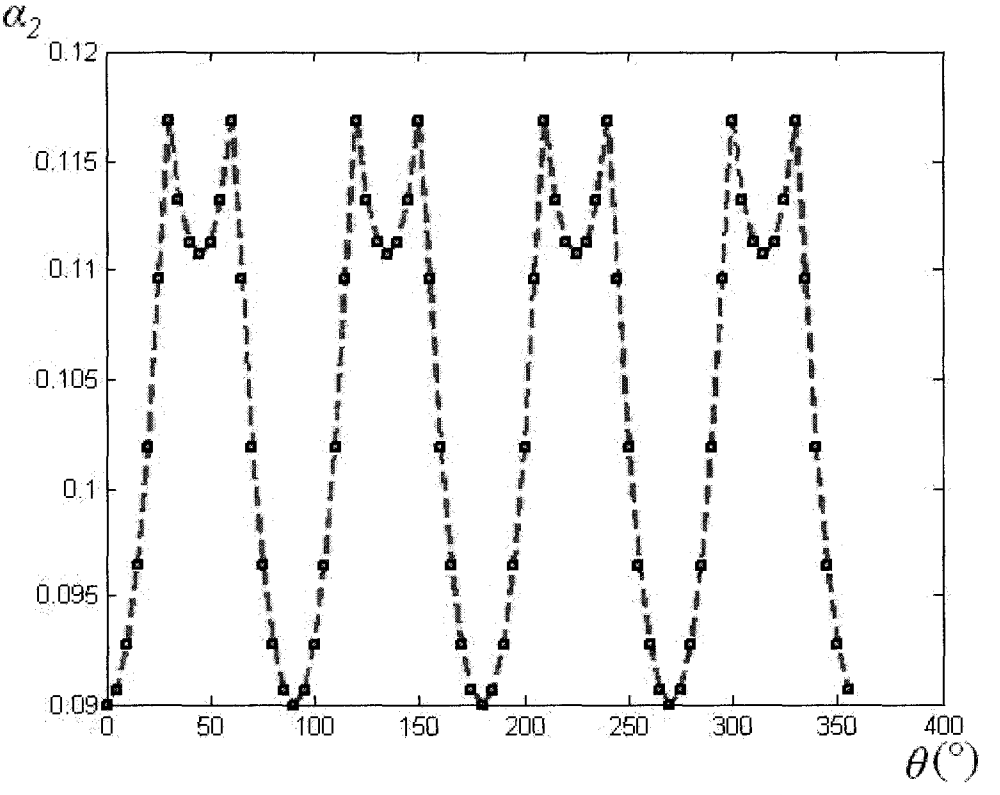

Fig. II.4.6 Lamé parameter α_2 for squarish toroidal shell B

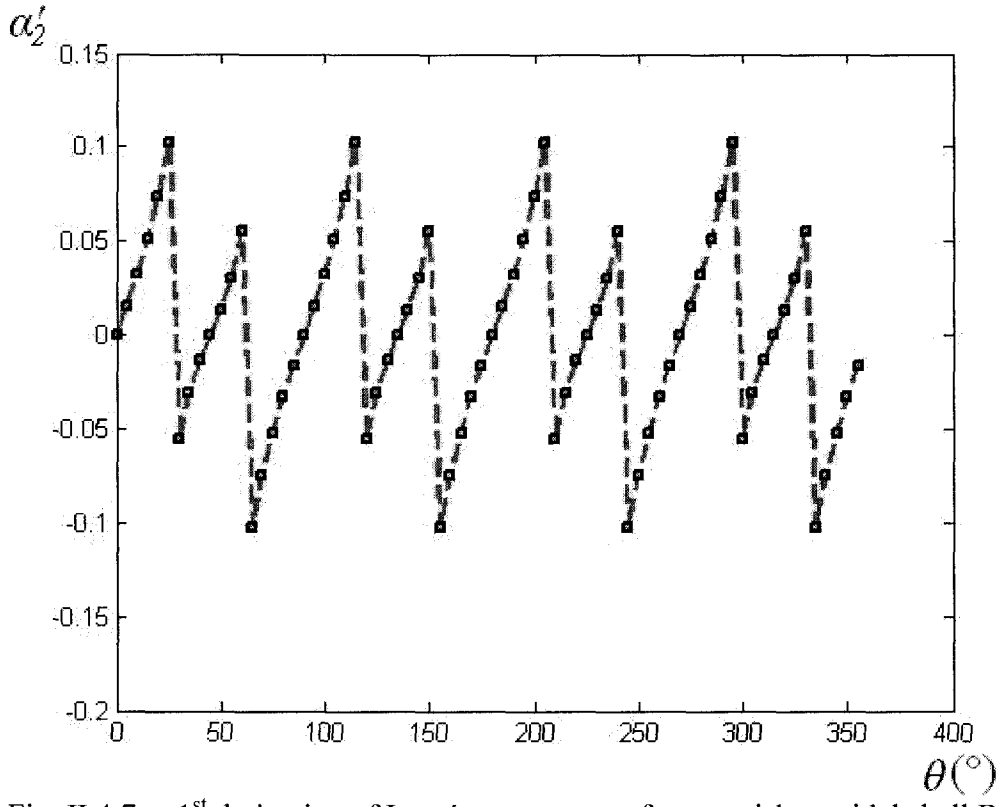

Fig. II.4.7 1st derivative of Lamé parameter α_2 for squarish toroidal shell B

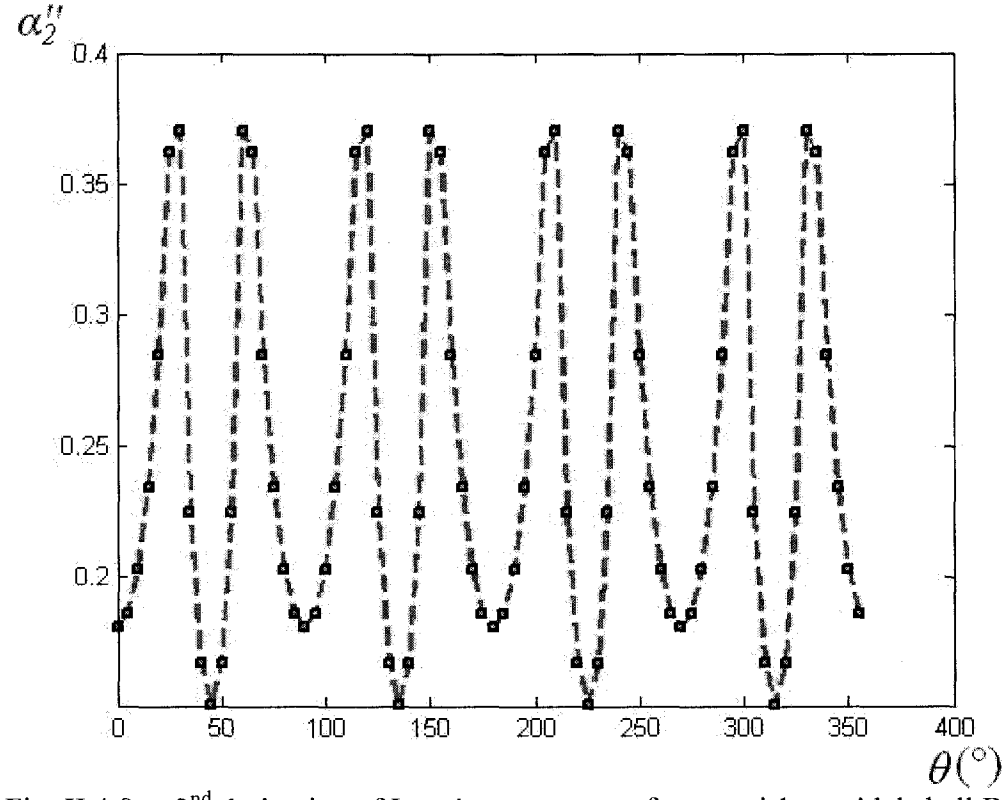

Fig. II.4.8 2nd derivative of Lamé parameter α_2 for squarish toroidal shell B

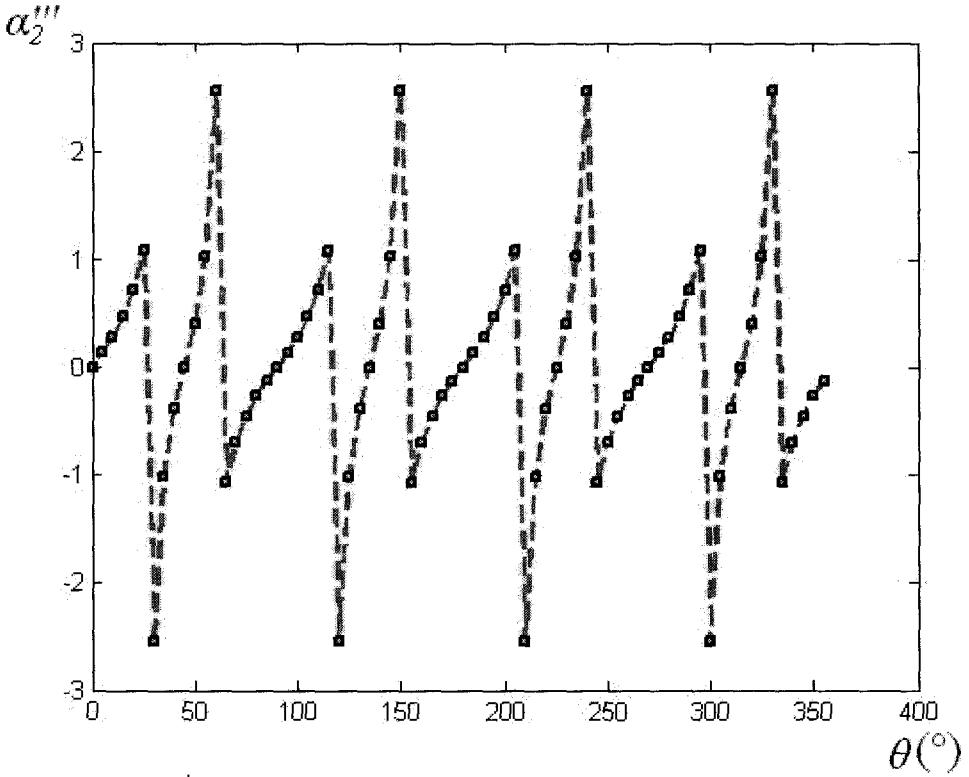

Fig. II.4.9 3rd derivative of Lamé parameter α_2 for squarish toroidal shell B

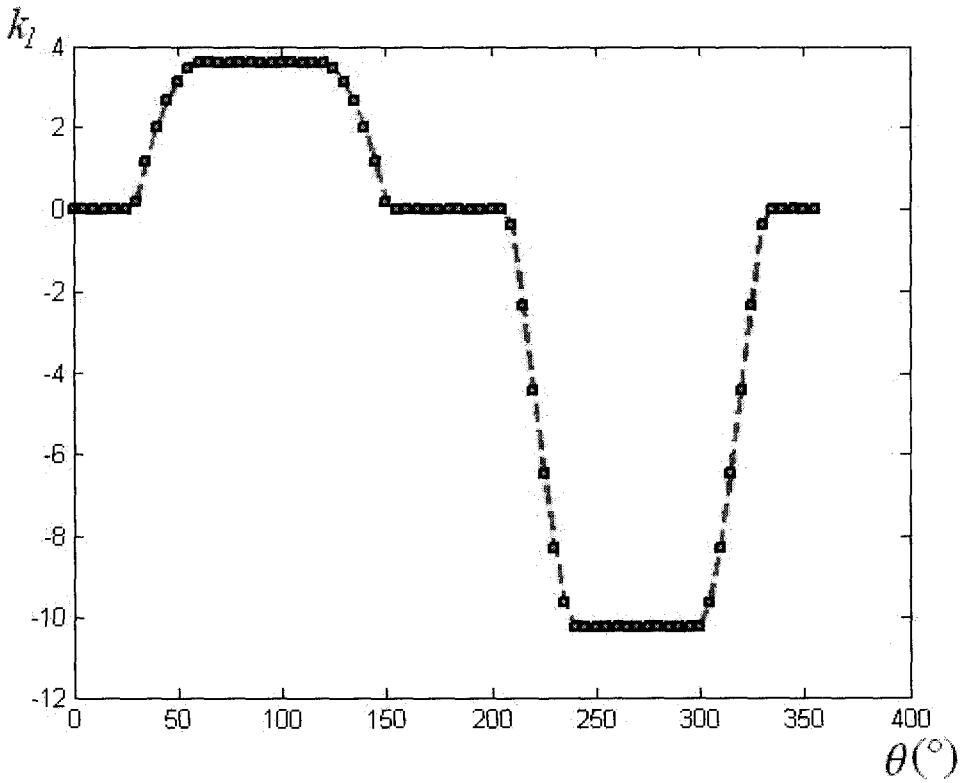

Fig. II.4.10 Curvature k_1 for squarish toroidal shell B

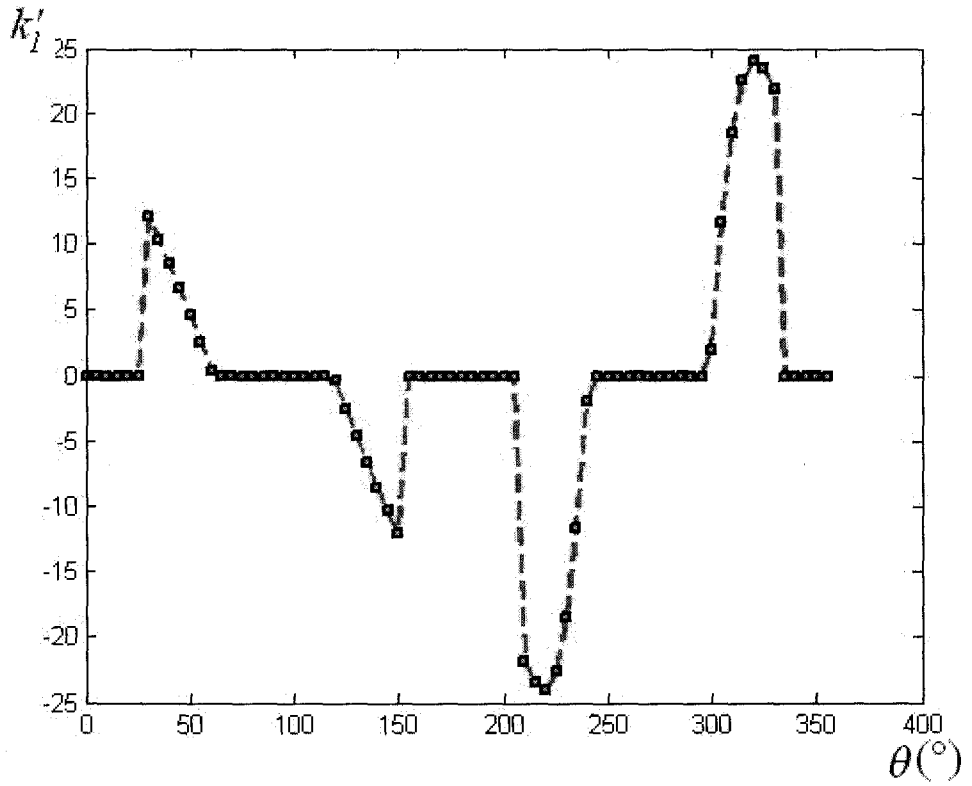

Fig. II.4.11 1st derivative of curvature k_1 for squarish toroidal shell B

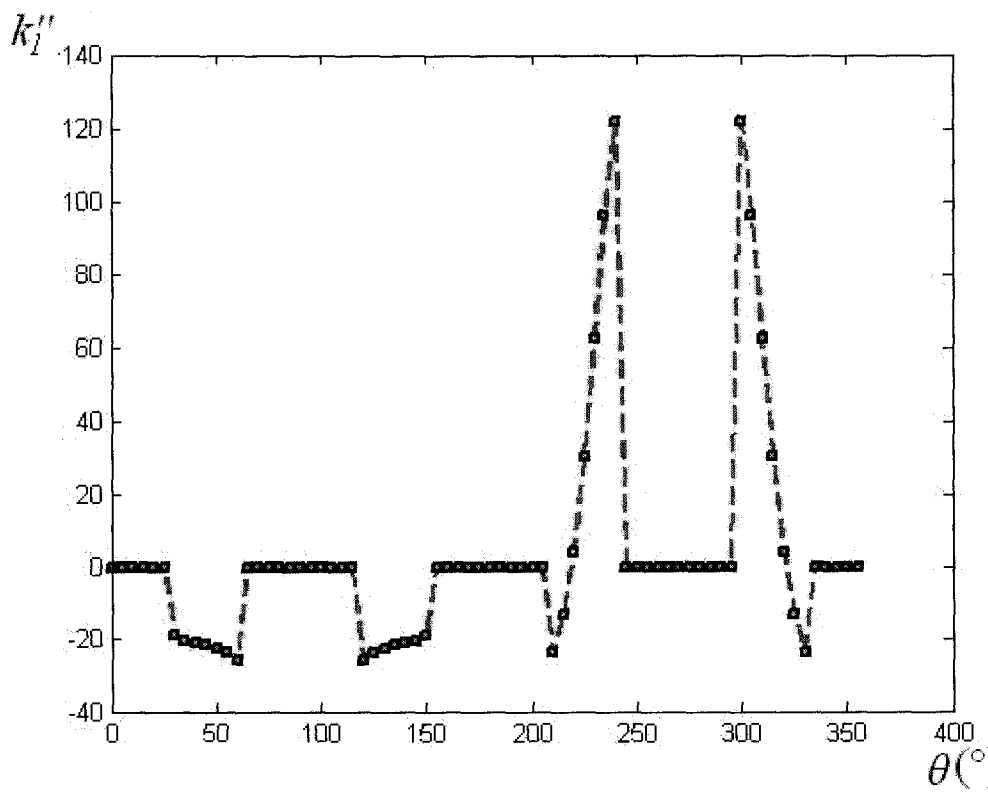

Fig. II.4.12 2nd derivative of curvature k_1 for squarish toroidal shell B

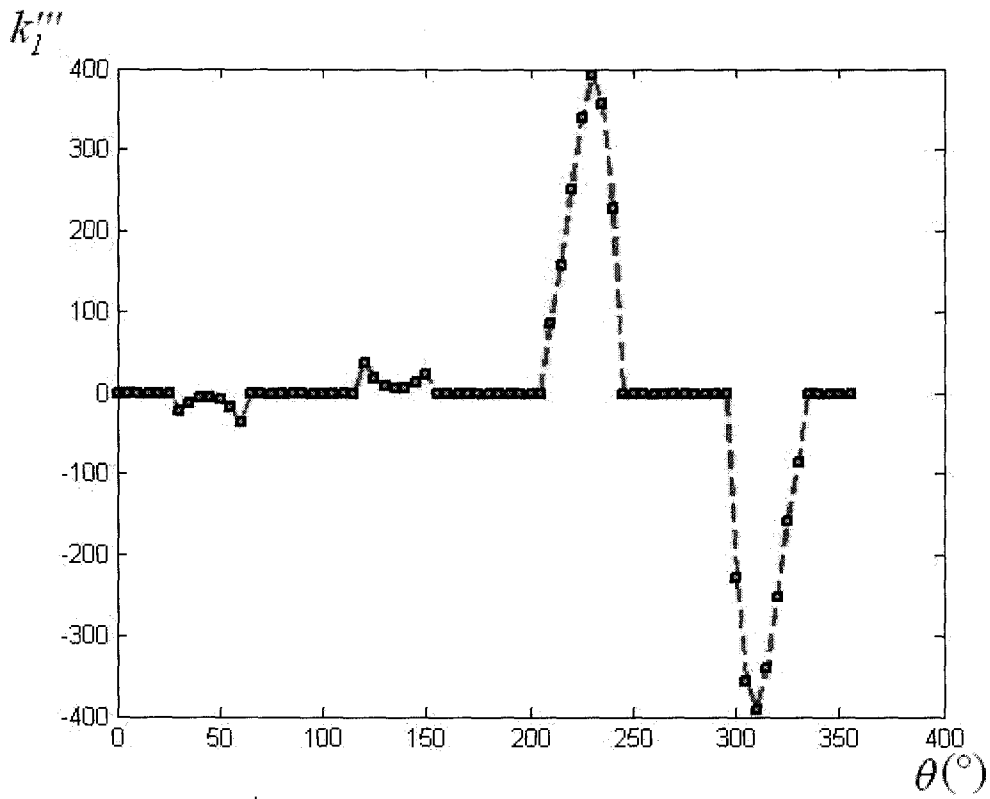

Fig. II.4.13 3rd derivative of curvature k_1 for squarish toroidal shell B

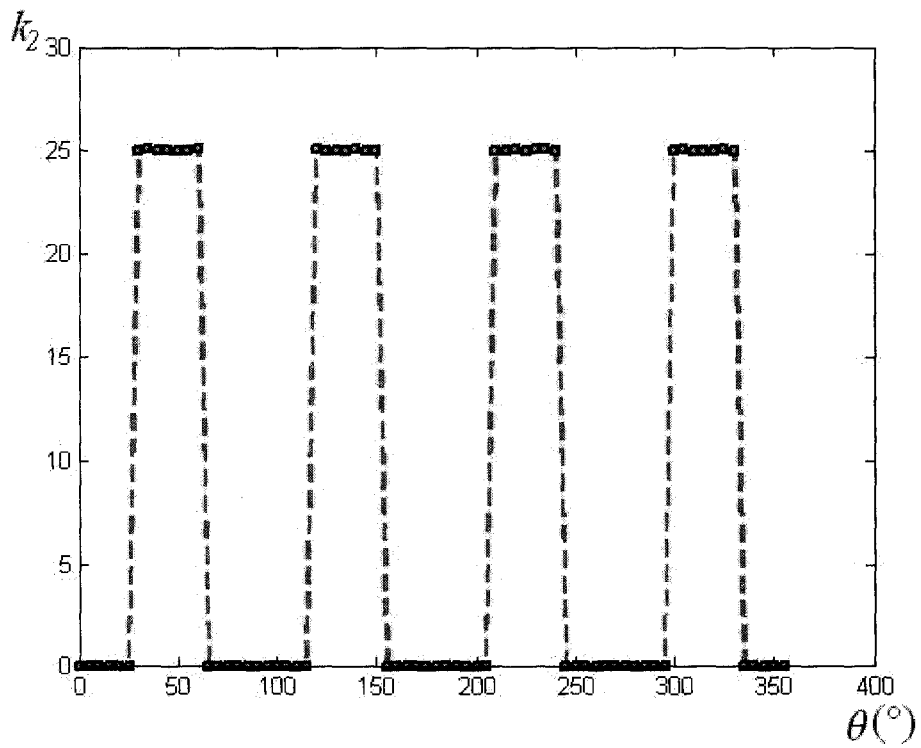

Fig. II.4.14 Curvature k_2 for squarish toroidal shell B

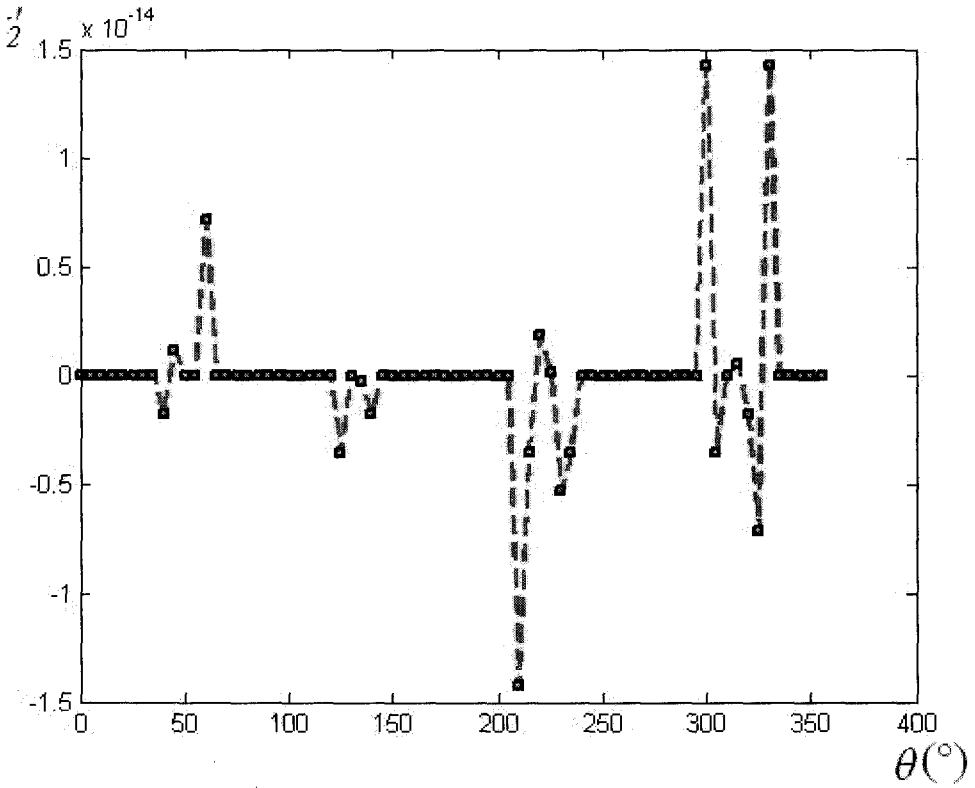

Fig. II.4.15 1st derivative of curvature k_2 for squarish toroidal shell B

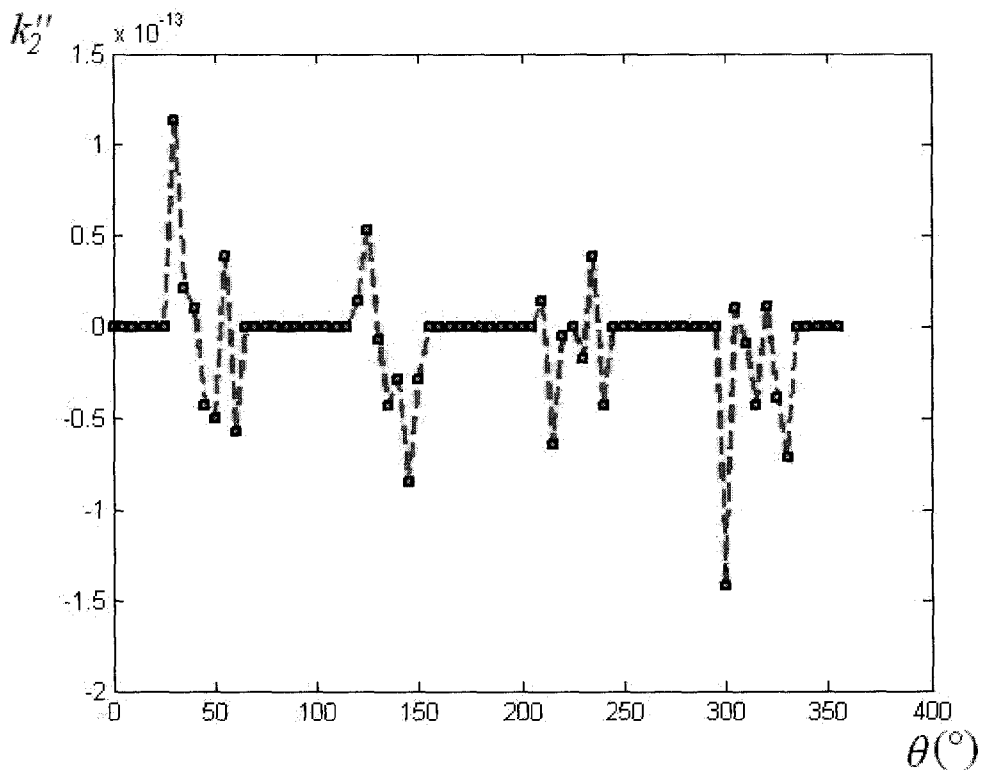

Fig. II.4.16 2nd derivative of curvature k_2 for squarish toroidal shell B

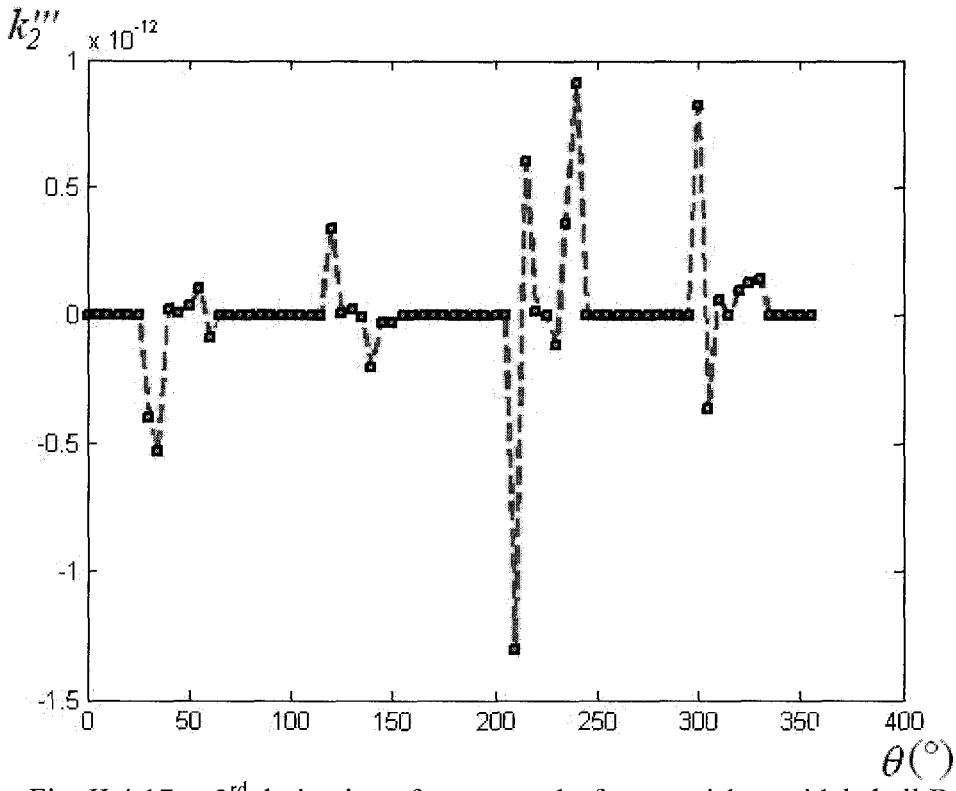

Fig. II.4.17 3rd derivative of curvature k_2 for squarish toroidal shell B

II.5 Conclusion

Figures in Sections II.3.4 and II.4.4 indicate that there are some discontinuities in the functions of the Lamé parameters, the curvatures, and their derivatives for the squarish toroidal shells A and B. These discontinuities may be the reason that the results obtained by the modified DQM program are not acceptable.

Comparing the DQM results for squarish toroidal shell A and for squarish toroidal shell B, the main difference is the distribution of the sampling points of the shells. According to the theory of the DQM, the distribution of the sampling points can be of great importance to the accuracy of the results of the DQM (Shu, 2000). The coordinate system of squarish toroidal shell B provides the sampling points with much more even spacing. Better results thus were obtained for frequencies for squarish toroidal shell B. It is noted that figures in

section II.4.4 have less discontinuity than those in section II.3.4. Although the results based on the second coordinate system is close to the results of FEM simulation, large errors still exist. It is considered that optimizing the distribution of the sampling points may further decrease the errors in the modified DQM program.